



## Architecture and morphodynamics of subcritical sediment waves in an ancient channel-lobe transition zone

Journal:	<i>Sedimentology</i>
Manuscript ID	SED-2016-OM-260.R2
Manuscript Type:	Original Manuscript
Date Submitted by the Author:	n/a
Complete List of Authors:	Hofstra, Menno; University of Leeds, School of Earth and Environment Peakall, Jeff; University of Leeds, Earth and Environment Hodgson, David; University of Leeds, Stevenson, Christopher; University of Liverpool, School of Earth, Ocean and Ecological Sciences
Keywords:	Karoo Basin, base-of-slope, channel-lobe transition, facies characteristics, process record, subcritical, sediment wave

1  
2  
3  
4  
5  
6  
7  
8  
9  
10  
11  
12  
13  
14  
15  
16  
17  
18  
19  
20  
21  
22  
23  
24  
25  
26  
27  
28  
29  
30  
31  
32  
33  
34  
35  
36  
37  
38  
39  
40  
41  
42  
43  
44  
45  
46  
47  
48  
49  
50  
51  
52  
53  
54  
55  
56  
57  
58  
59  
60

1 Architecture and morphodynamics of subcritical sediment waves in an ancient  
2 channel-lobe transition zone

3  
4  
5 M. Hofstra<sup>1†</sup>, J. Peakall<sup>1</sup>, D.M. Hodgson<sup>1</sup>, C.J. Stevenson<sup>2</sup>

6 <sup>1</sup>*Stratigraphy Group, School of Earth and Environment, University of Leeds, Leeds, LS2 9JT, UK*

7 <sup>2</sup>*School of Earth, Ocean and Ecological Sciences, University of Liverpool, L69 3GP, UK*

8  
9 *†corresponding author [Email: menno.hofstra.1@gmail.com]*

10  
11 **Running title:** Subcritical sediment wave architecture in a CLTZ

12 **Keywords:** channel-lobe transition; subcritical; sediment wave; base-of-slope; Karoo Basin;  
13 facies characteristics; process record

## 14 ABSTRACT

15 In modern systems, submarine channel-lobe transition zones (CLTZs) show a well-documented  
16 assemblage of depositional and erosional bedforms. In contrast, the stratigraphic record of CLTZs is  
17 poorly constrained, because preservation potential is low, and criteria have not been established to  
18 identify depositional bedforms in these settings. Several locations from an exhumed fine-grained  
19 base-of-slope system (Unit B, Laingsburg depocentre, Karoo Basin) show exceptional preservation of  
20 sandstone beds with distinctive morphologies and internal facies distributions. The regional  
21 stratigraphy, lack of a basal confining surface, wave-like morphology in dip section, size, and facies  
22 characteristics support an interpretation of subcritical sediment waves within a CLTZ setting. Some  
23 sediment waves show steep (10-25°) unevenly spaced (10-100 m) internal truncation surfaces that  
24 are dominantly upstream-facing, which suggests significant spatio-temporal fluctuations in flow  
25 character. Their architecture indicates individual sediment wave beds accrete upstream, in which  
26 each swell initiates individually. Lateral switching of the flow core is invoked to explain the sporadic  
27 upstream-facing truncation surfaces, and complex facies distributions vertically within each sediment  
28 wave. Variations in bedform character are related to the axial to marginal positions within a CLTZ.  
29 The depositional processes documented do not correspond with known bedform development  
30 under supercritical conditions. The proposed process model departs from established mechanisms of  
31 sediment wave formation by emphasising the evidence for subcritical rather than supercritical  
32 conditions, and highlights the significance of lateral and temporal variability in flow dynamics and  
33 resulting depositional architecture.

## 34 INTRODUCTION

35 Bedforms are rhythmic features that develop at the interface of fluid flow and a moveable bed (e.g.  
36 Southard, 1991; Van der Mark *et al.*, 2008; Baas *et al.*, 2016). Sediment waves are a type of long  
37 wavelength (tens of ms to kms) depositional bedform that vary in grain size from mud- to gravel-  
38 dominated, linked to their depositional setting (Fig. 1) (Wynn & Stow, 2002). They have been

1  
2  
3 39 identified in numerous modern channel-lobe transition zones (CLTZs) (Normark & Dickson, 1976;  
4  
5 40 Damuth, 1979; Lonsdale & Hollister, 1979; Normark *et al.*, 1980; Piper *et al.*, 1985; Malinverno *et al.*,  
6  
7 41 1988; Praeg & Schafer, 1989; Howe, 1996; Kidd *et al.*, 1998; Morris *et al.*, 1998; McHugh & Ryan,  
8  
9 42 2000; Migeon *et al.*, 2001; Normark *et al.*, 2002; Wynn & Stow, 2002; Wynn *et al.*, 2002a,b; Heiniö &  
10  
11 43 Davies, 2009), where they form part of a distinctive assemblage of depositional and erosional  
12  
13 44 bedforms (Mutti & Normark, 1987, 1991; Normark & Piper, 1991; Palanques *et al.*, 1995; Morris *et*  
14  
15 45 *al.*, 1998; Wynn *et al.*, 2002a,b; Macdonald *et al.*, 2011). However, the detailed sedimentological and  
16  
17 46 stratigraphic record of sediment waves from CLTZ and channel-mouth settings is not widely  
18  
19 47 documented.  
20  
21  
22 48 Vicente Bravo & Robles (1995) described hummock-like and wave-like depositional bedforms from  
23  
24 49 the Albian Black Flysch, NE Spain. The hummock-like bedforms (5 to 40 m wavelength and a few  
25  
26 50 decimetres to 1.5 m high) were interpreted to be genetically related to local scours. The wave-like  
27  
28 51 bedforms (5 and 30 m wavelength and a few cm to 0.7 m high) seen in longitudinal sections exhibit  
29  
30 52 symmetric to slightly asymmetric gravel-rich bedforms. Ponce & Carmona (2011) identified sandy  
31  
32 53 conglomeratic sediment waves with amplitudes up to 5 m and wavelengths ranging between 10 to  
33  
34 54 40 m at the northeast Atlantic coast of Tierra del Fuego, Argentina. Ito *et al.* (2014) described  
35  
36 55 medium- to very coarse-grained sandstone tractional structures from a Pleistocene canyon-mouth  
37  
38 56 setting within the Boso Peninsula, Japan, with wavelengths up to 40 m and crest heights up to 2 m.  
39  
40  
41 57 These coarse-grained examples from Japan, Argentina, and Spain lack detailed internal facies  
42  
43 58 descriptions and structure. Data on long wavelength finer-grained sediment waves in the rock record  
44  
45 59 are largely missing (Fig. 1), ascribed to their wavelength and poor exposure potential (Piper &  
46  
47 60 Kontopoulos, 1994). Modern examples that are dominantly fine grained (silt to mud) and show  
48  
49 61 substantial wavelengths (Fig. 1) are typically interpreted as large supercritical bedforms (Symonds *et*  
50  
51 62 *al.*, 2016), similar to cyclic steps. This is due to observations from geophysical data of their short lee-  
52  
53 63 sides and long depositional stoss-sides, and apparent single bedform structures with upstream  
54  
55 64 sediment wave migration as a sinusoidal wave (Cartigny *et al.*, 2014; Hughes-Clark, 2016; Covault *et*  
56  
57  
58  
59  
60

1  
2  
3 65 *al.*, 2017). Indeed, upstream migration of sediment waves is taken as an indicator of bedform  
4  
5 66 evolution under supercritical flow conditions (Symonds *et al.*, 2016). However, the processes  
6  
7 67 responsible for the inception and morphological evolution of sediment waves within CLTZ settings  
8  
9 68 remain poorly constrained, and high-resolution observations of their sedimentology are needed to  
10  
11 69 explore the balance of subcritical and supercritical processes in their inception, evolution, and  
12  
13 70 depositional record.

14  
15  
16 71 Here, we aim to improve understanding of sediment wave development in CLTZs through studying  
17  
18 72 multiple stratigraphic sections from well-constrained base-of-slope systems (Unit B, Laingsburg  
19  
20 73 depocentre, Karoo Basin) where distinctive fine to very-fine-grained sandstone depositional  
21  
22 74 bedforms with complex architecture, facies and stacking patterns are exposed. The objectives are: 1)  
23  
24 75 to document and interpret the depositional architecture and facies patterns of these sandstone  
25  
26 76 bedforms, 2) to discuss the topographic controls on their inception, 3) to propose a process model  
27  
28 77 for sediment wave development under subcritical rather than supercritical flow conditions, and, 4) to  
29  
30 78 consider the controls on the preservation potential of sediment wave fields in channel-lobe  
31  
32 79 transition zones.

## 33 34 35 80 **REGIONAL SETTING**

36  
37  
38 81 The southwest Karoo Basin is subdivided into the Laingsburg and the Tanqua depocentres. The Ecce  
39  
40 82 Group comprises a ~2 km-thick shallowing-upward succession from distal basin-floor through  
41  
42 83 submarine slope to shelf-edge and shelf deltaic settings (Wickens, 1994; Flint *et al.*, 2011). The deep-  
43  
44 84 water deposits of the Karoo Basin have a narrow grain size range from clay to upper fine sand. Within  
45  
46 85 the Laingsburg depocentre (Figs 2A and 3A), Unit B, the focus of this study, is stratigraphically  
47  
48 86 positioned between underlying proximal basin-floor fan deposits of Unit A (e.g. Sixsmith *et al.*, 2004;  
49  
50 87 Pr lat & Hodgson, 2013) and the overlying channelised slope deposits of the Fort Brown Formation  
51  
52 88 (Unit C-G; e.g. Hodgson *et al.*, 2011; Van der Merwe *et al.*, 2014). Unit B comprises a 200 m thick  
53  
54 89 section at the top of the Laingsburg Formation (Grecula *et al.*, 2003; Flint *et al.*, 2011; Brunt *et al.*,  
55  
56  
57  
58  
59  
60

1  
2  
3 90 2013), and is subdivided in three subunits, B1, B2 and B3 (Fig. 3A; Flint *et al.*, 2011; Brunt *et al.*,  
4  
5 91 2013). Unit B is well-exposed for more than 350 km<sup>2</sup> providing both down dip and across strike  
6  
7 92 control (Brunt *et al.*, 2013) with over 15 km long exposed sections along the limbs of the Baviaans  
8  
9 93 and Zoutkloof synclines and Faberskraal anticline (Fig. 2A). The study area is situated between well-  
10  
11 94 defined up-dip slope channels and down-dip basin-floor lobes (Figs 3B and 3C; Grecula *et al.*, 2003;  
12  
13 95 Pringle *et al.*, 2010; Brunt *et al.*, 2013). Therefore, the palaeogeographic setting is interpreted to be a  
14  
15 96 base-of-slope setting, where CLTZ-elements are more likely to be preserved (Figs 3B and 3C).

## 18 97 **METHODOLOGY AND DATASET**

19  
20  
21 98 Two areas of Unit B exposure were studied in detail: one located in the southern limb of the  
22  
23 99 Zoutkloof Syncline (Doornkloof) and one located in the southern limb of the Baviaans Syncline (Old  
24  
25 100 Railway) (Fig. 2). Stratigraphic correlations using closely-spaced sedimentary logs (m's to tens of m's),  
26  
27 101 photomontages, and walking out key surfaces and individual beds with a handheld GPS enabled  
28  
29 102 construction of architectural panels. Where the exposure allowed collection of sub-metre-scale  
30  
31 103 sedimentary logs individual beds were correlated over multiple kilometres. Within the Doornkloof  
32  
33 104 area (Fig. 2B) 11 long (>20-200 m) sedimentary logs, supported by 31 short (<5 m) detailed  
34  
35 105 sedimentary logs, were collected along a 2 km long E-W section. Particular emphasis was placed on  
36  
37 106 bed-scale changes in facies to construct detailed correlation panels. Additionally, a research borehole  
38  
39 107 drilled 330 m north of the studied outcrop section (DK01; 460983-6331775 UTM; Hofstra, 2016)  
40  
41 108 intersected the lower 92 m of Unit B (Figs 2A and 2B). Within the Old Railway area (Fig. 2C), eight  
42  
43 109 short and closely spaced (5-20 m distance) detailed sedimentary sections were collected.  
44  
45  
46 110 Palaeocurrents were collected from ripple-laminated bed tops and re-orientated, with 117  
47  
48 111 palaeoflow measurements at Doornkloof and 87 from the Old Railway area.

## 50 112 **FACIES AND ARCHITECTURE**

51  
52  
53 113 Both study areas contain sandstone-prone packages that comprise bedforms with substantial  
54  
55 114 downdip thickness and facies changes without evidence for confinement by an incision surface. The  
56  
57  
58  
59  
60

1  
2  
3 115 rate of thickness change and the range of sedimentary facies are markedly different from that  
4  
5 116 documented in basin-floor lobes (e.g. Prélat & Hodgson, 2013). Bed thicknesses change (metre scale)  
6  
7 117 in a downstream-orientated direction on short spatial-scales (tens of metres), compared to lateral  
8  
9 118 continuous bed thickness (hundreds of metres) known from lobes (e.g. Prélat *et al.*, 2010). Similarly,  
10  
11 119 facies change markedly over metre scales, in contrast to lobes where facies changes are transitional  
12  
13 120 over hundreds of metres (e.g. Prélat *et al.*, 2009). Depositional bedforms in both study areas are  
14  
15 121 present within a sandstone-prone (>90%) package of dominantly medium-bedded structured  
16  
17 122 sandstones, interbedded with thin-bedded and planar-laminated siltstones. The grain size range is  
18  
19 123 narrow, from siltstone to fine-grained sandstone, with a dominance of very-fine-grained sandstone.

#### 22 124 **Facies characteristics**

23  
24  
25 125 The sedimentary facies within the bedforms are subdivided into four types: structureless (F1),  
26  
27 126 banded to planar-laminated (F2), small-scale bedform structures (F3), and mudstone clast  
28  
29 127 conglomerates (F4).

30  
31 128 F1: Structureless sandstones show minimal variation or internal structure and are uniform in  
32  
33 129 grainsize (fine-grained sandstone). Locally, they may contain minor amounts of dispersed sub-  
34  
35 130 angular mudstone clasts (1-10 cm in diameter) and flame structures at bed bases.

36  
37  
38 131 Interpretation: These sandstones are interpreted as rapid fallout deposits from sand rich high-  
39  
40 132 density turbidity currents (Kneller & Branney, 1995; Stow & Johansson, 2000; Talling *et al.*, 2012)  
41  
42 133 with mudstone clasts representing traction-transported bedload. Flame structures at the bases of  
43  
44 134 structureless beds are associated with syn-depositional dewatering (Stow & Johansson, 2000).

45  
46  
47 135 F2: Banded and planar-laminated sandstones show large variations in character. The differentiation  
48  
49 136 between planar-laminated and banded facies is based on the thickness and character of the laminae  
50  
51 137 or bands. In banded sandstones, the bands are 0.5-3 cm thick and defined by alternations of clean  
52  
53 138 sand bands, and dirty sand bands rich in mudstone clasts and/or plant fragments. Planar-laminations  
54  
55 139 show <1 cm thick laminae that are defined by clear sand-to-silt grain-size changes. Furthermore,  
56  
57  
58  
59  
60

1  
2  
3 140 bands can be wavy or convolute, show substantial spatial thickness variations (<1 cm) at small (<1 m)  
4  
5 141 spatial scales, and exhibit subtle truncation at the bases of darker bands. Banded facies are  
6  
7 142 mudstone clast-rich where close to underlying mudstone clast conglomerates. In some places,  
8  
9 143 banded sandstone beds can be traced upstream into mudstone clast conglomerates. Where this  
10  
11 144 facies is observed, bed thicknesses typically exceed 0.5 m.

13  
14 145 Interpretation: Planar-lamination and banding are closely associated, and in many cases are difficult  
15  
16 146 to distinguish. This suggests that their depositional processes are closely related and are therefore  
17  
18 147 combined here into a single facies group. Planar laminated sandstones can be formed under dilute  
19  
20 148 flow conditions via the migration of low-amplitude bedwaves (Allen, 1984; Best & Bridge, 1992), or  
21  
22 149 under high-concentration conditions from traction carpets (Lowe, 1982; Sumner *et al.*, 2008; Talling  
23  
24 150 *et al.*, 2012; Cartigny *et al.*, 2013). The banded facies may be formed as traction carpet deposits from  
25  
26 151 high-density turbidity currents and are comparable to the Type 2 tractional structures of Ito *et al.*  
27  
28 152 (2014) and the H2 division of Haughton *et al.* (2009). Deposits related to traction carpets can show  
29  
30 153 significant variation in facies characteristics (e.g. Sohn, 1997; Cartigny *et al.*, 2013). Alternatively, the  
31  
32 154 banded facies may represent low-amplitude bedwave migration that formed under mud-rich  
33  
34 155 transitional flows (Baas *et al.*, 2016).

35  
36  
37  
38 156 F3: Fine-grained sandstones with decimetre-scale bedform structures. The majority (~80%) of this  
39  
40 157 facies is represented by climbing ripple-lamination, commonly with stoss-side preservation. Locally,  
41  
42 158 small-scale (wavelengths of decimetre-scale, and heights of a few cm) bedforms are present that  
43  
44 159 show convex-up laminae, biconvex tops, erosive to non-erosive basal surfaces, and laminae that can  
45  
46 160 thicken downwards (Figs 4A and 4C). In some cases, the bedforms show distinct low-angle climbing  
47  
48 161 (Fig. 5A). Isolated trains of decimetre-scale bedforms are present between banded/planar-laminated  
49  
50 162 facies (Figs 4B and 4C), whereas those exhibiting low-angle climbing can form above banded/planar-  
51  
52 163 laminated sandstone and in some cases transition into small-scale hummock-like features (Fig. 4A).  
53  
54 164 These hummock-like bedforms consist of erosively based, cross-cutting, concave- and convex-up,  
55  
56  
57  
58  
59  
60



1  
2  
3 165 low- to high-angle (up to 25°) laminae sets (Fig. 4A). They have decimetre to centimetre  
4  
5 166 wavelengths, and amplitudes up to 10 cm. Locally, internal laminae drape the lower bounding  
6  
7 167 surfaces and these tend to be low angle surfaces, whereas elsewhere laminae downlap onto the  
8  
9 168 basal surface, typically at higher angles (Fig. 4A). Where laminae are asymmetric they have accreted  
10  
11 169 in a downslope direction.

12  
13  
14 170 Furthermore, sinusoidal laminations are observed (Fig. 4A) with exceptional wavelengths (>20 cm)  
15  
16 171 and angles-of-climb (>45°) in comparison to conventional stoss-side preserved climbing ripples (15-  
17  
18 172 45°; 10-20 cm). These features also differ from convolute laminae/banding as they do show a  
19  
20 173 consistent wavelength and asymmetry. However, it is difficult to consistently make clear distinctions  
21  
22 174 between stoss-side preserved ripples and sinusoidal laminations. Hence, they are grouped together  
23  
24 175 into 'wavy bedform structures'.

25  
26  
27 176 F3 facies is most common at bed tops, but is also observed at bed bases, where laterally they are  
28  
29 177 overlain by an amalgamation surface. Locally, mudstone clasts (<1-4 cm) have been observed within  
30  
31 178 ripple-laminated segments.

32  
33  
34 179 Interpretation: Climbing ripple-lamination is interpreted as high rates of sediment fallout with  
35  
36 180 tractional reworking from flows within the lower flow regime (Allen, 1973; Southard & Boguchwal,  
37  
38 181 1990). The mudstone clasts are interpreted to be the result of overpassing of sediments on the bed  
39  
40 182 (Raudkivi, 1998; Garcia, 2008). When sedimentation rate exceeds the rate of erosion at the ripple  
41  
42 183 reattachment point, the stoss-side deposition is preserved and aggradational bedforms develop  
43  
44 184 (Allen, 1973). This is indicative of high rates of sediment fallout (Jopling & Walker, 1968; Allen, 1973;  
45  
46 185 Jobe *et al.*, 2012), attributed to rapid flow deceleration from moderate-to-low concentration  
47  
48 186 turbidity currents (Allen, 1973). Sinusoidal lamination is interpreted as a type of climbing ripple  
49  
50 187 lamination, marked by very high sedimentation rates, leading to similarity in thickness between stoss  
51  
52 188 and lee sides (Jopling & Walker, 1968; Allen, 1973; Jobe *et al.*, 2012).  
53  
54  
55  
56  
57  
58  
59  
60

1  
2  
3 189 The more convex bedforms (Figs 4A and 4C) bear similarities with washed out ripples that are  
4  
5 190 formed under high near-bed sediment concentration conditions at the transition from ripples to  
6  
7 191 upper stage plane beds in very fine sands (Baas & de Koning, 1995), and with combined-flow ripples  
8  
9 192 that have rounded tops and convex-up lee slopes (Harms, 1969; Yokokawa *et al.*, 1995; Tinterri,  
10  
11 193 2011). In turbidites, these bedforms have been termed 'rounded biconvex ripples with sigmoidal  
12  
13 194 laminae', and have been associated with reflected flow facies where turbidity currents have  
14  
15 195 interacted with topography (Tinterri, 2011; Tinterri & Muzzi Magalhaes, 2011; Zecchin *et al.*, 2013;  
16  
17 196 Tinterri & Tagliaferri, 2015). A third possibility is that these are decimetre-scale stable antidunes  
18  
19 197 since these can exhibit biconvex tops and in some cases convex-up cross-lamination (Alexander *et*  
20  
21 198 *al.*, 2001; Cartigny *et al.*, 2014; Fedele *et al.*, 2017), although these bedforms may also frequently  
22  
23 199 show concave laminae (Cartigny *et al.*, 2014). Typically, antidune laminae dip upstream (e.g.,  
24  
25 200 Alexander *et al.*, 2001; Cartigny *et al.*, 2014), although downstream migrating antidunes are known  
26  
27 201 from both open-channel flows (e.g., Kennedy, 1969) and gravity currents (Fedele *et al.*, 2017).

28  
29  
30 202 The 'hummocky-type' structures (Fig. 4A) with high-dip angles (up to 25°), draping of laminae, and  
31  
32 203 limited variation in laminae thickness, show similarities with anisotropic hummocky cross  
33  
34 204 stratification (HCS) from combined oscillatory-unidirectional flows (e.g., Dumas *et al.*, 2005; Dumas  
35  
36 205 & Arnott, 2006). Maximum dip angles of laminae in strongly anisotropic HCS can be around 25-30°  
37  
38 206 (Dumas *et al.*, 2005; Dumas & Arnott, 2006) much higher than for symmetrical forms, which are  
39  
40 207 typically less than 15° (Harms *et al.*, 1975; Tinterri, 2011). However, thickening and thinning of  
41  
42 208 laminae are expected in HCS (Harms *et al.*, 1975) and are not clearly observed in the hummocky-like  
43  
44 209 bedforms here. Such HCS-like hummocky bedforms have been interpreted from basin plain  
45  
46 210 turbidites to be related to reflected flows from topographic barriers (Tinterri, 2011; Tinterri & Muzzi  
47  
48 211 Magalhaes, 2011). Hummock-like bedforms in turbidites have also been interpreted as antidunes  
49  
50 212 (e.g., Skipper, 1971; Prave & Duke, 1990; Cartigny *et al.*, 2014). Antidunes are typically associated  
51  
52 213 with concave upward erosive surfaces, extensive cross-cutting sets if they are unstable antidunes,  
53  
54 214 bundles of upstream dipping laminae (if upstream migrating), laminae with low dip angles, low angle  
55  
56  
57  
58  
59  
60

1  
2  
3 215 terminations against the lower set boundary, some convex bedding, and structureless parts of fills  
4  
5 216 (e.g., Alexander *et al.*, 2001; Cartigny *et al.*, 2014; Fedele *et al.*, 2017). The hummock-like bedforms  
6  
7 217 in the present study share many similarities with these antidunes, however there is an absence of  
8  
9 218 structureless components, the draping of surfaces is more pronounced and more typical of HCS, the  
10  
11 219 approximately parallel nature of laminae within sets is more pronounced and the number of laminae  
12  
13 220 is greater. Furthermore, set bundles accrete downstream suggesting that if these are antidunes then  
14  
15 221 they are downstream-migrating forms. In summary, the hummock-like bedforms show greater  
16  
17 222 similarity to those HCS-like structures described from reflected flows (Tinterri, 2011; Tinterri & Muzzi  
18  
19 223 Magalhaes, 2011), rather than features associated with downstream migrating antidunes.

20  
21  
22 224 The observed combination of biconvex ripples and anisotropic hummock-like features, and the  
23  
24 225 transitions between these bedforms in some vertical sections, is also in agreement with that  
25  
26 226 observed in some turbidity currents interacting with topography (Tinterri, 2011; Tinterri & Muzzi  
27  
28 227 Magalhaes, 2011), further suggesting that the hummock-like features may be related to combined  
29  
30 228 flows, rather than the product of antidunes. This possibility of topographic-interaction induced  
31  
32 229 hummock-like and biconvex ripple forms is discussed further, after the topography of the sediment  
33  
34 230 waves is introduced.

35  
36  
37 231 F4: Mudstone clast conglomerate deposits form discrete patches (<20 m long and <0.3 m thick),  
38  
39 232 which commonly overlie erosion surfaces. Mudstone clasts (<1 cm – 10 cm diameter) vary from  
40  
41 233 subangular to well-rounded. They are dominantly clast supported with a matrix of fine-grained  
42  
43 234 sandstone.

44  
45  
46 235 Interpretation: Mudstone clast conglomerates are interpreted as lag deposits (e.g. Stevenson *et al.*,  
47  
48 236 2015) from energetic and bypassing high-density turbidity currents.

49  
50  
51 237 **Bed architecture and facies distribution: Doornkloof – Subunit B1**  
52  
53  
54  
55  
56  
57  
58  
59  
60

1  
2  
3 238 At Doornkloof (Fig. 2), subunit B1 has an average thickness of ~5 m (Fig. 5) and comprises thin- to  
4  
5 239 thick-bedded sandstones, thin-bedded siltstones and lenticular mudstone clast conglomerates (0.1-  
6  
7 240 0.3 m thick, 1-70 m wide) (Figs 5 and 6A-E). There are substantial variations in bed thicknesses and  
8  
9 241 sandstone-to-siltstone proportions along the 1.5 km long dip section (Fig. 5). Locally, medium- to  
10  
11 242 thick-bedded sandstones occur, which comprise bedforms within a package of thin-bedded siltstones  
12  
13 243 and sandstones. These bedforms show regional changes to more tabular thin-bedded sandstones  
14  
15 244 and siltstones (log 01/log 08, Fig. 5). Within the exposed section (~ 2 km), there are three sandstone-  
16  
17 245 prone bedform-dominated sections (200 m to 300 m in length) separated by siltstone-prone sections  
18  
19 246 (150 to 400 m in length), which have an overall tabular appearance (Fig. 6). The DK01 core (Figs 5 and  
20  
21 247 6) is located 330 m to the north of the western limit of Section I where subunit B1 is a ~5 m thick  
22  
23 248 package of interbedded thin structured sandstones and laminated siltstones (Fig. 6). Multiple erosion  
24  
25 249 surfaces are present at the base, and overall in the DK01 core the subunit B1 succession fines- and  
26  
27 250 thins-upward. Palaeoflow of the B1 subunit is dominantly ENE-orientated ( $082^\circ$ ) (Fig. 2B) but shows  
28  
29 251 some deviation within the eastern part of the section (log 42 – Figs 2B and 5) towards the NNE  
30  
31 252 ( $023^\circ$ ).  
32  
33  
34

35 253 The medium- to thick-bedded sandstones within the sandstone-prone sections of Section I,  
36  
37 254 orientated ( $079^\circ$ - $259^\circ$ ) subparallel to palaeoflow, show large lateral variations in thickness and facies.  
38  
39 255 The bedforms comprise structureless (F1), planar-laminated to banded (F2), and ripple-laminated  
40  
41 256 (F3) sandstones (Fig. 6A-E). The facies, architecture and thickness changes of one amalgamated bed  
42  
43 257 (*Bedform a*) are described in detail (Fig. 5). *Bedform a* thickens (up to 2.5 m) and thins (<20 cm)  
44  
45 258 multiple times, forming a down-dip pinch-and-swell morphology. Locally, the base of *Bedform a* is  
46  
47 259 marked by shallow erosion (<0.5 m deep; <30 m long) and in some places is amalgamated with the  
48  
49 260 underlying sandstone beds (Figs 5 and 7). Where *Bedform a* exceeds 0.5 m in thickness, banded (F2)  
50  
51 261 sandstone facies is dominant, and is in some places underlain by structureless (F1) divisions, or  
52  
53 262 exhibits climbing ripple-lamination at the bed top (F3). Where *Bedform a* is thin (<0.5 m thick), it is  
54  
55 263 dominated by climbing-ripple lamination (F3). Below *Bedform a*, lenses of mudstone conglomerate  
56  
57  
58  
59  
60

1  
2  
3 264 (<30 m long; 5-30 cm thick) can be observed at various locations over the complete section. In some  
4  
5 265 locations (e.g. log 16/18, Fig. 5), banded sandstone (F2) beds (Fig. 6D) can be observed intercalated  
6  
7 266 with mudstone clast conglomerate lenses (Fig. 7). These banded beds pinch out or show a transition  
8  
9 267 towards mudstone clast conglomerates upstream, and are amalgamated with *Bedform a*  
10  
11 268 downstream. At the same stratigraphic level as *Bedform a*, the DK01 core shows one pronounced 20  
12  
13 269 cm thick bed with angular mudstone clasts (<1-5 cm diameter) that can be correlated to *Bedform a*.  
14  
15  
16 270 In *Bedform a*, six truncation surfaces (10-25°) are identified within the eastern limit of the section  
17  
18 271 (Fig. 5), at places where the bedform exceeds 1 m in thickness. All truncation surfaces are sigmoid-  
19  
20 272 shaped and flatten out upstream and downstream within the bed (Fig. 6E). One eastward  
21  
22 273 (downstream) orientated truncation surface (Fig. 6B) in the lower part of the bed is observed at log  
23  
24 274 17 (Fig. 5). However, sigmoidal westward (upstream) facing truncation surfaces are most common in  
25  
26 275 the upper portion of the bed and are spaced 15-20 m apart. They cut banded (F2) and ripple-  
27  
28 276 laminated (F3) sandstone facies, and are sharply overlain by banded sandstone facies (F2) with bands  
29  
30 277 aligned parallel to the truncation surface, or by climbing-ripple laminated segments (Fig. 6E). Abrupt  
31  
32 278 upstream thinning (SW) and more gradual downstream thickening (NE) give *Bedform a*, an  
33  
34 279 asymmetric wave-like morphology in dip section. Small-scale bedforms (F3) are solely present at the  
35  
36 280 top of the wave-like morphology, and dominantly comprise climbing-ripple lamination, with  
37  
38 281 occasional wavy bedforms (stoss-side preserved climbing ripples and/or sinusoidal laminations) at  
39  
40 282 the thicker sections of the bedform (Fig. 5). At abrupt bed thickness changes associated with steep  
41  
42 283 westward-facing truncation surfaces (>15°) (logs 16/19/21, Fig. 5), shallow scour surfaces (<0.35 cm)  
43  
44 284 can be observed that cut into the top surface of *Bedform a*, overlain and onlapped by thin-bedded  
45  
46 285 siltstones and sandstones. Within the banded facies (F2), isolated lenses of ripple-lamination (F3) are  
47  
48 286 present (up to 30-40 cm long and 10 cm thick) (Fig. 5 – log 19). Mudstone and siltstone clasts (0.2-5  
49  
50 287 cm diameter) dispersed throughout structureless (F1) sections are typically well rounded, and rarely  
51  
52 288 sub-angular. At the eastern limit of Section I, stratigraphically below *Bedform a*, another ‘pinch-and-  
53  
54 289 swell’ sandstone bed abruptly increases in thickness downstream where *Bedform a* is amalgamated  
55  
56  
57  
58  
59  
60

1  
2  
3 290 with this bed below (log 21, Fig. 5). Where the bed thickens, *Bedform a* thins abruptly (log 23/24, Fig.  
4  
5 291 5). The thin-bedded and siltstone-prone deposits overlying *Bedform a* show more laterally constant  
6  
7 292 geometries, thicknesses and facies.  
8  
9

10 293 At the upstream end (SW) of Section 1, around log 02-07 (Fig. 5, middle panel), a package of  
11  
12 294 sandstone beds thickens locally (>100 m long, <5 m thick) above *Bedform a* (Fig. 8). *Bedform a*  
13  
14 295 pinches and swells multiple times within this log 02-07 interval to a maximum of 0.5 m thickness and  
15  
16 296 comprises similar facies as downstream (F1, F2, F3), but lacks internal truncation surfaces. The bed  
17  
18 297 directly above *Bedform a* thickens where *Bedform a* thins and *vice versa* (Fig. 8). Sandstone beds  
19  
20 298 above both this bed and *Bedform a*, in the top of the package, show only limited thickness variations  
21  
22 299 (~10 cm) and dominantly comprise climbing ripple-laminated sandstone (F2). All sandstone beds  
23  
24 300 above *Bedform a* either pinch-out or show a facies transition towards fine siltstone in both western  
25  
26 301 and eastern directions (Fig. 5).  
27  
28

### 29 302 **Bed architecture and facies distribution: Doornkloof – Subunit B2**

30  
31  
32 303 The sandstone bed morphology and facies characteristics at the base of subunit B2 share many  
33  
34 304 affinities with the deposits described within subunit B1 (Fig. 9). Palaeoflow of subunit B2 is generally  
35  
36 305 NE-orientated (040°) (n=68; Figs 2B and 9B) but with a high degree of dispersion, and a shift from  
37  
38 306 ENE (062°) in the western part of the section, to more northwards in the middle (19°) and eastern  
39  
40 307 part of the section (030°). This indicates that the section is dominantly subparallel to palaeoflow (dip  
41  
42 308 section) (Fig. 2B). Subunit B2 dominantly comprises medium-bedded (0.1-0.5 m thick) structured  
43  
44 309 sandstone (Fig. 9B). Closely spaced logs (m's to tens of m's) collected from the main face at the base  
45  
46 310 of B2 (Section II – Fig. 2B) permit tracing out of individual beds over a distance of 230 m and tracking  
47  
48 311 of internal facies changes (Fig. 6F-J). Two beds (*Bedform b* and *Bedform c*) change in thickness (0.5-2  
49  
50 312 m for *Bedform b* and 0.3-1.2 m for *Bedform c*) and contain multiple internal truncation surfaces of  
51  
52 313 which six are westward (upstream) facing and one is eastward (downstream) facing. Truncation  
53  
54 314 surfaces cut climbing ripple-laminated facies (F3) and banded facies (F2) with maximum angles  
55  
56  
57  
58  
59  
60

1  
2  
3 315 varying between 20-30° that shallow out and merge with the base of the bed (Figs 6G, 6H and 6J).  
4  
5 316 They flatten out in the downstream direction within the bed and are overlain by banded sandstone  
6  
7 317 facies (F2). In *Bedform b*, the rate of westward thinning is more abrupt than eastward, giving an  
8  
9 318 asymmetric wave-like morphology (Fig. 9B). This abrupt westward thinning is coincident with  
10  
11 319 locations of westward (upstream) orientated truncation surfaces. In the eastern part, 110 m  
12  
13 320 separates two truncation surfaces, in an area associated with bed thinning. However, towards the  
14  
15 321 western part of *Bedform b*, there is only 25-30 m between the westward (upstream) orientated  
16  
17 322 truncation surfaces, with no abrupt bed thinning.  
18  
19  
20 323 There is a high degree of longitudinal and vertical facies variability within *Bedform b* and *c* (Figs 4 and  
21  
22 324 9B). Commonly, longitudinal facies changes are accompanied by bed thickness changes. Locally, the  
23  
24 325 bases of thicker parts of the bedforms are mudstone clast-rich. Bed tops show small-scale bedform  
25  
26 326 structures (F3) at most locations. Banded sandstone facies overlie the truncation surfaces (Figs 6G,  
27  
28 327 6H and 6J). Ripple-laminated facies (F3) within the middle or lower parts of *Bedform b* and *c* indicate  
29  
30 328 flow directions that deviate (NW to N) from the regional palaeoflow (NE) (Figs 4A, 6F and 6H),  
31  
32 329 whereas the palaeoflow direction of the ripples at the top of the bedforms are consistent with the  
33  
34 330 regional palaeoflow. Detailed analysis of well-exposed sections (Fig. 4) indicates that many  
35  
36 331 laminated and banded sections are wavy and separated by low angle truncation or depositional  
37  
38 332 surfaces. Locally, small-scale bedform structures (F3) are present in patches (Figs 4B and 4C) (<10 cm  
39  
40 333 thick; couple of metres wide), which show downstream and/or upstream facies transitions to  
41  
42 334 banded/planar-laminated facies (F2), as well as examples of flame structures (Fig. 4C). The small-  
43  
44 335 scale bedform structures (F3) show a lot of variability, with hummock-like features observed above  
45  
46 336 biconvex ripples at both the downstream end of swells, and directly below truncation surfaces at the  
47  
48 337 upstream end of swells (Fig. 4A). Additionally, both hummock-like features and biconvex ripples  
49  
50 338 have been observed at the base of *Bedform b* (log 38; Fig. 9B). Similar to *Bedform a*, *Bedform b* & *c*  
51  
52 339 show wavy bedform structures at the top of swells, particularly where they are the thickest. *Bedform*  
53  
54 340 *b* is topped in the easternmost exposure by a scour surface that cuts at least 0.5 m into *Bedform b*  
55  
56  
57  
58  
59  
60

1  
2  
3 341 and is amalgamated with an overlying pinch-and-swell sandstone bed (Fig. 9B). Medium- to thin-  
4  
5 342 bedded structured sandstones are present above and below *Bedform b* and *c*, which do not show  
6  
7 343 any facies or thickness changes over the exposed section.  
8  
9  
10 344 The basal succession of subunit B2 in the DK01 core, at the same stratigraphic level as *Bedform b*  
11  
12 345 and *c*, comprises thick-bedded structureless (F1) to banded (F2) (>3 m) sandstones. Bed bases are  
13  
14 346 sharp and structureless and contain a variable amount of mudstone clasts (<1 cm). The middle to  
15  
16 347 upper parts of these beds show banded facies (F2) with clear mudstone clast-rich and -poor bands,  
17  
18 348 which pass through wavy lamination to climbing ripple (F3) and planar lamination at bed tops.  
19  
20 349 Above Section II, in both outcrop and core, a 15 m thick sandstone package shows a substantial  
21  
22 350 increase in bed thicknesses (max. 4.5 m), mainly due to bed amalgamation (Fig. 9A). Some of these  
23  
24 351 beds show a wave-like (asymmetric) morphology, similar to that observed in *Bedforms b and c*.  
25  
26 352 Abrupt bed thinning or pinch-out is common. These pinch-outs are primarily associated with  
27  
28 353 depositional geometry, with rare examples of bed truncation by erosion surfaces. Bounding surfaces  
29  
30 354 can be identified within the sandstone package, which are defined by successive upstream  
31  
32 355 depositional bed pinch-out points (Fig. 10), with local (<2 m long) shallow (<0.3 m) erosion surfaces.  
33  
34 356 These bounding surfaces separate multiple packages of downstream shingling (three to four)  
35  
36 357 sandstone beds. The packages of pinch-and-swell beds are stacked in an aggradational to slightly  
37  
38 358 upstream orientated manner (Fig. 10) and are topped by a >60 m thick package of tabular and  
39  
40 359 laterally continuous medium- to thin-bedded structured sandstones. At the same interval in the  
41  
42 360 DK01 core a transition can be observed from thick- to medium-bedded, dominantly banded (F2),  
43  
44 361 sandstones towards more medium- to thin-bedded structured (F3) sandstones.  
45  
46

#### 362 **Bed architecture: Old Railway – Subunit B2**

47  
48  
49  
50  
51 363 At this locality on the southern limb of the Baviaans Syncline, the lower 10 m of subunit B2 is  
52  
53 364 exposed for 100 m EW (Fig. 2C). Here, B2 is a medium- to thin-bedded sandstone-prone unit that  
54  
55 365 shows substantial lateral thickness changes without evidence of a basal erosion surface (Fig. 11).  
56  
57  
58  
59  
60



1  
2  
3 366 Mean palaeoflow is ESE (121°) (Fig. 2C), indicating the exposure is sub-parallel to depositional dip.  
4  
5 367 The sandstone beds are dominantly climbing ripple laminated (F3), with some banded/planar  
6  
7 368 laminated (F2) and structureless divisions (F1).  
8  
9 369 Multiple climbing ripple laminated beds contain dispersed small mudstone and siltstone clasts (Fig.  
10  
11 370 11C). The section is characterised by an alternation of beds showing typical pinch-and-swell  
12  
13 371 geometries (0.5-2 m) and more tabular thin-bedded (<0.5 m) sandstones. Locally, individual beds  
14  
15 372 pinch-and-swell multiple times over a distance of ~40 m, with wavelengths varying from 15 m to >40  
16  
17 373 m. Where there are swells, bed bases truncate underlying beds (Fig. 11D). Siltstones comprise only  
18  
19 374 ~10% of the succession and are thin-bedded and planar-laminated, with intercalated thin very fine-  
20  
21 375 grained sandstones (<1 cm).  
22  
23  
24 376 Towards the top of the section, a 40 cm thick very fine-grained sandstone bed abruptly fines and  
25  
26 377 thins downstream to a centimetre-thick siltstone bed (Fig. 12). This bed thickens and thins along a  
27  
28 378 ~20 m distance (Fig. 12) forming sandstone lenses, before regaining original thickness (40 cm).  
29  
30 379 Locally, within this zone, the bed longitudinally grades to siltstone and is perturbed from the top by  
31  
32 380 decimetre-scale scour surfaces (0.2-3 m long, couple of cm's deep). At log 04 (Fig. 11A), a bed that  
33  
34 381 pinches downstream has a downstream-orientated scour on its top surface, which is overlain by  
35  
36 382 thin-bedded sandstones and siltstones that pass upstream beyond the confines of the scour surface.  
37  
38 383 A downstream thickening bed with an erosive base truncates these beds. The majority of the  
39  
40 384 observed pinch-and-swell bedforms stack in a downstream direction (Fig. 11A). However, in the  
41  
42 385 middle of the package at log 1, one bed stacks in an upstream manner, giving the overall package an  
43  
44 386 aggradational character. This is similar to the stacking patterns observed within subunit B2 at the  
45  
46 387 Doornkloof section (Fig. 10).  
47  
48  
49

### 388 **Sediment waves within channel-lobe transition zones**

50  
51  
52  
53 389 The Doornkloof and Old Railway sections show bedforms with clear pinch-and-swell morphology  
54  
55 390 that are subparallel to flow direction. These bedforms developed in a base-of-slope setting without  
56  
57  
58  
59  
60

1  
2  
3 391 any evidence of a large-scale basal confining surface. Bed-scale amalgamation and scouring are  
4  
5 392 common in the two study areas, however the more significant component of downstream bed  
6  
7 393 thickness changes is depositional. Their geometry and dimensions (>1 m height; 10-100 m  
8  
9 394 wavelength), support their classification as sediment waves (Wynn & Stow, 2002). The bedforms  
10  
11 395 described from the Doornkloof area (*Beds a-c*) show clear asymmetric pinch-and-swell  
12  
13 396 morphologies, related to internal upstream-facing truncation surfaces (Figs 5 and 9). The well-  
14  
15 397 constrained base-of-slope setting (Brunt *et al.*, 2013), the lack of confining erosion surfaces, and the  
16  
17 398 lobe-dominated nature of Unit B downdip (Figs 3B and 3C) are consistent with an interpretation that  
18  
19 399 the sediment waves formed within a CLTZ setting.

## 22 400 **DISCUSSION**

### 25 401 **Topographic control on sediment wave inception**

27 402 The interpreted CLTZ setting for the sediment waves means that initial deposition is most likely  
28  
29 403 related to flow expansion at the channel-mouth (e.g. Hiscott, 1994a; Kneller, 1995; Mulder &  
30  
31 404 Alexander, 2001). The occurrence of abrupt downstream bedform thickening (e.g. *Bedform a*, Fig. 5),  
32  
33 405 indicates a marked decrease in flow capacity resulting in a temporary increase of deposition rates  
34  
35 406 (e.g. Hiscott, 1994a). Although deposition is expected in areas of flow expansion, this does not  
36  
37 407 explain why sediment wave deposition appears to be localised (e.g. log 02-07; Fig. 5). Both the  
38  
39 408 inception and development of the sediment waves are interpreted to be related to the presence of  
40  
41 409 seabed relief (dm's to m's amplitude). Seabed irregularities are common in base-of-slope settings,  
42  
43 410 and minor defects (such as scours lined with mudstone clast conglomerates; Fig. 7) could have  
44  
45 411 triggered deposition from flows close to the depositional threshold (Wynn *et al.*, 2002a). The  
46  
47 412 presence of bedforms overlying swells of older bedforms, such as at the upstream location of  
48  
49 413 *Bedform a* (Figs 5 (logs 2-7) and 8) or the sediment waves overlying *Bedform b* in subunit B2 (Fig. 10),  
50  
51 414 suggest that relief of older bedforms, and consequent flow deceleration, may also act as a nucleus  
52  
53 415 for later sediment wave development. The locally observed decimetre-scale deep scours probably  
54  
55  
56  
57  
58  
59  
60

1  
2  
3 416 had a more variable effect on sediment wave development. In some cases it resulted in topographic  
4  
5 417 relief that could help sediment wave nucleation (e.g. log 4, Fig. 11) and in other cases the scours  
6  
7 418 remove positive depositional relief (e.g. Fig. 12) and therefore they will have a slight negative effect  
8  
9 419 on sediment wave nucleation. The aggradational character of the sediment wave packages (Figs 10  
10  
11 420 and 11A) supports a depositional feedback mechanism. Depositional bedforms form positive  
12  
13 421 topography, which may help to nucleate sites of deposition and the development of composite  
14  
15 422 sediment waves forming the complicated larger-scale sediment wave architecture (Figs 10 and 11A).  
16  
17

18 423

19  
20 424 **Bed-scale process record**

21  
22  
23 425 The sediment wave deposits from CLTZ settings in Unit B are diverse and show significant facies  
24  
25 426 variations on the sub-metre scale. The characteristics of the sediment wave deposits from the two  
26  
27 427 Unit B datasets are discussed and compared.  
28  
29

30 428 *Bed-scale process record - Doornkloof section*

31 429 Facies of the sediment waves identified at the Doornkloof section are characterised by an  
32  
33 430 assemblage of structureless (F1), banded and planar laminated (F2), and climbing ripple laminated  
34  
35 431 (F3) sandstones. Local patches of structureless sandstone facies (F1) (Figs 5 and 9B) at bed bases,  
36  
37 432 suggest periods of more enhanced deposition rates (e.g. Stow & Johansson, 2000). However, the  
38  
39 433 sediment waves are dominated by banded facies, likely related either to traction-carpet deposition  
40  
41 434 (Sumner *et al.*, 2008; Cartigny *et al.*, 2013) or low-amplitude bedwave migration under transitional  
42  
43 435 flows (Baas *et al.*, 2016). This suggests deposition from high concentration flows during bedform  
44  
45 436 development. The high degree of F2 variation (band thickness, presence of shallow truncations,  
46  
47 437 wavy nature) is explained by: 1) turbulent bursts interacting with a traction carpet (Hiscott, 1994b);  
48  
49 438 2) waves forming at the density interface between a traction carpet and the overlying lower-  
50  
51 439 concentration flow, possibly as a result of Kelvin-Helmholtz instabilities (Figs 4 and 6) (Sumner *et al.*,  
52  
53 440 2008; Cartigny *et al.*, 2013); 3) the presence of bedwaves and associated development beneath  
54  
55  
56  
57  
58  
59  
60

1  
2  
3 441 mixed-load, mud-rich, transitional flows (Baas *et al.*, 2016), or some combination of these processes.  
4  
5 442 There is a strong spatial and stratigraphic relationship between mudstone clast conglomerates (F4)  
6  
7 443 (Figs 7 and 8) and banded sandstone facies (F2) with a high proportion of mudstone clasts. As the  
8  
9 444 deposits underlying the shallow erosion surfaces are predominantly siltstones, the mudstone clast  
10  
11 445 materials must have been entrained farther upstream, and are therefore interpreted as lag deposits  
12  
13 446 from bypass-dominated high-concentration flows (e.g. Stevenson *et al.*, 2015). As scours are typically  
14  
15 447 documented upstream of sediment waves in modern CLTZs (Wynn *et al.*, 2002a), the source of these  
16  
17 448 mudstone clasts is likely linked to local upstream scouring, supported by the angularity of the clasts  
18  
19 449 (Johansson & Stow, 1995). The transition from banded facies (F2) to climbing ripple-laminated facies  
20  
21 450 (F3), common at the top of individual beds, likely represents a change from net depositional high  
22  
23 451 concentration flows, to steady deposition from moderate to low concentration flows, and / or a  
24  
25 452 corresponding change from mud-rich transitional flows to mud-poor flows. The dominance of this  
26  
27 453 facies group (F3) at bed tops (Figs 5 and 9B) is interpreted as the product of less-energetic and more  
28  
29 454 depositional tails of bypassing flows.  
30  
31  
32 455 To understand the process record and evolution of the Unit B sediment waves, it is important to be  
33  
34 456 able to distinguish the record of a single flow event from a composite body comprised of deposits  
35  
36 457 from multiple flow events. The majority of the observed bed thickness changes within the sediment  
37  
38 458 waves at the Doornkloof section are attributed to depositional relief although internally they show  
39  
40 459 steep internal truncation surfaces (Figs 5, 6 and 9). The erosion surfaces may suggest that this  
41  
42 460 depositional architecture is the result of multiple depositional and erosional flow events. However,  
43  
44 461 several lines of evidence suggest these are deposits produced from a single flow event. The  
45  
46 462 preservation of upstream-facing truncation surfaces (Figs 5 and 9B), implies a significant component  
47  
48 463 of bedform accretion at the upstream end (Figs 13 and 14A). To be able to preserve upstream  
49  
50 464 younging truncation surfaces with angles up to 25° (close to the angle-of-repose), the erosion and  
51  
52 465 deposition within each bedform is likely to be the result of a single flow event. Within subunit B2, no  
53  
54 466 bed splitting is observed and all truncation surfaces of *Bedform b* and *c* merge towards the bed base  
55  
56  
57  
58  
59  
60

1  
2  
3 467 as a single surface (Fig. 9B), leaving underlying strata untouched. This suggests an origin from a  
4  
5 468 single flow event for the entire bedform.

6  
7 469 In subunit B1, all upstream facing truncation surfaces in the main sandstone body of *Bedform a*  
8  
9 470 merge onto a single surface within the composite deposit, in a similar manner to *Bedform b* and *c*,  
10  
11 471 further suggesting a single flow origin for the main sediment wave morphology. Additionally,  
12  
13 472 *Bedform a* can be followed out for ~ 1 km in the upstream direction, and shows many small-scale (<5  
14  
15 473 m longitudinal distance) purely depositional undulations at the western end (Figs 5 and 8). These  
16  
17 474 flow parallel undulations are stratigraphically equivalent to the deposits above the most upstream  
18  
19 475 truncation surface and therefore, represent the youngest depositional phase of *Bedform a*  
20  
21 476 development. The absence of erosion surfaces or bedding planes between these undulations further  
22  
23 477 suggests that the main body of *Bedform a* was formed as a single event bed. The evidence therefore  
24  
25 478 supports the initiation and development of each wave-like bedform in the Doornkloof section  
26  
27 479 (*Bedform a, b* and *c*) to be during the passage of a single flow event. Therefore, the internal scour  
28  
29 480 surfaces and bedform undulations are interpreted to be the result of spatio-temporal flow  
30  
31 481 fluctuations from a single flow event. In contrast, the mudstone clast patches that underlie *Bedform*  
32  
33 482 *a* show upstream pinch-out of sandstone beds and downstream amalgamation (Fig. 7) indicating  
34  
35 483 multiple flow events formed these patches and the lower sandstone body prior to the initiation of  
36  
37 484 the main bedform. The presence of these mudstone clast patches results in a marked difference in  
38  
39 485 bedform architecture and bed thickness for *Bedform a* compared to *Bedform b* and *c*.  
40  
41  
42  
43

#### 44 486 *Bed-scale process record - Old Railway section*

45  
46 487 In the Old Railway section (Fig. 11), erosional bed bases and bed amalgamation are common,  
47  
48 488 particularly where there is depositional thinning of underlying beds, indicating that the 'pinch-and-  
49  
50 489 swell' bedforms present at this section are the result of multiple flow events in contrast to the  
51  
52 490 Doornkloof area. However, bed amalgamation has limited impact on bedform thickness, as thickness  
53  
54 491 increase dominantly occurs downdip of the point of amalgamation and is therefore of a depositional  
55  
56  
57  
58  
59  
60

1  
2  
3 492 nature. The Old Railway bedforms classify as sediment waves (Wynn & Stow, 2002) with dimensions  
4  
5 493 of 15 to >40 m wavelength (extending outside outcrop limits) and 1-2 m amplitude. However, the  
6  
7 494 maximum bed thicknesses (1-1.5 m) are more limited than at the Doornkloof area (>2.5 m), climbing  
8  
9 495 ripple-laminated facies (F3) is more dominant, and banded facies (F2) are almost absent. The  
10  
11 496 sediment waves have a more uniform facies distribution and there is an absence of internal  
12  
13 497 truncation surfaces (Fig. 11). The dominance of F3 indicates rapid deposition from dilute turbulent  
14  
15 498 flows, which contrasts with the Doornkloof area.

16  
17  
18 499

19  
20  
21 500 **Subcritical sediment waves: comparison with supercritical bedforms**

22  
23 501 The Doornkloof and Old Railway outcrops are both characterised by composite sediment waves.  
24  
25 502 However, there are distinct differences between both areas. The Old Railway examples exhibit  
26  
27 503 comparatively simple sediment waves, composed of multiple event beds, and dominated by lower  
28  
29 504 flow-regime facies (F3) such as climbing ripple-lamination, accrete downstream, and lack significant  
30  
31 505 internal erosive surfaces. Morphologically, stoss sides can be comparable to or longer than lee sides  
32  
33 506 (Fig. 11). In contrast, the Doornkloof sediment waves were formed as single event beds and are  
34  
35 507 characterized by short stoss sides, long lee sides, and exhibit erosion and more energetic facies (F1,  
36  
37 508 F2, F4), with climbing ripple deposition (F3) becoming more dominant at the top of the beds (Fig.  
38  
39 509 13A). The Doornkloof waves migrate upstream through erosional truncation and draping at bed  
40  
41 510 swelling locations (up to >10 m; Fig. 9) followed by the development of another bed swell upstream  
42  
43 511 (Fig. 13A). This means that each swell initiates individually, rather than simultaneously as a  
44  
45 512 sinusoidal wave.

46  
47  
48  
49 513 The architecture of the Doornkloof sediment waves most closely resembles the smaller-scale type II  
50  
51 514 and type III antidunal bedforms described by Schminke *et al.* (1973). However, these bedform  
52  
53 515 architectures, which are an order of magnitude smaller, are interpreted to migrate through stoss-  
54  
55 516 side deposition by supercritical flows based on the field observations, and have never been

56  
57  
58  
59  
60

1  
2  
3 517 produced experimentally. In contrast, Kubo & Nakajima (2002) and Kubo (2004) observed sediment  
4  
5 518 wave architectures with short stoss sides, long lee sides and variable wavelengths, similar to the  
6  
7 519 Doornkloof sediment waves, under subcritical flow conditions in physical and numerical  
8  
9 520 experiments. The depositional patterns of these sediment waves were defined by upstream  
10  
11 521 migration of waveforms by individual growing mounds (Kubo & Nakajima, 2002; Kubo, 2004), and  
12  
13 522 are therefore highly analogous to the observations from the Doornkloof waves.

14  
15  
16 523 The nature and variability of small-scale bedform structures (F3) (e.g., Fig. 13A for the Doornkloof  
17  
18 524 waves) provide key indicators of flow type. This facies group consists of climbing ripples, sinusoidal  
19  
20 525 lamination, biconvex ripples, and hummock-like structures, with biconvex ripples sometimes  
21  
22 526 transitioning upwards into the hummocks. Climbing ripples and sinusoidal lamination are indicators  
23  
24 527 of subcritical flow (Allen, 1973; Southard & Boguchwal, 1990), and the biconvex ripples and  
25  
26 528 hummock-like structures have greater affinities with combined-flow ripples and hummocky cross  
27  
28 529 stratification than with antidunes, again suggesting deposition under subcritical flow conditions. In  
29  
30 530 particular, the vertical change from biconvex ripples to hummock-like bedforms observed in the  
31  
32 531 Doornkloof sediment waves is strongly analogous to structures associated with reflected flows in  
33  
34 532 other turbidites (Tinterri, 2011; Tinterri & Muzzi Magalhaes, 2011), rather than deposits associated  
35  
36 533 with supercritical flow conditions. The presence of topography in the form of the large-scale  
37  
38 534 sediment wave may have led to flow reflection (Tinterri, 2011) and deflection as and when the flow  
39  
40 535 waned. Importantly, these subcritical small-scale bedforms are observed over the full length of the  
41  
42 536 sediment waves, both on the stoss- and lee-side, at Doornkloof and the Old Railway (Figs 5, 9 and  
43  
44 537 11). This indicates subcritical deposition occurred across the entire sediment wave, and that the flow  
45  
46 538 remained subcritical throughout the depositional period over which the decimetre bedforms were  
47  
48 539 formed.

49  
50  
51  
52 540 The morphology and architecture of the sediment waves in this study contrast with large  
53  
54 541 supercritical bedforms, such as cyclic steps, since these exhibit short erosional lee-sides and long  
55  
56 542 depositional stoss-sides (Cartigny *et al.*, 2014; Hughes-Clark, 2016), and display upstream sediment  
57  
58  
59  
60

1  
2  
3 543 wave migration as a sinusoidal wave (Cartigny *et al.* 2014). Additionally, the sediment waves  
4  
5 544 described here are not single bedform structures such as described from supercritical bedforms  
6  
7 545 (e.g., Cartigny *et al.*, 2014; Covault *et al.*, 2017), but are composed of stacked smaller-scale  
8  
9 546 bedforms. The spatial and temporal extent of subcritical deposits also contrasts strongly with  
10  
11 547 ‘supercritical’ bedforms where subcritical deposition can be expected only in some or all of the  
12  
13 548 stoss-side, downdip of a hydraulic jump (Vellinga *et al.*, 2018). Furthermore, tractional subcritical  
14  
15 549 bedforms are predicted to be limited to the downstream parts of the stoss side in aggradational  
16  
17 550 cyclic steps, or to be mixed-in with supercritical and non-tractional subcritical facies in  
18  
19 551 transportational cyclic steps (Vellinga *et al.*, 2018; their Fig. 9). Note that decimeter-scale bedforms  
20  
21 552 themselves could not be modelled in the CFD simulations of Vellinga *et al.* (2018). Lastly, the overall  
22  
23 553 signature of subcritical deposits within dominantly supercritical bedforms was one dominated by  
24  
25 554 amalgamation of concave-up erosional surfaces and low-angle foresets and backsets creating  
26  
27 555 lenticular bodies (Vellinga *et al.*, 2018). These bodies scale with the size of the overall bedform, and  
28  
29 556 the backsets show clear downstream fining (Vellinga *et al.*, 2018). Again, the sediment waves studied  
30  
31 557 herein show radically different architecture to that formed in cyclic steps, characterised by stacked  
32  
33 558 decimeter-scale bedforms and an absence of large-scale (scaling with the sediment wave) foresets,  
34  
35 559 backsets and lenticular bodies.

36  
37  
38  
39 560 In summary, the morphology, architecture, composite nature, and small-scale bedform types, all  
40  
41 561 indicate that the sediment waves were clearly deposited under subcritical conditions. The subcritical  
42  
43 562 nature of these sediment waves, the observation of upstream accretion via deposition on the stoss  
44  
45 563 side, and the associated upstream migration of the crestline, observed at Doornkloof, challenge the  
46  
47 564 assumption that all upstream-orientated expansion of sediment waves is the product of supercritical  
48  
49 565 conditions (Wynn & Stow, 2002; Symons *et al.*, 2016). That said, the Doornkloof bedforms appear to  
50  
51 566 have migrated sporadically over short distances (m’s to tens of m’s) through upstream accretion (Fig.  
52  
53 567 9B), before undergoing growth of new sediment wave lenses upstream, thus the entire bedform  
54  
55 568 does not continuously migrate as observed in some modern sediment wave examples (e.g., Hughes-



1  
2  
3 569 Clark, 2016). The presence of these subcritical sediment waves in the downstream parts of CLTZs  
4  
5 570 also challenges the idea that mid-sized fans, like those in the Karoo, likely exhibit flows close to  
6  
7 571 critical Froude numbers, at and beyond the CLTZ (Hamilton *et al.*, 2017), although such conditions  
8  
9 572 are likely in upstream parts of CLTZ where scouring occurs.  
10

11 573

#### 14 574 **Spatio-temporal flow fluctuations**

16 575 The large-scale erosive truncations, and the wide variability of decimetre-scale bedforms in space  
17  
18 576 and time, observed in the Doornkloof waves indicate marked spatio-temporal flow fluctuations from  
19  
20 577 a single flow event. In contrast, the continuity of facies and absence of significant erosive surfaces  
21  
22 578 suggests that the Old Railway sediment waves were formed by flows with very limited spatio-  
23  
24 579 temporal variation. Here, we focus on these spatio-temporal fluctuations indicated by the  
25  
26 580 Doornkloof waves, and later address the issue of how the different types of sediment waves shown  
27  
28 581 in the Doornkloof and Old Railway outcrops could coexist.  
29  
30

31 582 Fluctuations in velocity and concentration can be expected in environments where turbidity currents  
32  
33 583 exit confinement (e.g. Kneller & McCaffrey, 1999, 2003; Ito, 2008; Kane *et al.*, 2009; Ponce &  
34  
35 584 Carmona, 2011), and where flows pass over depositional and erosional relief on the seabed (e.g.  
36  
37 585 Groenenberg *et al.*, 2010; Eggenhuisen *et al.*, 2011). Similar steep internal scour surfaces to those  
38  
39 586 observed in the Doornkloof bedforms were interpreted to be generated by energetic sweeps from a  
40  
41 587 stratified flow (Hiscott, 1994b). Furthermore, a similar depositional history of waxing and waning  
42  
43 588 behaviour within a single flow was inferred from the sediment waves of the Miocene Austral  
44  
45 589 foreland Basin, Argentina (Ponce & Carmona, 2011). However, the depositional model proposed by  
46  
47 590 Ponce & Carmona (2011) assumes each independent lens-shaped geometry is created and reworked  
48  
49 591 simultaneously, and subsequently draped as a result of flow deceleration. The Doornkloof sediment  
50  
51 592 wave architecture cannot be explained by this process as the 'lenses' are clearly not disconnected  
52  
53 593 (Figs 5 and 13). The distribution of truncation surfaces within the sediment waves of subunit B2 does  
54  
55  
56  
57  
58  
59  
60

1  
2  
3 594 however suggest there can be both phases of upstream swell formation as well as upstream  
4  
5 595 migration of the crest line (e.g. *Bedform c* at log 34-35). To explain the large fluctuations in flow  
6  
7 596 concentration and depositional behaviour in CLTZ settings (Fig. 13), a number of factors can be  
8  
9 597 considered. Here, we consider each of these factors in turn, and assess their potential for explaining  
10  
11 598 the development of the sediment waves observed in this study.

12  
13  
14 599 *Flow splitting in updip channel-levée systems*

15  
16  
17 600 Waxing and waning flow behaviour can be induced by splitting of the flow in the channel-levée  
18  
19 601 system updip, where the primary 'channelised' flow may reach the sediment wave field earlier than  
20  
21 602 the secondary 'overbank' flow (Peakall *et al.*, 2000). However, this would imply significant velocity  
22  
23 603 and concentration differences and therefore significant depositional facies differences between the  
24  
25 604 two stages, which does not fit the observations (Figs 13 and 14A). Furthermore, it would not explain  
26  
27 605 the number of flow fluctuations interpreted within a single flow event bed (Figs 13 and 14A).

28  
29  
30 606 *Mixed load (sand-clay) bedforms*

31  
32  
33 607 An alternative explanation for the sediment wave architecture could be that these bedforms formed  
34  
35 608 by flows with sand-clay mixtures. Complicated bedform architectures with both erosional and  
36  
37 609 depositional components have been created experimentally (Baas *et al.*, 2016). However, there are a  
38  
39 610 number of issues with this hypothesis: 1) the bedforms described from the two case studies are one  
40  
41 611 to two orders of magnitude larger than the 'muddy' bedforms described within flume tanks (Baas *et*  
42  
43 612 *al.*, 2016), and 2) the presence of clean climbing ripple-lamination suggests that at least part of the  
44  
45 613 flow was not clay-rich during deposition (Baas *et al.*, 2013; Schindler *et al.*, 2015).

46  
47  
48 614 *Froude number fluctuations*

49  
50  
51 615 The net-depositional record of waxing and waning flow conditions (Fig. 14A) observed at a single  
52  
53 616 given location within the Doornkloof sediment waves (Fig. 13) could be hypothesised to be a record  
54  
55 617 of temporal fluctuations around the critical Froude number separating sub- and supercritical flow  
56  
57  
58  
59  
60

1  
2  
3 618 conditions. However, the evidence for subcritical deposition across the full length of the sediment  
4  
5 619 waves, and over the timescale of bedform development, demonstrates that fluctuations around the  
6  
7 620 critical Froude number cannot be directly responsible for the formation of these sediment waves.  
8  
9 621 That said, fluctuations in velocity and capacity within a subcritical flow downstream of a zone of  
10  
11 622 hydraulic jumps may still play a role in controlling the observed sedimentation patterns. Fluctuations  
12  
13 623 of the turbidity current Froude number are expected in areas of abrupt flow expansion such as at  
14  
15 624 the base-of-slope (Garcia, 1993; Wynn *et al.*, 2002b). Turbidity currents that undergo rapid  
16  
17 625 transitions from supercritical to subcritical conditions forming a single hydraulic jump, or repeated  
18  
19 626 hydraulic jumps across a CLTZ (Sumner *et al.*, 2013; Dorrell *et al.*, 2016), have been linked to  
20  
21 627 bedform formation (Vicente Bravo & Robles, 1995; Wynn & Stow, 2002; Wynn *et al.*, 2002b; Symons  
22  
23 628 *et al.*, 2016), and have been linked to the formation of erosive scours in upstream parts of CLTZs in  
24  
25 629 the Karoo Basin (Hofstra *et al.*, 2015). Due to the presence of multiple interacting hydraulic jumps  
26  
27 630 across a CLTZ, Froude number fluctuations around unity may be expected (Sumner *et al.*, 2013;  
28  
29 631 Dorrell *et al.*, 2016). Such velocity fluctuations would change the capacity of the flow (Fig. 14A),  
30  
31 632 however whether this would translate to periodic changes in sediment concentration is less clear  
32  
33 633 due in part to the lack of concentration measurements from natural and experimental subaqueous  
34  
35 634 hydraulic jumps. That said, in turbidity currents generally, there is a close coupling between velocity  
36  
37 635 and concentration changes (Felix *et al.*, 2005). Fluctuating velocities, and potentially concentration,  
38  
39 636 related to variations in Froude numbers around critical may enable complicated and variable  
40  
41 637 bedform architectures to be formed.

#### 42 638 *The 'hose effect'*

43  
44  
45  
46  
47  
48 639 A spatial control in flow character could also be invoked to explain the development of sediment  
49  
50 640 waves, based on flow-deposit interactions and the momentum of the flow core (Fig. 14B). As a  
51  
52 641 turbidity current exits channel confinement it does not directly lose its momentum (e.g. Choi &  
53  
54 642 Garcia, 2001). The flow core may shift around during bedform aggradation due to interactions with  
55  
56  
57  
58  
59  
60

1  
2  
3 643 depositional and erosional relief around the channel-mouth. Most studies on flow-deposit  
4  
5 644 interactions focus on temporal changes in flow conditions (e.g. Kneller & McCaffrey, 2003;  
6  
7 645 Groenenberg *et al.*, 2010), but rarely consider lateral changes within a single turbidity current  
8  
9 646 (Hiscott, 1994a). A single location within a sediment wave field may receive periods of high and low  
10  
11 647 energy linked to the lateral shifting of the flow core, where the energetic flow core can be linked to  
12  
13 648 periods of erosion and/or high concentration flow deposition, and the flow margin to deposition  
14  
15 649 from the less energetic and dilute parts of the flow. In this scenario, the upstream-orientated  
16  
17 650 truncation surfaces are the result of the interaction of the flow core with its self-produced obstacle  
18  
19 651 (Fig. 14B), linked to the inability to sustain the compensation process over time. Upstream  
20  
21 652 fluctuations in Froude number, related to an area of scour formation and hydraulic jumps, would  
22  
23 653 result in longitudinal waxing and waning flow behaviour downstream and could explain the  
24  
25 654 combination of both erosion and high concentration flow deposition of the flow core.  
26  
27  
28 655 The compensational effects will form a stratigraphic record of fluctuating energy levels (Figs 13A and  
29  
30 656 14A). The lateral flow movement may explain deviation in palaeoflow direction between intra-bed  
31  
32 657 ripple-laminated intervals compared to sediment wave bed tops, observed within the Doornkloof  
33  
34 658 subunit B2 sediment waves (Figs 4A, 6F, 13 and 14), as it could represent (partial) flow deflection  
35  
36 659 affected by the evolving sediment wave morphology. Similar behaviour within a single unconfined  
37  
38 660 flow has been invoked in basin-floor settings of the Cloridorme Formation (Parkash, 1970; Parkash &  
39  
40 661 Middleton, 1970) and at levée settings of the Amazon Channel (Hiscott *et al.*, 1997). The 'hose  
41  
42 662 effect' would result in a composite depositional record as the core of the flow sporadically moves  
43  
44 663 laterally, repeatedly superimposing high energy conditions onto lower energy conditions, therefore  
45  
46 664 explaining the inconsistency in sediment wave wavelengths. With this spatial process, the locus of  
47  
48 665 deposition will move laterally whilst the waning flow can lead to deposition progressively migrating  
49  
50 666 upstream. The hose effect may explain how sediment waves are able to build upstream accreting  
51  
52 667 geobodies without being deposited under supercritical conditions. The mechanism also provides an  
53  
54 668 explanation for the range and spatial variability of the observed small-scale bedform structures (F3),  
55  
56  
57  
58  
59  
60

1  
2  
3 669 and for the similarities with small-scale bedforms interpreted to have been formed by turbidity  
4  
5 670 currents interacting with topography (Tinterri, 2011; Tinterri & Muzzi Magalhaes, 2011). As the flow  
6  
7 671 migrates laterally, flows will interact at an angle with the growing sediment wave, thus encouraging  
8  
9 672 interaction of incident and reflected flow.

10  
11 673 As noted earlier, there is strong field-evidence (Parkash, 1970; Parkash & Middleton, 1970; Hiscott *et*  
12  
13 674 *al.*, 1997) for the 'hose effect' mechanism. However, the hose effect has not been experimentally or  
14  
15 675 numerically modelled, which reflects the ubiquity of bedform experiments in two-dimensional  
16  
17 676 flumes, and a paucity of three-dimensional flow effects on bedform development.

18  
19  
20 677 *Spatio-temporal flow fluctuations - summary*

21  
22  
23 678 In summary, the combination of waxing and waning flow behaviour in the subcritical flow core,  
24  
25 679 downstream of a zone of hydraulic jumps (Dorrell *et al.*, 2016), as well as spatial compensational  
26  
27 680 processes (hose effect) are invoked as the most probable mechanisms to explain the complicated  
28  
29 681 architecture and facies patterns of the Doornkloof sediment waves.

30  
31  
32 682

33  
34 683 **Spatial variations within a sediment wave field**

35  
36  
37 684 As noted earlier, there are major differences between the sediment waves at the Old Railway  
38  
39 685 outcrop with a low degree of spatial and temporal variability, and the high spatio-temporal  
40  
41 686 variability observed in the Doornkloof sediment waves. Here, we will attempt to explain such  
42  
43 687 variation between sediment waves in the same system. One potential mechanism is the character of  
44  
45 688 the feeder channel, including factors such as channel dimensions and magnitude of the incoming  
46  
47 689 flows. However, previous studies (Brunt *et al.*, 2013) suggest that the dimensions of feeder channels  
48  
49 690 within the Unit B base-of-slope system were similar, implying that the character of sediment waves  
50  
51 691 is unrelated to variations in feeder channel character.

52  
53  
54  
55  
56  
57  
58  
59  
60

1  
2  
3 692 Alternatively, the differences between the Doornkloof and Old Railway areas may be related to their  
4  
5 693 position relative to the mouth of the feeder channel. A dominance of lower flow-regime facies (F3)  
6  
7 694 such as climbing ripple-lamination is commonly associated with overbank or off-axis environments  
8  
9 695 (e.g. Kane & Hodgson, 2011; Brunt *et al.*, 2013; Rotzien *et al.*, 2014). As the Old Railway is  
10  
11 696 characterised by such facies, it could represent a fringe position through a sediment wave field (Fig.  
12  
13 697 15). In contrast, the Doornkloof section is characterized by erosion and more energetic facies (F1, F2,  
14  
15 698 F4), suggesting it was situated in a more axial position in the sediment wave field (Fig. 15A).  
16  
17 699 Furthermore, within the Doornkloof area, climbing ripple deposition (F3) becomes more dominant at  
18  
19 700 the top of the beds, likely reflecting progressive decrease in flow velocity and concentration (Figs 5,  
20  
21 701 8 and 9B). These spatial and temporal variations can be integrated with the hypothesised lateral  
22  
23 702 shifting of the flow core (the hose effect). The hose effect is likely to have more influence on  
24  
25 703 deposits within axial parts of the channel-mouth, such as within the Doornkloof area, where the flow  
26  
27 704 is most powerful. In contrast, the lateral fringes of the channel-mouth are most likely subject to  
28  
29 705 deposition from flow margins (Fig. 15B), such as at the Old Railway section. This results in more  
30  
31 706 steady flow conditions and relatively uniform deposition of facies and explains the difference in  
32  
33 707 characteristics between the Old Railway sediment waves, which are dominated by F3 facies and  
34  
35 708 shows little evidence of erosion, and the Doornkloof sediment waves, which are dominated by F1  
36  
37 709 and F2 facies with substantial evidence of erosion.  
38  
39  
40  
41 710 The differences in the expression of the Unit B sediment waves suggest that the stratigraphic record  
42  
43 711 of CLTZ environments exhibit substantial spatial variability. The process model shows that initial  
44  
45 712 sediment wave architecture can involve both upstream orientated accretion (Doornkloof area), and  
46  
47 713 downstream orientated accretion (Old Railway section), depending on the position with respect to  
48  
49 714 the channel mouth. Despite the lack of 3D control on morphology, we predict that this variance in  
50  
51 715 depositional behaviour between axial and fringe areas will have influence on planform crest  
52  
53 716 morphology and will lead to the crest curvatures, which are commonly observed within the modern  
54  
55 717 seafloor (e.g. Wynn *et al.*, 2002b). Similar observations on the importance of spatial variation have  
56  
57  
58  
59  
60

1  
2  
3 718 been made for the erosional bedform area (Fig. 15) of channel lobe transition zones (Hofstra *et al.*,  
4  
5 719 2015).

6  
7 720

8  
9  
10 721 **Preservation of sediment waves in channel lobe transition zones**

11  
12 722 Two questions that remain unanswered are: 1) what conditions promoted stratigraphic preservation  
13  
14 723 of the sediment waves in the examples herein, and 2) how likely is preservation of sediment waves  
15  
16 724 in the stratigraphic record of channel lobe transition zones? Here, we interpret that the preservation  
17  
18 725 of the sediment waves in the two field areas is related to the strongly aggradational character of  
19  
20 726 subunits B1 and B2. This is also evident from the lobe deposits downdip that show strong  
21  
22 727 aggradation and limited progradation (Fig. 3; Brunt *et al.*, 2013), in comparison to lobe deposits  
23  
24 728 elsewhere in the Karoo Basin (e.g., Hodgson *et al.*, 2006; van der Merwe *et al.*, 2014). Furthermore,  
25  
26 729 subunit B1 is abruptly overlain by a regional mudstone aiding preservation, whereas subunit B2 is  
27  
28 730 overlain by thick levée successions (subunit B3), marking the progradation of the slope system across  
29  
30 731 the CLTZ (Brunt *et al.*, 2013). This scenario has similarities to that proposed by Pemberton *et al.*  
31  
32 732 (2016) who suggested that preservation of scours in a CLTZ was linked to a rapidly prograding slope  
33  
34 733 system.

35  
36  
37  
38 734 For sediment waves in CLTZ settings in general, there are several scenarios that can be proposed to  
39  
40 735 facilitate their preservation. During system initiation at the start of a waxing-to-waning sediment  
41  
42 736 supply cycle, possibly driven by a relative sea-level fall and initial slope incision, the position of the  
43  
44 737 CLTZ on the base-of-slope might be relatively stable as slope conduits evolve prior to slope  
45  
46 738 progradation. The stratigraphic record of the resulting deposits is likely limited in thickness, and  
47  
48 739 probably preferentially associated with scour-fills (e.g., Pemberton *et al.*, 2016). The position of the  
49  
50 740 CLTZ could be fixed through physiographic features, such as a tectonic or diapiric break-in-slope,  
51  
52 741 which would aid the stratigraphic preservation of the CLTZ. Several studies have shown that when  
53  
54 742 submarine channel-levee systems avulse they do not return to their original route (e.g. Armitage *et*

55  
56  
57  
58  
59  
60

1  
2  
3 743 *al.*, 2012; Ortiz-Karpf *et al.*, 2015; Morris *et al.*, 2016), which would help to preserve sediment waves  
4  
5 744 in an abandoned CLTZ. The stratigraphic evidence for this control would be in the sediment waves  
6  
7 745 abruptly overlain by mudstone or thin-bedded successions indicative of overbank deposition. Finally,  
8  
9 746 the preservation potential of sediment waves in CLTZs will be higher at the point of maximum  
10  
11 747 regression/progradation of the system (Hodgson *et al.*, 2016). Similar arguments were applied to the  
12  
13 748 preservation of scour-fills in CLTZ by Hofstra *et al.* (2015).

14  
15  
16 749 In summary, we hypothesise that preservation of sediment waves may require i) updip avulsion, ii)  
17  
18 750 represent the point of maximum system progradation, or iii) form during a period of relative spatial  
19  
20 751 stability, followed by system progradation. Subsequent rapid progradation of a slope system is then  
21  
22 752 important for long-term preservation, though an off-axis location relative to large-scale slope  
23  
24 753 channels is critical in order to avoid cannibalisation of the CLTZ deposits (e.g., Hofstra *et al.*, 2015).  
25  
26 754 Such propagation of channel-levée systems (e.g. Hodgson *et al.*, 2016), suggests that the  
27  
28 755 preservation potential of sediment waves in axial positions, for example the interpreted position of  
29  
30 756 the Doornkloof section, is lower than sediment wave deposits in fringe positions, such as the  
31  
32 757 interpreted position of the Old Railway section (Fig. 15A).

33  
34  
35 758

## 36 37 38 759 **CONCLUSIONS**

39  
40 760 Detailed morphologies, architectures and facies of fine-sand grained sediment waves are reported  
41  
42 761 from an ancient channel-lobe transition zone. The sediment waves are constructed from banded and  
43  
44 762 planar-laminated sandstones, as well as from progressive aggradation of a range of small-scale  
45  
46 763 bedforms, including climbing ripples, sinusoidal lamination, biconvex ripples, and hummocky-like  
47  
48 764 structures, interpreted as the products of subcritical deposition, with periods of flow reflection and  
49  
50 765 deflection forming the biconvex ripples and hummocks. Morphologically, the sediment waves  
51  
52 766 exhibit long-lee sides, and short erosively-cut stoss sides, and show upstream accretion over short  
53  
54 767 distances (m's to tens of m's), punctuated by the upstream development of new sediment wave  
55  
56  
57  
58  
59  
60



1  
2  
3 768 lenses. Consequently, the observations from these exhumed deposits challenge some current  
4  
5 769 models of sediment wave development, which suggest that entire sediment waves continuously  
6  
7 770 migrate upstream under supercritical conditions. In particular, the outcrops demonstrate that the  
8  
9 771 formation of sediment waves in an upstream direction, as well as upstream migration of crestlines, is  
10  
11 772 not solely the product of supercritical flows, but can also occur in subcritical conditions. The  
12  
13 773 progressive development of the sediment waves is argued to be the product of lateral migration of  
14  
15 774 the expanding flow across the channel-lobe transition zone, potentially coupled to fluctuations in  
16  
17 775 velocity and flow capacity related to upstream hydraulic jumps. Variations in sediment waves, from  
18  
19 776 more complex forms with multiple erosive surfaces and complex internal facies, to simple  
20  
21 777 accretionary forms with abundant climbing ripples, is linked to position across the channel-lobe  
22  
23 778 transition zone, from axial to lateral fringes respectively. The preservation potential of sediment  
24  
25 779 waves in CLTZs into the stratigraphic record is low due to subsequent system progradation and  
26  
27 780 erosion. However, preservation is higher where there is updip avulsion and abandonment of a CLTZ,  
28  
29 781 in off axis areas where sediment waves might be overlain by overbank sediments, and / or at the  
30  
31 782 point of maximum system progradation.  
32  
33  
34  
35  
36  
37  
38  
39  
40  
41  
42  
43  
44  
45  
46  
47  
48  
49  
50  
51  
52  
53  
54  
55  
56  
57  
58  
59  
60

1  
2  
3  
4  
5  
6  
7  
8  
9  
10  
11  
12  
13  
14  
15  
16  
17  
18  
19  
20  
21  
22  
23  
24  
25  
26  
27  
28  
29  
30  
31  
32  
33  
34  
35  
36  
37  
38  
39  
40  
41  
42  
43  
44  
45  
46  
47  
48  
49  
50  
51  
52  
53  
54  
55  
56  
57  
58  
59  
60

783 **ACKNOWLEDGEMENTS**

784 This work forms part of the results of the LOBE 2 joint industry consortium research project. We are  
785 grateful for the financial support from: Anadarko, Bayerngas Norge, BG Group, BHP Billiton, BP,  
786 Chevron, Dong Energy, E.ON, GDF Suez, Maersk Oil, Marathon Oil, Petrobras, Shell, Statoil, Total,  
787 VNG Norge, and Woodside. We are grateful to Matthieu Cartigny, Brian Romans and an anonymous  
788 reviewer for the constructive reviews and for the input of Associate Editor Jaco Baas, which greatly  
789 improved this manuscript. We also acknowledge the landowners from the Laingsburg area for access  
790 to their land. Finally, Renée de Bruijn, Nienke Lips and Yvonne Sychala are thanked for their  
791 assistance in the field.

792 **REFERENCES**

- 793 **Alexander, J., Bridge, J.S., Cheel, R.J. and Leclair, S.F.** (2001) Bedforms and associated sedimentary  
794 structures formed under supercritical water flows over aggrading sand beds. *Sedimentology*, **48**,  
795 133-152.
- 796 **Allen, J.R.L.** (1973) A classification of climbing-ripple cross-lamination. *Journal of the Geological*  
797 *Society of London*, **129**, 537-541.
- 798 **Allen, J.R.L.** (1984) Parallel lamination developed from upper-stage plane beds: a model based on  
799 the larger coherent structures of the turbulent boundary layer. *Sedimentary Geology*, **39**, 227-242.
- 800 **Armitage, D.A., McHargue, T., Fildani, A. and Graham, S.A.** (2012) Postavulsion channel evolution:  
801 Niger Delta continental slope. *AAPG Bulletin*, **96**, 823-843.
- 802 **Baas, J.H. and de Koning, H.** (1995) Washed-out ripples: Their equilibrium dimensions, migration  
803 rate, and relation to suspended-sediment concentration in very fine sand. *Journal of Sedimentary*  
804 *Research*, **65**, 431-435.
- 805 **Baas, J.H., Davies, A.G. and Malarkey, J.** (2013) Bedform development in mixed sand-mud: The  
806 contrasting role of cohesive forces in flow and bed. *Geomorphology*, **182**, 19-32.
- 807 **Baas, J.H., Best, J.L. and Peakall, J.** (2016) Predicting bedforms and primary current stratification in  
808 cohesive mixtures of mud and sand. *Journal of the Geological Society*, **173**, 12-45.
- 809 **Best, J. and Bridge, J.** (1992) The morphology and dynamics of low amplitude bedwaves upon upper  
810 stage plane beds and the preservation of planar laminae. *Sedimentology*, **39**, 737-752.
- 811 **Bouma, A.H. and Boerma, J.A.K.** (1968) Vertical disturbances in piston cores. *Marine Geology*, **6**,  
812 231-241.

- 1  
2  
3 813 **Brunt, R.L., Hodgson, D.M., Flint, S.S., Pringle, J.K., Di Celma, C., Prélat, A. and Grecula, M.** (2013)  
4  
5 814 Confined to unconfined: Anatomy of a base of slope succession, Karoo Basin, South Africa. *Marine*  
6  
7 815 *and Petroleum Geology*, **41**, 206-221.  
8  
9 816 **Campion, K.T., Dixon, B.T. and Scott, E.D.** (2011) Sediment waves and depositional implications for  
10  
11 817 fine-grained rocks in the Cerro Toro Formation (Upper Cretaceous), Silla Syncline, Chile. *Marine and*  
12  
13 818 *Petroleum Geology*, **28**, 761-784.  
14  
15  
16 819 **Cartigny, M.J., Eggenhuisen, J.T., Hansen, E.W. and Postma, G.** (2013) Concentration-dependent  
17  
18 820 flow stratification in experimental high-density turbidity currents and their relevance to turbidite  
19  
20 821 facies models. *Journal of Sedimentary Research*, **83**, 1047-1065.  
21  
22  
23 822 **Cartigny, M.J.B., Ventra, D., Postma, G. and Van Den Berg, J.H.** (2014) Morphodynamics and  
24  
25 823 sedimentary structures of bedforms under supercritical-flow conditions: New insights from flume  
26  
27 824 experiments. *Sedimentology*, **61**, 712-748.  
28  
29  
30 825 **Choi, S.U. and Garcia, M.H.** (2001) Spreading of gravity plumes on an incline. *Coastal Engineering*  
31  
32 826 *Journal*, **43**, 221-237.  
33  
34  
35 827 **Covault, J.A., Kostic, S., Paull, C.K., Sylvester, Z. and Fildani, A.** (2017) Cyclic steps and related  
36  
37 828 supercritical bedforms: Building blocks of deep-water depositional systems, western North America.  
38  
39 829 *Marine Geology*, **393**, 4-20, doi:10.1016/j.margeo.2016.12.009  
40  
41  
42 830 **Damuth, J.E.** (1979) Migrating sediment waves created by turbidite currents in northern South China  
43  
44 831 Basin. *Geology*, **7**, 520-523.  
45  
46 832 **Dorrell, R.M., Peakall, J., Sumner, E.J., Parsons, D.R., Darby, S.E., Wynn, R.B., Özsoy, E. and Tezcan,**  
47  
48 833 **D.** (2016) Flow dynamics and mixing processes in hydraulic jump arrays: Implications for channel-  
49  
50 834 lobe transition zones. *Marine Geology*, **381**, 181-193.  
51  
52  
53  
54  
55  
56  
57  
58  
59  
60

- 1  
2  
3 835 **Dumas, S. and Arnott, R.W.C.** (2006) Origin of hummocky and swaley cross-stratification— The  
4  
5 836 controlling influence of unidirectional current strength and aggradation rate. *Geology*, **34**, 1073-  
6  
7 837 1076.  
8  
9  
10 838 **Dumas, S., Arnott, R.W.C. and Southard, J.B.** (2005) Experiments on oscillatory-flow and combined-  
11  
12 839 flow bed forms: Implications for interpreting parts of the shallow-marine sedimentary record.  
13  
14 840 *Journal of Sedimentary Research*, **75**, 501-513.  
15  
16  
17 841 **Eggenhuisen, J.T., McCaffrey, W.D., Haughton, P.D. and Butler, R.W.** (2011) Shallow erosion  
18  
19 842 beneath turbidity currents and its impact on the architectural development of turbidite sheet  
20  
21 843 systems. *Sedimentology*, **58**, 936-959.  
22  
23  
24 844 **Fedele, J.J., Hoyal, D., Barnaal, Z., Tulenko, J. and Awatt, S.** (2017) Bedforms created by gravity  
25  
26 845 flows. In: Budd, D.A., Hajek, E.A. and Purkis, S.J. (Eds) *Autogenic Dynamics and Self-organization in*  
27  
28 846 *Sedimentary Systems*. SEPM Special Publication 106, 95-121.  
29  
30  
31 847 **Felix, M., Sturton, S. and Peakall, J.** (2005) Combined measurements of velocity and concentration  
32  
33 848 in experimental turbidity currents. *Sedimentary Geology*, **179**, 31-47.  
34  
35  
36 849 **Flint, S.S., Hodgson, D.M., Sprague, A., Brunt, R.L., Van Der Merwe, W.C., Figueiredo, J., Prélat, A.,**  
37  
38 850 **Box, D., Di Celma, C. and Kavanagh, J.P.** (2011) Depositional architecture and sequence stratigraphy  
39  
40 851 of the Karoo basin floor to shelf edge succession, Laingsburg depocentre, South Africa. *Marine and*  
41  
42 852 *Petroleum Geology*, **28**, 658-674.  
43  
44  
45 853 **Garcia, M.H.** (1993) Hydraulic jumps in sediment-driven bottom currents. *Journal of Hydraulic*  
46  
47 854 *Engineering*, **119**, 1094-1117.  
48  
49  
50 855 **Garcia, M.H.** (2008) *Sedimentation Engineering: Process, Measurements, Modeling and Practice*.  
51  
52 856 American Society of Civil Engineers, Reston, Virginia.  
53  
54  
55  
56  
57  
58  
59  
60

- 1  
2  
3 857 **Grechula, M., Flint, S.S., Wickens, H.DeV. and Johnson, S.D.** (2003) Upward-thickening patterns and  
4  
5 858 lateral continuity of Permian sand-rich turbidite channel fills, Laingsburg Karoo, South Africa.  
6  
7 859 *Sedimentology*, **50**, 831-853.  
8  
9  
10 860 **Groenenberg, R.M., Hodgson, D.M., Pr lat, A., Luthi, S.M. and Flint, S.S.** (2010) Flow-deposit  
11  
12 861 interaction in submarine lobes: insights from outcrop observations and realizations of a process-  
13  
14 862 based numerical model. *Journal of Sedimentary Research*, **80**, 252-267.  
15  
16  
17 863 **Hamilton, P., Gaillot, G., Strom, K., Fedele, J. and Hoyal, D.** (2017) Linking hydraulic properties in  
18  
19 864 supercritical submarine distributary channels to depositional lobe geometry. *Journal of Sedimentary*  
20  
21 865 *Research*, **87**, 935-950.  
22  
23  
24 866 **Harms, J.C.** (1969) Hydraulic significance of some sand ripples. *Geological Society of America*  
25  
26 867 *Bulletin*, **80**, 363-396.  
27  
28  
29 868 **Harms, J.C., Southard, J.B., Spearing, D.R. and Walker, R.G.** (1975) *Depositional environments as*  
30  
31 869 *interpreted from primary sedimentary structures and stratification sequences*. Society for  
32  
33 870 Sedimentary Geology (SEPM) Short Course 2, pp. 161.  
34  
35  
36 871 **Haughton, P., Davis, C., McCaffrey, W. and Barker, S.** (2009) Hybrid sediment gravity flow deposits-  
37  
38 872 classification, origin and significance. *Marine and Petroleum Geology*, **26**, 1900-1918.  
39  
40  
41 873 **Heini , P. and Davies R.J.** (2009) Trails of depressions and sediment waves along submarine  
42  
43 874 channels on the continental margin of Espirito Santo Basin, Brazil. *Geological Society of America*  
44  
45 875 *Bulletin*, **121**, 698-711.  
46  
47  
48 876 **Hiscott, R.N.** (1994a) Loss of capacity, not competence, as the fundamental process governing  
49  
50 877 deposition from turbidity currents. *Journal of Sedimentary Research*, **64**, 209-214.  
51  
52  
53 878 **Hiscott, R.N.** (1994b) Traction-carpet stratification in turbidites-fact or fiction? *Journal of*  
54  
55 879 *Sedimentary Research*, **64**, 204-208.  
56  
57  
58  
59  
60

- 1  
2  
3 880 **Hiscott, R.N., Hall, F.R., and Pirmez, C.** (1997) Turbidity-current overspill from the Amazon Channel:  
4  
5 881 texture of the silt/sand load, paleoflow from anisotropy of magnetic susceptibility, and implications  
6  
7 882 for flow processes. In: *Proceedings of the Ocean Drilling Program, Scientific Results* (Eds. Flood, R.D.,  
8  
9 883 Piper, D.J.W., Klaus, A. and Peterson, I.C.), **155**, 53-78.
- 10  
11 884 **Hodgson, D.M., Flint, S.S., Hodgetts, D., Drinkwater, N.J., Johannessen, E.P. and Luthi, S.M.** (2006)  
12  
13 885 Stratigraphic evolution of fine-grained submarine fan systems, Tanqua depocenter, Karoo Basin,  
14  
15 886 South Africa. *Journal of Sedimentary Research*, **76**, 20-40.
- 16  
17  
18 887 **Hodgson, D.M., Di Celma, C.N., Brunt, R.L. and Flint, S.S.** (2011) Submarine slope degradation and  
19  
20 888 aggradation and the stratigraphic evolution of channel-levee systems. *Journal of the Geological*  
21  
22 889 *Society*, **168**, 625-628.
- 23  
24  
25 890 **Hodgson, D.M., Kane, I.A., Flint, S.S., Brunt, R.L. and Ortiz-Karpf, A.** (2016). Time-transgressive  
26  
27 891 confinement on the slope and the progradation of basin-floor fans: Implications for the sequence  
28  
29 892 stratigraphy of deep-water deposits. *Journal of Sedimentary Research*, **86**, 73-86.
- 30  
31  
32 893 **Hofstra, M.** (2016) The Stratigraphic Record of Submarine Channel-lobe Transition Zones.  
33  
34 894 Unpublished PhD thesis, University of Leeds, Leeds, 331p.
- 35  
36  
37 895 **Hofstra, M., Hodgson, D.M., Peakall, J. and Flint, S.S.** (2015) Giant scour-fills in ancient channel-lobe  
38  
39 896 transition zones: Formative processes and depositional architecture. *Sedimentary Geology*, **329**, 98-  
40  
41 897 114.
- 42  
43  
44 898 **Howe, J.A.** (1996) Turbidite and contourite sediment waves in the northern Rockall Trough, North  
45  
46 899 Atlantic Ocean. *Sedimentology*, **43**, 219-234.
- 47  
48 900 **Hughes Clarke, J.E.** (2016) First wide-angle view of channelized turbidity currents links migrating  
49  
50 901 cyclic steps to flow characteristics. *Nature Communications*, 7:11896, doi: 10.1038/ncomms11896.  
51  
52  
53  
54  
55  
56  
57  
58  
59  
60

- 1  
2  
3 902 **Ito, M.** (2008) Downfan transformation from turbidity currents to debris flows at a channel-to-lobe  
4  
5 903 transitional zone: the lower Pleistocene Otadai Formation, Boso Peninsula, Japan. *Journal of*  
6  
7 904 *Sedimentary Research*, **78**, 668-682.
- 8  
9 905 **Ito, M.** (2010) Are coarse-grained sediment waves formed as downstream-migrating antidunes?  
10  
11 906 Insight from an early Pleistocene submarine canyon on the Boso Peninsula, Japan. *Sedimentary*  
12  
13 907 *Geology*, **226**, 1-8.
- 14  
15  
16 908 **Ito, M.** and **Saito, T.** (2006) Gravel waves in an ancient canyon: Analogous features and formative  
17  
18 909 processes of coarse-grained bedforms in a submarine-fan system, the lower Pleistocene of the Boso  
19  
20 910 Peninsula, Japan. *Journal of Sedimentary Research*, **76**, 1274-1283.
- 21  
22  
23 911 **Ito, M., Ishikawa, K.** and **Nishida, N.** (2014) Distinctive erosional and depositional structures formed  
24  
25 912 at a canyon mouth: A lower Pleistocene deep-water succession in the Kasuza forearc basin on the  
26  
27 913 Boso Peninsula, Japan. *Sedimentology*, **61**, 2042-2062.
- 28  
29  
30 914 **Jobe, Z.R., Lowe, D.R.** and **Morris, W.R.** (2012) Climbing-ripple successions in turbidite systems:  
31  
32 915 depositional environments, sedimentation rates and accumulation times. *Sedimentology*, **59**, 867-  
33  
34 916 898.
- 35  
36  
37 917 **Johansson, M.** and **Stow, D.A.V.** (1995) A classification scheme for shale clasts in deep water  
38  
39 918 sandstones. In: Hartley, A.J. and Prosser, D.J. (eds.) *Characterization of Deep Marine Clastic Systems*,  
40  
41 919 Geological Society Special Publication 94, 221-241.
- 42  
43  
44 920 **Jopling, A.V.** and **Walker, R.G.** (1968) Morphology and origin of ripple-drift cross-lamination, with  
45  
46 921 examples from the Pleistocene of Massachusetts. *Journal of Sedimentary Research*, **38**, 971-984.
- 47  
48  
49 922 **Kane, I.A.** and **Hodgson, D.M.** (2011) Sedimentological criteria to differentiate submarine channel  
50  
51 923 levee subenvironments: exhumed examples from the Rosario Fm. (Upper Cretaceous) of Baja  
52  
53 924 California, Mexico, and the Fort Brown Fm. (Permian), Karoo basin, S. Africa. *Marine and Petroleum*  
54  
55 925 *Geology*, **28**, 807-823.
- 56  
57  
58  
59  
60



- 1  
2  
3 926 **Kane, I.A., McCaffrey, W.D. and Martinsen, O.J.** (2009) Allogenic vs. autogenic controls on  
4  
5 927 megaflute formation. *Journal of Sedimentary Research*, **79**, 643-651.  
6  
7 928 **Kennedy, J.F.** (1969) The formation of sediment ripples, dunes and antidunes. *Annual Review of*  
8  
9 929 *Fluid Mechanics*, **1**, 147-168.  
10  
11  
12 930 **Kidd, R.B., Lucchi, R.G., Gee, M. and Woodside, J.M.** (1998) Sedimentary processes in the Stromboli  
13  
14 931 Canyon and Marsili Basin, SE Tyrrhenian Sea: results from side-scan sonar surveys. *Geo-Marine*  
15  
16 932 *Letters*, **18**, 146-154.  
17  
18  
19 933 **Kneller, B.** (1995) Beyond the turbidite paradigm: physical models for deposition of turbidites and  
20  
21 934 their implications for reservoir prediction. In: *Characterization of Deep Marine Clastic Systems* (Eds.  
22  
23 935 Hartley, A.J. and Prosser, D.J.) *Geol. Soc. London, Spec. Publ.*, **94**, 31-49.  
24  
25  
26 936 **Kneller, B.C. and Branney, M.J.** (1995) Sustained high-density turbidity currents and the deposition  
27  
28 937 of thick massive sands. *Sedimentology*, **42**, 607-616.  
29  
30  
31 938 **Kneller, B.C. and McCaffrey, W.D.** (1999) Depositional effects of flow nonuniformity and  
32  
33 939 stratification within turbidity currents approaching a bounding slope: deflection, reflection, and  
34  
35 940 facies variation. *Journal of Sedimentary Research*, **69**, 980-991.  
36  
37  
38 941 **Kneller, B.C. and McCaffrey, W.D.** (2003) The interpretation of vertical sequences in turbidite beds:  
39  
40 942 the influence of longitudinal flow structure. *Journal of Sedimentary Research*, **73**, 706-713.  
41  
42  
43 943 **Kubo, Y.** (2004) Experimental and numerical study of topographic effects on deposition from two-  
44  
45 944 dimensional, particulate-driven density currents. *Sedimentary Geology*, **164**, 311-326.  
46  
47  
48 945 **Kubo, Y. and Nakajima, T.** (2002) Laboratory experiments and numerical simulation of sediment-  
49  
50 946 wave formation by turbidity currents. *Marine Geology*, **192**, 105-121.  
51  
52  
53 947 **Lonsdale, P. and Hollister, C.D.** (1979) Near-bottom traverse of Rockall Trough-Hydrographic and  
54  
55 948 geological inferences. *Oceanologica Acta*, **2**, 91-105.  
56  
57  
58  
59  
60

- 1  
2  
3 949 **Lowe, D.R.** (1982) Sediment gravity flows: II Depositional models with special reference to the  
4  
5 950 deposits of high-density turbidity currents. *Journal of Sedimentary Research*, **52**, 279-297.  
6  
7 951 **Macdonald, H.A., Wynn, R.B., Huvenne, V.A., Peakall, J., Masson, D.G., Weaver, P.P. and McPhail,**  
8  
9 952 **S.D.** (2011) New insights into the morphology, fill, and remarkable longevity (>0.2 m.y.) of modern  
10  
11 953 deep-water erosional scours along the northeast Atlantic margin. *Geosphere*, **7**, 845-867.  
12  
13  
14 954 **Malinverno, A., Ryan, W.B., Auffret, G. and Pautot, G.** (1988) Sonar images of the path of recent  
15  
16 955 failure events on the continental margin off Nice, France. In: *Sedimentological Consequences of*  
17  
18 956 *Convulsive Geologic Events*, (Ed. Clifton, H.E.), *Geological Society of America Special Paper*, **229**, 59-  
19  
20 957 76.  
21  
22  
23 958 **McHugh, C.M. and Ryan, W.B.** (2000) Sedimentary features associated with channel overbank flow:  
24  
25 959 examples from the Monterey Fan. *Marine Geology*, **163**, 199-215.  
26  
27  
28 960 **Migeon, S., Savoye, B., Zanella, E., Mulder, T., Faugères, J.C. and Weber, O.** (2001) Detailed seismic-  
29  
30 961 reflection and sedimentary study of turbidite waves on the Var Sedimentary Ridge (SE France):  
31  
32 962 significance for sediment transport and deposition and for the mechanisms of sediment-wave  
33  
34 963 construction. *Marine and Petroleum Geology*, **18**, 179-208.  
35  
36  
37 964 **Morris, S.A., Kenyon, N.H., Limonov, A.F. and Alexander, J.** (1998) Downstream changes of large-  
38  
39 965 scale bedforms in turbidites around the Valencia channel mouth, north-west Mediterranean:  
40  
41 966 implications for palaeoflow reconstruction. *Sedimentology*, **45**, 365-377.  
42  
43  
44 967 **Morris, E.A., Hodgson, D.M., Brunt, R.L. and Flint, S.S.** (2014) Origin, evolution and anatomy of silt-  
45  
46 968 prone submarine external levées. *Sedimentology*, **61**, 1734-1763.  
47  
48  
49 969 **Morris, E.A., Hodgson, D.M., Flint, S., Brunt, R.L., Luthi, S.M. and Kolenberg, Y.** (2016) Integrating  
50  
51 970 outcrop and subsurface data to assess the temporal evolution of a submarine channel–levee system.  
52  
53 971 *AAPG Bulletin*, **100**, 1663-1691.  
54  
55  
56  
57  
58  
59  
60

- 1  
2  
3 972 **Mulder, T. and Alexander, J.** (2001) The physical character of subaqueous sedimentary density flows  
4  
5 973 and their deposits. *Sedimentology*, **48**, 269-299.  
6  
7 974 **Mukti, M.M.R. and Ito, M.** (2010) Discovery of outcrop-scale fine-grained sediment waves in the  
8  
9 975 lower Halang Formation, an upper Miocene submarine-fan succession in West Java. *Sedimentary*  
10  
11 976 *Geology*, **231**, 55-62.  
12  
13  
14 977 **Mutti, E. and Normark, W.R.** (1987) Comparing examples of modern and ancient turbidite systems:  
15  
16 978 problems and concepts. In: *Marine Clastic Sedimentology: Concepts and Case Studies* (Eds. Leggett,  
17  
18 979 J.K. and Zuffa, G.G.) *Graham and Trotman, Oxford*, pp. 1-38.  
19  
20  
21 980 **Mutti, E. and Normark, W.R.** (1991) An integrated approach to the study of turbidite systems. In:  
22  
23 981 *Seismic Facies and Sedimentary Processes of Submarine Fans and Turbidite Systems* (Eds. Weimer, P.  
24  
25 982 and Link, M.H.) *Springer, New York*, pp. 75-106.  
26  
27  
28 983 **Nakajima, T., Satoh, M. and Okamura, Y.** (1998) Channel-levee complexes, terminal deep-sea fan  
29  
30 984 and sediment wave fields associated with the Toyama Deep-Sea Channel system in the Japan Sea.  
31  
32 985 *Marine Geology*, **147**, 25-41.  
33  
34  
35 986 **Normark, W.R. and Dickson, F.H.** (1976) Sublacustrine fan morphology in Lake Superior. *AAPG*  
36  
37 987 *Bulletin*, **60**, 1021-1036.  
38  
39  
40 988 **Normark, W.R. and Piper, D.J.W.** (1991) Initiation processes and flow evolution of turbidity currents:  
41  
42 989 Implications for the depositional record. In: *From Shoreline to Abyss: Contributions in Marine*  
43  
44 990 *Geology in Honor of Francis Parker Shepard* (Ed. Osborne, R.H.), *SEPM Special Publication*, **46**, 207-  
45  
46 991 230.  
47  
48 992 **Normark W.R., Hess, G.R., Stow, D.A.V. and Bowen, A.J.** (1980) Sediment waves on the Monterey  
49  
50 993 Fan levee: a preliminary physical interpretation. *Marine Geology*, **37**, 1-18.  
51  
52  
53 994 **Normark, W.R., Piper, D.J., Posamentier, H. Pirmez, C. and Migeon, S.** (2002) Variability in form and  
54  
55 995 growth of sediment waves on turbidite channel levees. *Marine Geology*, **192**, 23-58.  
56  
57  
58  
59  
60

- 1  
2  
3 996 **Ortiz-Karpp, A., Hodgson, D.M. and McCaffrey, W.D.** (2015) The role of mass-transport complexes in  
4  
5 997 controlling channel avulsion and the subsequent sediment dispersal patterns on an active margin:  
6  
7 998 the Magdalena Fan, offshore Colombia. *Marine and Petroleum Geology*, **64**, 58-75.  
8  
9 999 **Palanques, A., Kenyon, N.H., Alonso, B. and Limonov, A.** (1995) Erosional and depositional patterns  
10  
11 1000 in the Valencia mouth: An example of a modern channel-lobe transition zone channel. *Marine*  
12  
13 1001 *Geophysical Researches*, **17**, 503-517.  
14  
15  
16 1002 **Parkash, B.** (1970) Downcurrent changes in sedimentary structures in Ordovician turbidite  
17  
18 1003 greywackes. *Journal of Sedimentary Research*, **40**, 572-590.  
19  
20  
21 1004 **Parkash, B. and Middleton, G.V.** (1970) Downcurrent textural changes in Ordovician turbidite  
22  
23 1005 greywackes. *Sedimentology*, **14**, 259-293.  
24  
25  
26 1006 **Peakall, J., McCaffrey, W.D. and Kneller, B.C.** (2000) A process model for the evolution, morphology,  
27  
28 1007 and architecture of sinuous submarine channels. *Journal of Sedimentary Research*, **70**, 434-448.  
29  
30  
31 1008 **Pemberton, E.A.L., Hubbard, S.M., Fildani, A., Romans, B. and Stright, L.** (2016) The stratigraphic  
32  
33 1009 expression of decreasing confinement along a deep-water sediment routing system: Outcrop  
34  
35 1010 example from southern Chile. *Geosphere*, **12**, 114-134.  
36  
37  
38 1011 **Piper, D.J.W. and Kontopoulos, N.** (1994) Bed forms in submarine channels: comparison of ancient  
39  
40 1012 examples from Greece with studies of Recent turbidite systems. *Journal of Sedimentary Research*,  
41  
42 1013 **64**, 247-252.  
43  
44  
45 1014 **Piper, D.J.W., Shor, A.N., Farre, J.A., O'Connell, S. and Jacobi, R.** (1985) Sediment slides and  
46  
47 1015 turbidity currents on the Laurentian Fan: Sidescan sonar investigations near the epicenter of the  
48  
49 1016 1929 Grand Banks earthquake. *Geology*, **13**, 538-541.  
50  
51  
52 1017 **Ponce, J.J. and Carmona, N.** (2011) Coarse-grained sediment waves in hyperpycnal clinoform  
53  
54 1018 systems, Miocene of the Austral foreland basin, Argentina. *Geology*, **39**, 763-766.  
55  
56  
57  
58  
59  
60

- 1  
2  
3 1019 **Postma, G., Kleverlaan, K. and Cartigny, M.J.B.** (2014) Recognition of cyclic steps in sandy and  
4  
5 1020 gravelly turbidite sequences and consequences for the Bouma facies. *Sedimentology*, **61**, 2268-2290.  
6  
7 1021 **Praeg, D.B. and Schafer, C.T.** (1989) Seabed features of the Labrador slope and rise near 55° N  
8  
9 1022 revealed by SEAMARC I sidescan sonar imagery. *Atlantic Geoscience Centre, Bedford Institute of*  
10  
11 1023 *Oceanography*.  
12  
13  
14 1024 **Prave, A.R. and Duke, W.L.** (1990) Small-scale hummocky cross-stratification in turbidites: a form of  
15  
16 1025 antidune stratification? *Sedimentology*, **37**, 531-539.  
17  
18  
19 1026 **Prélat, A. and Hodgson, D.M.** (2013) The full range of turbidite bed thickness patterns in submarine  
20  
21 1027 lobes: controls and implications. *Journal of the Geological Society*, **170**, 209-214.  
22  
23  
24 1028 **Prélat, A., Hodgson D.M. and Flint, S.S.** (2009) Evolution, architecture and hierarchy of distributary  
25  
26 1029 deep-water deposits: a high-resolution outcrop investigation from the Permian Karoo Basin, South  
27  
28 1030 Africa. *Sedimentology*, **56**, 2132-2154.  
29  
30  
31 1031 **Prélat, A., Covault J.A., Hodgson D.M., Fildani, A. and Flint, S.S.** (2010) Intrinsic controls on the  
32  
33 1032 range of volumes, morphologies, and dimensions of submarine lobes. *Sedimentary Geology*, **232**, 66-  
34  
35 1033 76.  
36  
37 1034 **Pringle, J.K., Brunt, R.L., Hodgson, D.M. and Flint, S.S.** (2010) Capturing stratigraphic and  
38  
39 1035 sedimentological complexity from submarine channel complex outcrops to digital 3D models, Karoo  
40  
41 1036 Basin, South Africa. *Petroleum Geoscience*, **16**, 307-330.  
42  
43  
44 1037 **Raudkivi, A.J.** (1998) *Loose Boundary Hydraulics*. A.A. Balkema, Rotterdam, The Netherlands, pp 260.  
45  
46  
47 1038 **Rotzien, J.R., Lowe, D.R., King, P.R. and Browne, G.H.** (2014) Stratigraphic architecture and  
48  
49 1039 evolution of a deep-water slope channel-levee and overbank apron: The Upper Miocene Upper  
50  
51 1040 Mount Messenger Formation, Taranaki Basin. *Marine and Petroleum Geology*, **52**, 22-41.  
52  
53  
54 1041 **Schindler, R.J., Parsons, D.R., Ye, L., Hope, J.A., Baas, J.H., Peakall, J., Manning, A.J., Aspden, R.J.,**  
55  
56 1042 **Malarkey, J., Simmons, S., Paterson, D.M., Lichtman, I.D., Davies, A.G., Thorne, P.D. and Bass, S.J.**  
57  
58  
59  
60

- 1  
2  
3 1043 (2015) Sticky stuff: Redefining bedform prediction in modern and ancient environments. *Geology*,  
4  
5 1044 **43**, 399-402.  
6  
7 1045 **Schminke, H.U., Fisher, R.V. and Waters, A.C.** (1973) Antidune and chute and pool structures in the  
8  
9 1046 base surge deposits of the Laacher See area, Germany. *Sedimentology*, **20**, 553-574.  
10  
11  
12 1047 **Sixsmith, P., Flint, S.S., Wickens, H.D. and Johnson, S.** (2004) Anatomy and stratigraphic  
13  
14 1048 development of a basin floor turbidite system in the Laingsburg Formation, main Karoo Basin, South  
15  
16 1049 Africa. *Journal of Sedimentary Research*, **74**, 239-254.  
17  
18  
19 1050 **Skipper, K.**, (1971) Antidune cross-stratification in a turbidite sequence, Cloridorme Formation,  
20  
21 1051 Gaspé, Quebec. *Sedimentology*, **17**, 51-68.  
22  
23  
24 1052 **Sohn, Y.K.** (1997) On traction-carpet sedimentation. *Journal of Sedimentary Research*, **67**, 502-509.  
25  
26  
27 1053 **Southard, J.B.** (1991) Experimental determination of bed-form stability. *Annual Review of Earth and*  
28  
29 1054 *Planetary Sciences*, **19**, 423-455.  
30  
31 1055 **Southard, J.B. and Boguchwal, L.A.** (1990) Bed configurations in steady unidirectional water flows.  
32  
33 1056 Part 2. Synthesis of flume data. *Journal of Sedimentary Research*, **60**, 658-679.  
34  
35  
36 1057 **Stow, D.A. and Johansson, M.** (2000) Deep-water massive sands: nature, origin and hydrocarbon  
37  
38 1058 implications. *Marine and Petroleum Geology*, **17**, 145-174.  
39  
40  
41 1059 **Stevenson, C.J., Jackson, C.A-L., Hodgson, D.M., Hubbard, S.M. and Eggenhuisen, J.T.** (2015) Deep-  
42  
43 1060 water sediment bypass. *Journal of Sedimentary Research*, **85**, 1058-1081.  
44  
45  
46 1061 **Sumner, E.J., Amy, L.A. and Talling, P.J.** (2008) Deposit structure and processes of sand deposition  
47  
48 1062 from decelerating sediment suspensions. *Journal of Sedimentary Research*, **78**, 529-547.  
49  
50  
51 1063 **Sumner, E.J., Peakall, J., Parsons, D.R., Wynn, R.B., Darby, S.E., Dorrell, R.M., McPhail, S.D.,**  
52  
53 1064 **Perrett, J., Webb, A. and White, D.** (2013) First direct measurements of hydraulic jumps in an active  
54  
55 1065 submarine density current. *Geophysical Research Letters*, **40**, 5904-5908.  
56  
57  
58  
59  
60

- 1  
2  
3 1066 **Symons, W.O., Sumner, E.J., Talling, P.J., Cartigny, M.J. and Clare, M.A.** (2016) Large-scale sediment  
4  
5 1067 waves and scours on the modern seafloor and their implications for the prevalence of supercritical  
6  
7 1068 flows. *Marine Geology*, **371**, 130-148.
- 8  
9 1069 **Talling, P.J., Masson, D.G., Sumner, E.J. and Malgesini, G.** (2012) Subaqueous sediment density  
10  
11 1070 flows: Depositional processes and deposit types. *Sedimentology*, **59**, 1937-2003.
- 12  
13  
14 1071 **Tinterri, R.** (2011). Combined flow sedimentary structures and the genetic link between sigmoidal  
15  
16 1072 and hummocky cross-stratification. *GeoActa (Bologna)*, **10**, 1-43.
- 17  
18  
19 1073 **Tinterri, R. and Muzzi Magalhaes, P.** (2011) Synsedimentary structural control on foredeep  
20  
21 1074 turbidites: An example from Miocene Marnoso-arenacea Formation, Northern Apennines, Italy.  
22  
23 1075 *Marine and Petroleum Geology*, **28**, 629-657.
- 24  
25  
26 1076 **Tinterri, R. and Tagliaferri, A.** (2015) The syntectonic evolution of foredeep turbidites related to  
27  
28 1077 basin segmentation: Facies response to the increase in tectonic confinement (Marnoso-arenacea  
29  
30 1078 Formation, Miocene, Northern Apennines, Italy). *Marine and Petroleum Geology*, **67**, 81-110.
- 31  
32  
33 1079 **Van der Mark, C.F., Blom, A. and Hulscher, S.J.M.H.** (2008) Quantification of variability in bedform  
34  
35 1080 geometry. *Journal of Geophysical Research: Earth Surface*, **113**, F03020, doi:10.1029/2007JF000940.
- 36  
37  
38 1081 **Van Der Merwe, W.C., Hodgson, D.M., Brunt, R.L. and Flint, S.S.** (2014) Depositional architecture of  
39  
40 1082 sand-attached and sand-detached channel-lobe transition zones on an exhumed stepped slope  
41  
42 1083 mapped over a 2500 km<sup>2</sup> area. *Geosphere*, **10**, 1076-1093.
- 43  
44  
45 1084 **Vellinga, A.J., Cartigny, M.J.B., Eggenhuisen, J.T. and Hansen, E.W.M.** (2018) Morphodynamics and  
46  
47 1085 depositional signature of low-aggradation cyclic steps: New insights from a depth resolved model.  
48  
49 1086 *Sedimentology*, **65**, 540-560.
- 50  
51 1087 **Vicente Bravo, J.V. and Robles, S.** (1995) Large-scale mesotopographic bedforms from the Albian  
52  
53 1088 Black Flysch, northern Spain: characterization, setting and comparison with recent analogues. In:  
54  
55 1089 *Atlas of Deep Water Environments; Architectural Style in Turbidite Systems* (Eds. Pickering, K.T.,  
56  
57  
58  
59  
60

- 1  
2  
3 1090 Hiscott, R.N., Kenyon, N.H., Ricci-Lucchi, F. and Smith, R.D.A.), *Chapman and Hall, London*, pp. 216-  
4  
5 1091 226.  
6  
7 1092 **Wickens H.DeV.** (1994) Basin floor fan building turbidites of the southwestern Karoo Basin, Permian  
8  
9 1093 Ecca Group, South Africa. *PhD-Thesis. University of Port Elizabeth*.  
10  
11  
12 1094 **Winn, R.D. and Dott, R.H.** (1977) Large-scale traction-produced structures in deep-water fan-  
13  
14 1095 channel conglomerates in southern Chile. *Geology*, **5**, 41-44.  
15  
16 1096 **Wynn, R.B. and Stow, D.A.** (2002) Classification and characterisation of deep-water sediment waves.  
17  
18 1097 *Marine Geology*, **192**, 7-22.  
19  
20  
21 1098 **Wynn, R.B., Kenyon, N.H., Masson, D.G., Stow D.A. and Weaver, P.P.** (2002a) Characterization and  
22  
23 1099 recognition of deep-water channel-lobe transition zones. *AAPG Bulletin*, **86**, 1441-1462.  
24  
25  
26 1100 **Wynn, R.B., Piper, D.J.W. and Gee, M.J.R.** (2002b) Generation and migration of coarse-grained  
27  
28 1101 sediment waves in turbidity current channels and channel-lobe transition zones. *Marine Geology*,  
29  
30 1102 **192**, 59-78.  
31  
32  
33 1103 **Yokokawa, M., Matsuda, F. and Endo, N.** (1995) Sand particle movement on migrating combined-  
34  
35 1104 flow ripples. *Journal of Sedimentary Research*, **A65**, 40-44.  
36  
37  
38 1105 **Zecchin, M., Caffau, M., Di Stefano, A., Maniscalco, R., Lenaz, D., Civile, D., Muto, F. and Crantelli,**  
39  
40 1106 **S.** (2013) The Messinian succession of the Crotona Basin (southern Italy) II: Facies architecture and  
41  
42 1107 stratal surfaces across the Miocene-Pliocene boundary. *Marine and Petroleum Geology*, **48**, 474-492.  
43  
44  
45  
46  
47  
48  
49  
50  
51  
52  
53  
54  
55  
56  
57  
58  
59  
60



1  
2  
3 1108 **FIGURE CAPTIONS**  
4

5 1109 **Figure 1.** Sediment wave dimensions (crest height *versus* wavelength) from modern and ancient  
6 systems grouped on the basis of type of dataset (A), setting (B) and grain size (C). Data taken from  
7 1110 Normark & Dickson (1976); Winn & Dott (1977); Damuth (1979); Lonsdale & Hollister (1979); Piper *et*  
8 1111 *al.* (1985); Malinverno *et al.* (1988); Praeg & Schafer (1989); Piper & Kontopoulos (1994); Vicente  
9 1112 Bravo & Robles (1995); Howe (1996); Kidd *et al.* (1998); Morris *et al.* (1998); Nakajima *et al.* (1998);  
10 1113 McHugh & Ryan (2000); Migeon *et al.* (2001); Wynn *et al.* (2002a,b); Normark *et al.* (2002); Ito &  
11 1114 Saito (2006); Heinio & Davies (2009); Ito (2010); Mukti & Ito (2010); Campion *et al.* (2011); Ponce &  
12 1115 Carmona (2011); Ito *et al.* (2014); Morris *et al.* (2014); Postma *et al.* (2014). Note that a lack of sand-  
13 1116 prone sediment waves in modern examples can be ascribed to difficulties in retrieving piston cores  
14 1117 within such sediments (e.g. Bouma & Boerma, 1968). The raw data are available as supplementary  
15 1118 material to this manuscript.  
16 1119

17  
18 1120 **Figure 2.** (A) Location map of the Laingsburg depocentre within the Western Cape. The transparent  
19 1121 overlay with black lining indicates the total exposed area of Unit B. Important outcrop areas are  
20 1122 highlighted, including the sections studied in this paper: Doornkloof and Old Railway; white  
21 1123 diamonds indicate locations discussed in Brunt *et al.* (2013). (B) Zoomed-in map of the Doornkloof  
22 1124 section including palaeocurrent distributions, sub-divided into subunit B1 and subunit B2. The  
23 1125 outcrop outlines are indicated by solid lines. Red line indicates Section I (Figure 5), blue line on DK-  
24 1126 unit B2 represents Section II (Figure 9). (C) Zoomed-in map of the Old Railway section including  
25 1127 palaeocurrent distributions.  
26 1128

27  
28 1129 **Figure 3.** (A) Simplified stratigraphic column of the deep-water stratigraphy within the Laingsburg  
29 1130 depocentre, based on Flint *et al.* (2011). (B-C) Palaeogeographic reconstruction of subunit B2 (B) and  
30 1131 subunit B1 (C) based on the regional study of Brunt *et al.* (2013). The two outcrop locations  
31 1132 discussed in this paper are indicated by the diamonds.  
32  
33  
34  
35  
36  
37  
38  
39  
40  
41  
42  
43  
44  
45  
46  
47  
48  
49  
50  
51  
52  
53  
54  
55  
56  
57  
58  
59  
60

1  
2  
3 1132 **Figure 4.** Examples of Internal bed structure and facies changes within subunit B2 (Doornkloof), with  
4  
5 1133 one example from *Bedform c* (A) and two from *Bedform b* (B and C) (see Fig. 9B for locations). All  
6  
7 1134 these examples show vertical internal facies changes, which include planar-lamination, wavy-  
8  
9 1135 lamination/banding and ripple-lamination.

10  
11 1136 **Figure 5.** Complete stratigraphic panel of the Doornkloof section showing the subdivision of Unit B,  
12  
13 1137 the location of the two detailed sedimentary sections (I, II), and the position of the DK01 core. The  
14  
15 1138 thin siltstone interval (TSI; Brunt *et al.*, 2013) between the AB interfan and subunit B1 has been used  
16  
17 1139 as a stratigraphic datum. The middle correlation panel shows section I of subunit B1; the position of  
18  
19 1140 *Bedform a* and the palaeoflow patterns have been indicated, as well as the location of the  
20  
21 1141 correlation panel in Figure 8. The bottom correlation panel shows the detailed facies distribution  
22  
23 1142 within *Bedform a* and its internal truncation surfaces. Outcrop photograph locations shown in Figure  
24  
25 1143 6 (A-D) and Figure 7 have been indicated.

26  
27  
28  
29 1144 **Figure 6.** Representative outcrop photographs from Section I and II and descriptive DK01 core log of  
30  
31 1145 subunit B1, with (A) *Bedform a* with ripple-top morphology on top of a local mudstone clast  
32  
33 1146 conglomerate deposit; (B) Eastward-orientated internal truncation surface (dotted line) in banded  
34  
35 1147 division within *Bedform a*; (C) Mudstone clast conglomerate layer below *Bedform a*; (D) Mudstone  
36  
37 1148 clast-rich banded section of *Bedform a*; (E) Westward-orientated internal truncation surface (dotted  
38  
39 1149 line) with climbing ripple-laminated facies within *Bedform a*; (F) Climbing ripple-lamination in  
40  
41 1150 between banded sandstone and sigmoidal lamination, as part of *Bedform b*; (G) Lower section of  
42  
43 1151 westward orientated truncation surface in *Bedform b*; (H) Upper section of westward orientated  
44  
45 1152 truncation surface in *Bedform b*; (I) Banded sandstone division in *Bedform b*; (J) West-facing  
46  
47 1153 truncation surface in *Bedform c*. See Figure 5 and Figure 9B for locations. Interpreted position of  
48  
49 1154 *Bedform a* is indicated (by an asterisk) within the DK01 core log.

50  
51  
52 1155 **Figure 7.** Mudstone clast conglomerate patch at the bottom of *Bedform a*, with clean true-scale  
53  
54 1156 photopanel (top) and interpreted vertically exaggerated ( $V_e = 1.8$ ) photopanel (bottom). It shows a  
55  
56  
57  
58  
59  
60

1  
2  
3 1157 basal erosion surface overlying thin-bedded sandstones, multiple 'floating' sandstone patches,  
4  
5 1158 upstream orientated pinch-out and downstream orientated amalgamation. Location of photograph  
6  
7 1159 is shown in the lowest panel of Figure 5.  
8

9 1160 **Figure 8.** Facies correlation panel of local sandstone swell in subunit B1. *Bedform a* is located at the  
11 1161 base of the package. Top panel shows its location within subunit B1. See middle panel of Figure 5 for  
12  
13 1162 more detailed facies correlation panel of the complete subunit B1, log locations, and lower panel of  
14  
15 1163 Figure 5 for symbol explanations.  
16  
17

18 1164 **Figure 9.** (A) Panoramic view of the base of subunit B2 at the DK-section. The outlines of *Bedform b*  
19  
20 1165 and *c* are indicated with white lines. Numbers indicate the position of sedimentary logs. (B) Facies  
21  
22 1166 correlation of the II-section with *Bedform b* and *c*. The top panel shows the thickness variability of  
23  
24 1167 these beds and the surrounding stratigraphy, comprised of structured sandstones (ripple- or planar-  
25  
26 1168 laminated); the lower panel shows the internal facies distribution of *Bedform b* and *c*. Rose diagrams  
27  
28 1169 show palaeoflow measurements around Section II. Internal truncation surfaces and location of the  
29  
30 1170 facies photos shown in Figure 4 and Figure 6 (F-J) have been indicated. See Figure 2B and Figure 5 for  
31  
32 1171 location of section II and for meaning of log symbols.  
33  
34

35 1172 **Figure 10.** Bedset architecture within the main subunit B2 outcrop face in the Doornkloof area.  
36  
37 1173 Bounding surfaces have been defined based on successive bed pinch-out with multiple (3-4)  
38  
39 1174 downstream-orientated stacked and weakly amalgamated bedforms.  
40  
41

42 1175 **Figure 11.** Subunit B2 within the Old Railway area. A- Facies correlation panels of the section with  
43  
44 1176 bedform distribution (top) and facies distribution (bottom). B- Zoomed-in facies correlation panel of  
45  
46 1177 most eastern section with C – mudstone clasts within a climbing-ripple laminated bed, indicating  
47  
48 1178 sediment overpassing, and D – bed splitting indicating erosion and amalgamation. See Figure 2 for  
49  
50 1179 location and lowest panel in Figure 5 for meaning of log symbols. Location of Figure 12 is indicated.  
51  
52

53 1180 **Figure 12.** Sketch of bed showing transient pinch-out to a thin siltstone bed (see Figure 11B for  
54  
55 1181 location), with (A1) pinch-out to siltstone, and (A2) local scouring of bed top.  
56  
57  
58  
59  
60

1  
2  
3 1182 **Figure 13.** (A) Idealised model to illustrate the variation in sedimentary structure within sediment  
4  
5 1183 wave swells in the Doornkloof area. (B) Interpretation of changes in depositional behaviour through  
6  
7 1184 time, linked to the observed internal facies changes in (A). T1-T7 refer to successive time periods,  
8  
9 1185 and show the evolution of the sediment waves, and what this means in terms of flow conditions  
10  
11 1186 over time. F1 consists of structureless sands.

12  
13  
14 1187 **Figure 14.** (A) Process explanation of the upstream-orientated accretion process, linked to flow  
15  
16 1188 capacity changes over time. Flow capacity may be linked to temporal variations in velocity from  
17  
18 1189 upstream hydraulic jumps, and/or to the lateral migration of the flow, shown in part B. (B)  
19  
20 1190 Illustration of the inferred spatial contribution (hose effect) during formation of the sediment waves.  
21  
22 1191 Lateral migration of the flow core during a single event is linked to capacity changes at a single  
23  
24 1192 location, as well as the formation of new swells upstream. The steps are interlinked between A and  
25  
26 1193 B; 'x' marks the same location throughout. Step 5 represents another phase of erosion, and thus a  
27  
28 1194 return to step 2.

29  
30  
31 1195 **Figure 15.** (A) Spatial division within a channel-lobe transition zone between a depositional bedform  
32  
33 1196 area (DB) and an erosional bedform area (EB) following Wynn *et al.* (2002a). Differences in sediment  
34  
35 1197 wave deposit facies and architecture are explained by spatial differences between the axis and fringe  
36  
37 1198 areas of the deposition-dominated fields (DB) of a CLTZ. (B) Sketch model showing how the 'hose  
38  
39 1199 effect' within an active flow will dominantly influence sediment wave development in axial areas.  
40  
41  
42  
43  
44  
45  
46  
47  
48  
49  
50  
51  
52  
53  
54  
55  
56  
57  
58  
59  
60

1

1  
2  
3  
4  
5  
6  
7 1 | Architecture and morphodynamics of subcritical sediment waves in an ancient  
8  
9 2 | channel-lobe transition zone

3

4

10  
11  
12  
13  
14  
15  
16 5 | M. Hofstra<sup>1†</sup>, J. Peakall<sup>1</sup>, D.M. Hodgson<sup>1</sup>, C.J. Stevenson<sup>2</sup>

17  
18 6 | <sup>1</sup>Stratigraphy Group, School of Earth and Environment, University of Leeds, Leeds, LS2 9JT, UK

19  
20 7 | <sup>2</sup>School of Earth, Ocean and Ecological Sciences, University of Liverpool, L69 3GP, UK

8

21  
22  
23  
24  
25 9 | †corresponding author [Email:

26  
27 10 | [eeemh@leeds.ac.uk](mailto:eeemh@leeds.ac.uk) [menno.hofstra.1@gmail.com](mailto:menno.hofstra.1@gmail.com)]

11

28  
29  
30  
31  
32 12 | **Running title:** ~~Sediment~~Subcritical sediment wave architecture in a CLTZ

33  
34  
35 13 | **Keywords:** channel-lobe transition; subcritical; sediment wave; base-of-slope; Karoo Basin;

36  
37 14 | facies characteristics; process record

38

39

40

41

42

43

44

45

46

47

48

49

50

51

52

53

54

55

56

57

58

59

60

## 15 ABSTRACT

16 In modern systems, submarine channel-lobe transition zones (CLTZs) show a well-documented  
17 assemblage of depositional and erosional bedforms. In contrast, the stratigraphic record of CLTZs is  
18 poorly constrained, because preservation potential is low, and criteria have not been established to  
19 identify depositional bedforms in these settings. Several locations from an exhumed fine-grained  
20 base-of-slope system (Unit B, [Laingsburg depocentre](#), Karoo Basin) show exceptional preservation of  
21 sandstone beds with distinctive morphologies and internal facies distributions. The regional  
22 stratigraphy, lack of a basal confining surface, wave-like morphology in dip section, size, and facies  
23 characteristics support an interpretation of [subcritical](#) sediment waves within a CLTZ setting. Some  
24 sediment waves show steep (10-25°) unevenly spaced (10-100 m) internal truncation surfaces that  
25 are dominantly upstream-facing, which suggests significant spatio-temporal fluctuations in flow  
26 character. Their architecture indicates individual sediment wave beds accrete upstream, in which  
27 each swell initiates individually. ~~These depositional processes do not correspond with known~~  
28 ~~bedform development under supercritical conditions.~~ Lateral switching of the flow core is invoked to  
29 explain the sporadic upstream-facing truncation surfaces, and complex facies distributions vertically  
30 within each sediment wave. Variations in bedform character are related to the axial to marginal  
31 positions within a CLTZ. ~~This~~ [The depositional processes documented do not correspond with known](#)  
32 [bedform development under supercritical conditions. The proposed process](#) model departs from  
33 established mechanisms of sediment wave formation by emphasising the evidence for subcritical  
34 rather than supercritical conditions, and highlights the significance of lateral and temporal variability  
35 in flow dynamics and resulting depositional architecture.

## 36 INTRODUCTION

37 Bedforms are rhythmic features that develop at the interface of fluid flow and a moveable bed (e.g.  
38 Southard, 1991; Van der Mark *et al.*, 2008; Baas *et al.*, 2016). Sediment waves are a type of long  
39 wavelength (tens of ms to kms) depositional bedform that vary in grain size from mud- to gravel-

1  
2  
3  
4  
5  
6 40 dominated, linked to their depositional setting (Fig. 1) (Wynn & Stow, 2002). They have been  
7  
8 41 identified in numerous modern channel-lobe transition zones (CLTZs) (Normark & Dickson, 1976;  
9  
10 42 Damuth, 1979; Lonsdale & Hollister, 1979; Normark *et al.*, 1980; Piper *et al.*, 1985; Malinverno *et al.*,  
11  
12 43 1988; Praeg & Schafer, 1989; Howe, 1996; Kidd *et al.*, 1998; Morris *et al.*, 1998; McHugh & Ryan,  
13  
14 44 2000; Migeon *et al.*, 2001; Normark *et al.*, 2002; Wynn & Stow, 2002; Wynn *et al.*, 2002a,b;  
15  
16 45 ~~Heiniö~~Heiniö & Davies, 2009), where they form part of a distinctive assemblage of depositional and  
17  
18 46 erosional bedforms (Mutti & Normark, 1987, 1991; Normark & Piper, 1991; Palanques *et al.*, 1995;  
19  
20 47 Morris *et al.*, 1998; Wynn *et al.*, 2002a,b; Macdonald *et al.*, 2011). However, the detailed  
21  
22 48 sedimentological and stratigraphic record of sediment waves from CLTZ and channel-mouth settings  
23  
24 49 is not widely documented.

25 50 Vicente Bravo & Robles (1995) described hummock-like and wave-like depositional bedforms from  
26  
27 51 the Albian Black Flysch, NE Spain. The hummock-like bedforms (5 to 40 m wavelength and a few  
28  
29 52 decimetres to 1.5 m high) were interpreted to be genetically related to local scours. The wave-like  
30  
31 53 bedforms (5 and 30 m wavelength and a few cm to 0.7 m high) seen in longitudinal sections exhibit  
32  
33 54 symmetric to slightly asymmetric gravel-rich bedforms. Ponce & Carmona (2011) identified sandy  
34  
35 55 conglomeratic sediment waves with amplitudes up to 5 m and wavelengths ranging between 10 to  
36  
37 56 40 m at the northeast Atlantic coast of Tierra del Fuego, Argentina. Ito *et al.* (2014) described  
38  
39 57 medium- to very coarse-grained sandstone tractional structures from a Pleistocene canyon-mouth  
40  
41 58 setting within the Boso Peninsula, Japan, with wavelengths up to 40 m and crest heights up to 2 m.  
42  
43 59 These coarse-grained examples from Japan, Argentina, and Spain lack detailed internal facies  
44  
45 60 descriptions and structure. ~~Therefore, the processes responsible for the inception and morphological~~  
46  
47 61 ~~evolution of sediment waves within CLTZ settings remain poorly constrained. Furthermore, data~~Data  
48  
49 62 on long wavelength finer-grained sediment waves in the rock record are largely missing (Fig. 1),  
50  
51 63 ascribed to their wavelength and poor exposure potential (Piper & Kontopoulos, 1994), ~~in contrast~~  
52  
53 64 ~~to modern~~. Modern examples that are dominantly fine grained (silt to mud) and show substantial  
54  
55 65 wavelengths (Fig. 1) are typically interpreted as large supercritical bedforms (Symonds *et al.*,  
56  
57  
58  
59  
60

2016), similar to cyclic steps. This is due to observations from geophysical data of their short lee-sides and long depositional stoss-sides, and apparent single bedform structures with upstream sediment wave migration as a sinusoidal wave (Cartigny *et al.*, 2014; Hughes-Clark, 2016; Covault *et al.*, 2017). Indeed, upstream migration of sediment waves is taken as an indicator of bedform evolution under supercritical flow conditions (Symonds *et al.*, 2016). However, the processes responsible for the inception and morphological evolution of sediment waves within CLTZ settings remain poorly constrained, and high-resolution observations of their sedimentology are needed to explore the balance of subcritical and supercritical processes in their inception, evolution, and depositional record.

Here, we aim to improve understanding of sediment wave development in CLTZs through studying multiple stratigraphic sections from well-constrained base-of-slope systems (Unit B, Laingsburg depocentre, Karoo Basin) where distinctive fine to very-fine-grained sandstone depositional bedforms with complex architecture, facies and stacking patterns are exposed. The objectives are: 1) to document and interpret the depositional architecture and facies patterns of these sandstone bedforms, and 2) to discuss their origin and formative processes, 2) to discuss the topographic controls on their inception, 3) to propose a process model for sediment wave development under subcritical rather than supercritical flow conditions, and, 4) to consider the controls on the preservation potential of sediment wave fields in channel-lobe transition zones.

#### REGIONAL SETTING

The southwest Karoo Basin is subdivided into the Laingsburg and the Tanqua depocentres. The Ecca Group comprises a ~2 km-thick shallowing-upward succession from distal basin-floor through submarine slope to shelf-edge and shelf deltaic settings (Wickens, 1994; Flint *et al.*, 2011). The deep-water deposits of the Karoo Basin have a narrow grain size range from clay to upper fine sand. Within the Laingsburg depocentre, (Figs 2A and 3A), Unit B, the focus of this study, is stratigraphically positioned between underlying proximal basin-floor fan deposits of Unit A (e.g. Sixsmith *et al.*, 2004;



91 Prélat & Hodgson, 2013) and the overlying channelised slope deposits of the Fort Brown Formation  
92 (Unit C-G; e.g. Hodgson *et al.*, 2011; Van der Merwe *et al.*, 2014). Unit B comprises a 200 m thick  
93 section at the top of the Laingsburg Formation (Grecula *et al.*, 2003; Flint *et al.*, 2011; Brunt *et al.*,  
94 2013), and is subdivided in three subunits, B1, B2 and B3 (Fig. 3A; Flint *et al.*, 2011; Brunt *et al.*,  
95 2013). Unit B is well-exposed for more than 350 km<sup>2</sup> providing both down dip and across strike  
96 control (Brunt *et al.*, 2013) with over 15 km long exposed sections along the limbs of the Baviaans  
97 and Zoutkloof synclines and Faberskraal anticline (Fig. 2A). The study area is situated between well-  
98 defined up-dip slope channels and down-dip basin-floor lobes (Fig. 3B and 3C; Grecula *et al.*,  
99 2003; Pringle *et al.*, 2010; Brunt *et al.*, 2013). Therefore, the palaeogeographic setting is interpreted  
100 to be a base-of-slope setting, where CLTZ-elements are more likely to be preserved (Fig. 3B and  
101 3C).

## 102 METHODOLOGY AND DATASET

103 Two areas of Unit B exposure were studied in detail: one located in the southern limb of the  
104 Zoutkloof Syncline (Doornkloof) and one located in the southern limb of the Baviaans Syncline (Old  
105 Railway) (Fig. 2). Stratigraphic correlations using closely-spaced sedimentary logs, (m's to tens of  
106 m's), photomontages, and walking out key surfaces and individual beds with a handheld GPS enabled  
107 construction of architectural panels. Where the exposure allowed collection of sub-metre-scale  
108 sedimentary logs individual beds were correlated over multiple kilometres. Within the Doornkloof  
109 area (Fig. 2B) 11 long (>20-200 m) sedimentary logs, supported by 31 short (<5 m) detailed  
110 sedimentary logs, were collected along a 2 km long E-W section. Particular emphasis was placed on  
111 bed-scale changes in facies to construct detailed correlation panels. Additionally, a research borehole  
112 drilled 330 m north of the studied outcrop section (DK01; 460983-6331775 UTM; Hofstra, 2016)  
113 intersected the lower 92 m of Unit B (Figs 2A and 2B). Within the Old Railway area (Fig. 2C), eight  
114 short and closely spaced (5-20 m distance) detailed sedimentary sections were collected.

1  
2  
3  
4  
5  
6 115 Palaeocurrents were collected from ripple-laminated bed tops and re-orientated, with 117

7  
8 116 palaeoflow measurements at Doornkloof and 87 from the Old Railway area.  
9

10 117 **FACIES AND ARCHITECTURE**  
11

12 118 Both study areas contain sandstone-prone packages that comprise bedforms with substantial

13  
14 119 downdip thickness and facies changes without evidence for confinement by an incision surface. The

15  
16 120 rate of thickness change and the range of sedimentary facies are markedly different from that

17  
18 121 documented in basin-floor lobes (e.g. Pr lat & Hodgson, 2013). Bed thicknesses change (metre scale)

19  
20 122 in a downstream-orientated direction on short spatial-scales (tens of metres), compared to lateral

21  
22 123 continuous bed thickness (hundreds of metres) known from lobes (e.g. Pr lat *et al.*, 2010). Similarly,

23  
24 124 facies change markedly over metre scales, in contrast to lobes where facies changes are transitional

25  
26 125 over hundreds of metres (e.g. Pr lat *et al.*, 2009). Depositional bedforms in both study areas are

27 126 present within a sandstone-prone (>90%) package of dominantly medium-bedded structured

28  
29 127 sandstones, interbedded with thin-bedded and planar-laminated siltstones. The grain size range is

30  
31 128 narrow, from siltstone to fine-grained sandstone, with a dominance of very-fine-grained sandstone.  
32

33 129 **Facies characteristics**  
34

35 130 The sedimentary facies within the bedforms are subdivided into four types: structureless (F1),

36  
37 131 banded to planar-laminated (F2), small-scale bedform structures (F3), and mudstone clast

38  
39 132 conglomerates (F4).  
40

41 133 F1: Structureless sandstones show minimal variation or internal structure and are uniform in

42  
43 134 grainsize (fine-grained sandstone). Locally, they may contain minor amounts of dispersed sub-

44  
45 135 angular mudstone clasts (1-10 cm) in diameter) and flame structures at bed bases.  
46

47 136 Interpretation: These sandstones are interpreted as rapid fallout deposits from sand rich high-

48  
49 137 density turbidity currents (Kneller & Branney, 1995; Stow & Johansson, 2000; Talling *et al.*, 2012)

50  
51 138 with mudstone clasts representing traction-transported bedload. Flame structures at the bases of

52  
53 139 structureless beds are associated with syn-depositional dewatering (Stow & Johansson, 2000).  
54  
55  
56  
57  
58  
59  
60

1  
2  
3  
4  
5  
6 140 F2: Banded and planar-laminated sandstones show large variations in character. The differentiation  
7  
8 141 between planar-laminated and banded facies is based on the thickness and character of the laminae  
9  
10 142 or bands. In banded sandstones, the bands are 0.5-3 cm thick and defined by alternations of clean  
11  
12 143 sand bands, and dirty sand bands rich in mudstone chipsclasts and/or plant fragments. Planar-  
13  
14 144 laminations show <1 cm thick laminae that are defined by clear sand-to-silt grain-size changes.  
15  
16 145 Furthermore, bands can be wavy or convolute, show substantial spatial thickness variations (<1 cm)  
17  
18 146 at small (<1 m) spatial scales, and exhibit subtle truncation at the bases of darker bands. Banded  
19  
20 147 facies are mudstone clast-rich where close to underlying mudstone clast conglomerates.  
21  
22 148 Occasionally in some places, banded sandstone beds can be traced upstream into mudstone clast  
23  
24 149 conglomerates. Where this facies is observed, bed thicknesses typically exceed 0.5 m.  
25  
26 150 Interpretation: Planar-lamination and banding are closely associated, and in many cases are difficult  
27  
28 151 to distinguish. This suggests that their depositional processes are closely related and are therefore  
29  
30 152 combined here into a single facies group. Planar laminated sandstones can be formed under dilute  
31  
32 153 flow conditions via the migration of low-amplitude bedwaves (Allen, 1984; Best & Bridge, 1992), or  
33  
34 154 under high-concentration conditions from traction carpets (Lowe, 1982; Sumner *et al.*, 2008; Talling  
35  
36 155 *et al.*, 2012; Cartigny *et al.*, 2013). The banded facies are interpreted may be formed as traction  
37  
38 156 carpet deposits from high-density turbidity currents and are comparable to the Type 2 tractional  
39  
40 157 structures of Ito *et al.* (2014) and the H2 division of Haughton *et al.* (2009). Deposits related to  
41  
42 158 traction carpets can show large significant variation in facies characteristics (e.g. Sohn, 1997; Cartigny  
43  
44 159 *et al.*, 2013). Alternatively, the banded facies may represent low-amplitude bedwave migration that  
45  
46 160 formed under mud-rich transitional flows (Baas *et al.*, 2016).  
47  
48 161 F3: Fine-grained sandstones with decimetre-scale bedform structures. The majority (~80%) of this  
49  
50 162 facies is represented by climbing ripple-lamination, commonly with stoss-side preservation. Locally,  
51  
52 163 small-scale (wavelengths of decimetre-scale, and heights of a few cm) bedforms are present that  
53  
54 164 show convex-up laminae, biconvex tops, erosive to non-erosive basal surfaces, and laminae that can  
55  
56  
57  
58  
59  
60

1  
2  
3  
4  
5  
6 165 thicken downwards (Figs 4A and 4C). In some cases, the bedforms show distinct low-angle climbing  
7  
8 166 (Fig. 5A). Isolated trains of decimetre-scale bedforms are present between banded/planar-laminated  
9  
10 167 facies (Figs 4B and 4C), ~~whilst~~whereas those exhibiting low-angle climbing can form above  
11  
12 168 banded/planar-laminated sandstone and in some cases transition into small-scale hummock-like  
13  
14 169 features (Fig. 4A). These hummock-like bedforms consist of erosively based, cross-cutting, concave-  
15  
16 170 and convex-up, low- to high-angle (up to 25°) laminae sets (Fig. 4A). They have decimetre to  
17  
18 171 centimetre wavelengths, and amplitudes up to 10 cm. Locally, internal laminae drape the lower  
19  
20 172 bounding surfaces and these tend to be low angle surfaces, ~~whilst~~whereas elsewhere laminae  
21  
22 173 downlap onto the basal surface, typically at higher angles (Fig. 4A). Where laminae are asymmetric  
23  
24 174 they ~~accrete~~have accreted in a downslope direction.  
25  
26 175 Furthermore, sinusoidal laminations are observed (Fig. 4A) with exceptional wavelengths (>20 cm)  
27  
28 176 and angles-of-climb (>45°) in comparison to conventional stoss-side preserved climbing ripples (15-  
29  
30 177 45°; 10-20 cm). These features also differ from convolute laminae/banding as they do show a  
31  
32 178 consistent wavelength and asymmetry. However, it is difficult to consistently make clear distinctions  
33  
34 179 between stoss-side preserved ripples and sinusoidal laminations. Hence, they are grouped together  
35  
36 180 into 'wavy bedform structures'.  
37  
38 181 F3 facies is most common at bed tops, but is also observed at bed bases, where laterally they are  
39  
40 182 overlain by an amalgamation surface. Locally, mudstone clasts (<1-4 cm) have been observed within  
41  
42 183 ripple-laminated segments.  
43  
44 184 Interpretation: Climbing ripple-lamination is interpreted as high rates of sediment fallout with  
45  
46 185 tractional reworking from flows within the lower flow regime (Allen, 1973; Southard & Boguchwal,  
47  
48 186 1990). The mudstone ~~-~~clasts are interpreted to be the result of overpassing of sediments on the bed  
49  
50 187 (Raudkivi, 1998; Garcia, 2008). When sedimentation rate exceeds the rate of erosion at the ripple  
51  
52 188 reattachment point, the stoss-side deposition is preserved and aggradational bedforms develop  
53  
54 189 (Allen, 1973). This is indicative of high rates of sediment fallout (Jopling & Walker, 1968; Allen, 1973;  
55  
56  
57  
58  
59  
60

1  
2  
3  
4  
5  
6 190 Jobe *et al.*, 2012), attributed to rapid flow deceleration from moderate-to-low concentration  
7  
8 191 turbidity currents (Allen, 1973). Sinusoidal lamination is interpreted as a type of climbing ripple  
9  
10 192 lamination, marked by very high sedimentation rates, leading to similarity in thickness between stoss  
11  
12 193 and lee sides (Jopling & Walker, 1968; Allen, 1973; Jobe *et al.*, 2012).

13  
14 194 The more convex bedforms (Figs 4A and 4C) bear similarities with washed out ripples that are  
15  
16 195 formed under high near-bed sediment concentration conditions at the transition from ripples to  
17  
18 196 upper stage plane beds in very fine sands (Baas & de Koning, 1995), and with combined-flow ripples  
19  
20 197 that have rounded tops and convex-up lee slopes (Harms, 1969; Yokokawa *et al.*, 1995; Tinterri,  
21  
22 198 2011). In turbidites, these bedforms have been termed 'rounded biconvex ripples with sigmoidal  
23  
24 199 laminae', and have been associated with reflected flow facies where turbidity currents have  
25  
26 200 interacted with topography (Tinterri, 2011; Tinterri & Muzzi Magalhaes, 2011; Zecchin *et al.*, 2013;  
27  
28 201 Tinterri & Tagliaferri, 2015). A third possibility is that these are decimetre-scale stable antidunes  
29  
30 202 since these can exhibit biconvex tops and in some cases convex-up cross-lamination (Alexander *et*  
31  
32 203 *al.*, 2001; Cartigny *et al.*, 2014; Fedele *et al.*, 2017), although these bedforms may also frequently  
33  
34 204 show concave laminae (Cartigny *et al.*, 2014). Typically, antidune laminae dip upstream (e.g.,  
35  
36 205 Alexander *et al.*, 2001; Cartigny *et al.*, 2014), although downstream migrating antidunes are known  
37  
38 206 from both open-channel flows (e.g., Kennedy, 1969) and gravity currents (Fedele *et al.*, 2017).

39 207 The 'hummocky-type' structures (Fig. 4A) with high-dip angles (up to 25°), draping of laminae, and  
40  
41 208 limited variation in laminae thickness, show similarities with anisotropic hummocky cross  
42  
43 209 stratification (HCS) from combined oscillatory-unidirectional flows (e.g., Dumas *et al.*, 2005; Dumas  
44  
45 210 & Arnott, 2006). Maximum dip angles of laminae in strongly anisotropic HCS can be around 25-30°  
46  
47 211 (Dumas *et al.*, 2005; Dumas & Arnott, 2006) much higher than for symmetrical forms, which are  
48  
49 212 typically less than 15° (Harms *et al.*, 1975; Tinterri, 2011). However, thickening and thinning of  
50  
51 213 laminae are expected in HCS (Harms *et al.*, 1975) and are not clearly observed in the hummocky-like  
52  
53 214 bedforms here. Such HCS-like hummocky bedforms have been interpreted from basin plain  
54  
55  
56  
57  
58  
59  
60

1  
2  
3  
4  
5  
6 215 turbidites to be related to reflected flows from topographic barriers (Tinterri, 2011; Tinterri & Muzzi  
7  
8 216 Magalhaes, 2011). Hummock-like bedforms in turbidites have also been interpreted as antidunes  
9  
10 217 (e.g., Skipper, 1971; Prave & Duke, 1990; Cartigny *et al.*, 2014). Antidunes are typically associated  
11  
12 218 with concave upward erosive surfaces, extensive cross-cutting sets if they are unstable antidunes,  
13  
14 219 bundles of upstream dipping laminae (if upstream migrating), laminae with low dip angles, low angle  
15  
16 220 terminations against the lower set boundary, some convex bedding, and structureless parts of fills  
17  
18 221 (e.g., Alexander *et al.*, 2001; Cartigny *et al.*, 2014; Fedele *et al.*, 2017). The hummock-like bedforms  
19  
20 222 in the present study share many similarities with these antidunes, however there is an absence of  
21  
22 223 structureless components, the draping of surfaces is more pronounced and more typical of HCS, the  
23  
24 224 approximately parallel nature of laminae within sets is more pronounced and the number of laminae  
25  
26 225 is greater. Furthermore, set bundles accrete downstream suggesting that if these are antidunes then  
27  
28 226 they are downstream-migrating forms. In summary, the hummock-like bedforms show greater  
29  
30 227 similarity to those HCS-like structures described from reflected flows (Tinterri, 2011; Tinterri & Muzzi  
31  
32 228 Magalhaes, 2011), rather than features associated with downstream migrating antidunes.

33  
34 229 The observed combination of biconvex ripples and anisotropic hummock-like features, and the  
35  
36 230 transitions between these bedforms in some vertical sections, is also in agreement with that  
37  
38 231 observed in some turbidity currents interacting with topography (Tinterri, 2011; Tinterri & Muzzi  
39  
40 232 Magalhaes, 2011), further suggesting that the hummock-like features may be related to combined  
41  
42 233 flows, rather than the product of antidunes. This possibility of topographic-interaction induced  
43  
44 234 hummock-like and biconvex ripple forms is discussed further, after the topography of the sediment  
45  
46 235 waves is introduced.

47 236 F4: Mudstone clast conglomerate deposits form discrete patches (<20 m long and <0.3 m thick),  
48  
49 237 which commonly overlie erosion surfaces. Mudstone clasts (<1 cm – 10 cm diameter) vary from  
50  
51 238 subangular to well-rounded. They are dominantly clast supported with a matrix of fine-grained  
52  
53 239 sandstone.  
54  
55  
56  
57  
58  
59  
60

240 Interpretation: Mudstone clast conglomerates are interpreted as lag deposits (e.g. Stevenson *et al.*,  
 241 2015) from energetic and bypassing high-density turbidity currents.

#### 242 **Bed architecture and facies distribution: Doornkloof – Subunit B1**

243 At Doornkloof (Fig. 2), subunit B1 has an average thickness of ~5 m (Fig. 5) and comprises thin- to  
 244 thick-bedded sandstones, thin-bedded siltstones and lenticular mudstone clast conglomerates (0.1-  
 245 0.3 m thick, 1-70 m wide) (Figs 5 and 6A-E). There are substantial variations in bed thicknesses and  
 246 sandstone-to-siltstone proportions along the 1.5 km long dip section (Fig. 5). Locally, medium- to  
 247 thick-bedded sandstones occur, which comprise bedforms within a package of thin-bedded siltstones  
 248 and sandstones. These bedforms show regional changes to more tabular thin-bedded sandstones  
 249 and siltstones (log 01/log 08, Fig. 5). Within the exposed section (~ 2 km), there are three sandstone-  
 250 prone bedform-dominated sections (200 m to 300 m in length) separated by siltstone-prone sections  
 251 (150 to 400 m in length), which have an overall tabular appearance (Fig. 6). The ~~Dk01~~DK01 core (Figs  
 252 5 and 6) is located 330 m to the north of the western limit of Section I where subunit B1 is a ~5 m  
 253 thick package of interbedded thin structured sandstones and laminated siltstones (Fig. 6). Multiple  
 254 erosion surfaces are present at the base, and overall in the DK01 core the subunit B1 succession  
 255 fines- and thins-upward. Palaeoflow of the B1 subunit is dominantly ENE-orientated (082°) (Fig. 2B)  
 256 but shows some deviation within the eastern part of the section (log 42 – Figs 2B and 5) towards the  
 257 NNE (023°).

258 The medium- to thick-bedded sandstones within the sandstone-prone sections of Section I,  
 259 orientated (079°-259°) subparallel to palaeoflow, show large lateral variations in thickness and facies.  
 260 The bedforms comprise structureless (F1), planar-laminated to banded (F2), and ripple-laminated  
 261 (F3) sandstones (Fig. 6A-E). The facies, architecture and thickness changes of one amalgamated bed  
 262 (*Bedform a*) are described in detail (Fig. 5). *Bedform a* thickens (up to 2.5 m) and thins (<20 cm)  
 263 multiple times, forming a down-dip pinch-and-swell morphology. Locally, the base of *Bedform a* is  
 264 marked by shallow erosion (<0.5 m deep; <30 m long) and ~~occasionally amalgamates in some places~~

1  
2  
3  
4  
5  
6 265 | is amalgamated with the underlying sandstone beds (Figs 5 and 7). Where *Bedform a* exceeds 0.5 m  
7  
8 266 | in thickness, banded (F2) sandstone facies is dominant, and is occasionally in some places underlain  
9  
10 267 | by structureless (F1) divisions, or exhibits climbing ripple-lamination at the bed top (F3). Where  
11  
12 268 | *Bedform a* is thin (<0.5 m thick), it is dominated by climbing-ripple lamination (F3). Below *Bedform a*,  
13  
14 269 | lenses of mudstone conglomerate (<30 m long; 5-30 cm thick) can be observed at various locations  
15  
16 270 | over the complete section. In some locations (e.g. log 16/18, Fig. 5), banded sandstone (F2) beds  
17  
18 271 | (Fig. 6D) can be observed intercalated with mudstone clast conglomerate lenses (Fig. 7). These  
19  
20 272 | banded beds pinch out or show a transition towards mudstone clast conglomerates upstream, and  
21  
22 273 | amalgamate are amalgamated with *Bedform a* downstream. At the same stratigraphic level as  
23  
24 274 | *Bedform a*, the DK01 core shows one pronounced 20 cm thick bed with angular mudstone clasts (<1-  
25  
26 275 | 5 cm diameter) that can be correlated to *Bedform a*.

27 276 | In *Bedform a*, six truncation surfaces (10-25°) are identified within the eastern limit of the section  
28  
29 277 | (Fig. 5), at places where the bedform exceeds 1 m in thickness. All truncation surfaces are sigmoid-  
30  
31 278 | shaped and flatten out upstream and downstream within the bed (Fig. 6E). One eastward  
32  
33 279 | (downstream) orientated truncation surface (Fig. 6B) in the lower part of the bed is observed at log  
34  
35 280 | 17 (Fig. 5). However, sigmoidal westward (upstream) facing truncation surfaces are most common in  
36  
37 281 | the upper portion of the bed and are spaced 15-20 m apart. They cut banded (F2) and ripple-  
38  
39 282 | laminated (F3) sandstone facies, and are sharply overlain by banded sandstone facies (F2) with bands  
40  
41 283 | aligned parallel to the truncation surface, or by climbing-ripple laminated segments (Fig. 6E). Abrupt  
42  
43 284 | upstream thinning (SW) and more gradual downstream thickening (NE) gives give *Bedform a*, an  
44  
45 285 | asymmetric wave-like morphology in dip section. Small-scale bedforms (F3) are solely present at the  
46  
47 286 | top of the wave-like morphology, and dominantly comprise climbing-ripple lamination, with  
48  
49 287 | occasional wavy bedforms (stoss-side preserved climbing ripples and/or sinusoidal laminations) at  
50  
51 288 | the thicker sections of the bedform (Fig. 5). At abrupt bed thickness changes associated with steep  
52  
53 289 | westward-facing truncation surfaces (>15°) (logs 16/19/21, Fig. 5), shallow scour surfaces (<0.35 cm)  
54  
55 290 | can be observed cutting that cut into the top surface of *Bedform a*, overlain and onlapped by thin-



291 bedded siltstones and sandstones. Within the banded facies (F2), isolated lenses of ripple-lamination  
 292 (F3) are present (up to 30-40 cm long and 10 cm thick) (Fig. 5 – log 19). Mudstone and siltstone clasts  
 293 (0.2-5 cm diameter) dispersed throughout structureless (F1) sections are typically well rounded, and  
 294 rarely sub-angular. At the eastern limit of Section I, stratigraphically below *Bedform a*, another  
 295 ‘pinch-and-swell’ sandstone bed abruptly increases in thickness downstream where *Bedform a*  
 296 amalgamatesis amalgamated with this bed below (log 21, Fig. 5). Where the bed thickens, *Bedform a*  
 297 thins abruptly (log 23/24, Fig. 5). The thin-bedded and siltstone-prone deposits overlying *Bedform a*  
 298 show more laterally constant geometries, thicknesses and facies.

299 At the upstream end (SW) of Section 1, around log 02-07 (Fig. 5, middle panel), a package of  
 300 sandstone beds thickens locally (>100 m long, <5 m thick) above *Bedform a* (Fig. 8). *Bedform a*  
 301 pinches and swells multiple times within this log 02-07 interval to a maximum of 0.5 m thickness and  
 302 comprises similar facies as downstream (F1, F2, F3), but lacks internal truncation surfaces. The bed  
 303 directly above *Bedform a* thickens where *Bedform a* thins and *vice versa* (Fig. 8). Sandstone beds  
 304 above both this bed and *Bedform a*, in the top of the package, show only limited thickness variations  
 305 (~10 cm) and dominantly comprise climbing ripple-laminated sandstone (F2). All sandstone beds  
 306 above *Bedform a* either pinch-out or show a facies transition towards fine siltstone in both western  
 307 and eastern directions (Fig. 5).

#### 308 **Bed architecture and facies distribution: Doornkloof – Subunit B2**

309 The sandstone bed morphology and facies characteristics at the base of subunit B2 share many  
 310 affinities with the deposits described within subunit B1 (Fig. 9). Palaeoflow of subunit B2 is generally  
 311 NE-orientated (040°) (n=68; Figs 2B and 9B), but shows with a wide spread high degree of dispersion,  
 312 and a shift from ENE (062°) in the western part of the section, to more northwards in the middle  
 313 (19°) and eastern part of the section (030°). This indicates that the section is dominantly subparallel  
 314 to palaeoflow (dip section) (Fig. ~~3B~~2B). Subunit B2 dominantly comprises medium-bedded (0.1-0.5 m  
 315 thick) structured sandstone (Fig. 9B). Closely spaced logs (m's to tens of m's) collected from the

1  
2  
3  
4  
5  
6 316 | main face at the base of B2 (Section II – Fig. 2B) permit tracing out of individual beds over a distance  
7  
8 317 | of 230 m and tracktracking of internal facies changes (Fig. 6F-J). Two beds (*Bedform b* and *Bedform*  
9  
10 318 | *c*) change in thickness (0.5-2 m for *Bedform b* and 0.3-1.2 m for *Bedform c*) and contain multiple  
11  
12 319 | internal truncation surfaces of which six are westward (upstream) facing and one is eastward  
13  
14 320 | (downstream) facing. Truncation surfaces cut climbing ripple-laminated facies (F3) and banded facies  
15  
16 321 | (F2) with maximum angles varying between 20-30° that shallow out and merge with the base of the  
17  
18 322 | bed (Figs 6G, 6H and 6J). They flatten out in the downstream direction within the bed and are  
19  
20 323 | overlain by banded sandstone facies (F2). In *Bedform b*, the rate of westward thinning is more  
21  
22 324 | abrupt than eastward, giving an asymmetric wave-like morphology (Fig. 9B). This abrupt westward  
23  
24 325 | thinning is coincident with locations of westward (upstream) orientated truncation surfaces. In the  
25  
26 326 | eastern part, 110 m separates two truncation surfaces, in an area associated with bed thinning.  
27  
28 327 | However, towards the western part of *Bedform b*, there is only 25-30 m between the westward  
29  
30 328 | (upstream) orientated truncation surfaces, with no abrupt bed thinning.  
31  
32 329 | There is a high degree of longitudinal and vertical facies variability within *Bedform b* and *c* (Figs 4 and  
33  
34 330 | 9B). Commonly, longitudinal facies changes are accompanied by bed thickness changes. Locally, the  
35  
36 331 | bases of thicker parts of the bedforms are mudstone clast-rich. Bed tops show small-scale bedform  
37  
38 332 | structures (F3) at most locations. Banded sandstone facies overlie the truncation surfaces (Figs 6G,  
39  
40 333 | 6H and 6J). Ripple-laminated facies (F3) within the middle or lower parts of *Bedform b* and *c* indicate  
41  
42 334 | flow directions that deviate (NW to N) from the regional palaeoflow (NE) (Figs 4A, 6F and 6H),  
43  
44 335 | whilewhereas the palaeoflow direction of the ripples at the top of the bedforms are consistent with  
45  
46 336 | the regional palaeoflow. Detailed analysis of well-exposed sections (Fig. 4) indicates that many  
47  
48 337 | laminated and banded sections are wavy and separated by low angle truncation or depositional  
49  
50 338 | surfaces. Locally, small-scale bedform structures (F3) are present in patches (Figs 4B and 4C) (<10 cm  
51  
52 339 | thick; couple of metres wide), which show downstream and/or upstream facies transitions to  
53  
54 340 | banded/planar-laminated facies (F2), as well as examples of flame structures (Fig. 4C). The small-  
55  
56 341 | scale bedform structures (F3) show a lot of variability, with hummock-like features observed above  
57  
58  
59  
60

1  
2  
3  
4  
5  
6 342 biconvex ripples at both the downstream end of swells, and directly below truncation surfaces at the  
7  
8 343 upstream end of swells (Fig. 4A). Additionally, both hummock-like features and biconvex ripples  
9  
10 344 have been observed at the base of *Bedform b* (log 38; Fig. 9B). Similar to *Bedform a*, *Bedform b* & *c*  
11  
12 345 show wavy bedform structures at the top of swells, particularly where they are the thickest. *Bedform*  
13  
14 346 *b* is topped in the easternmost exposure by a scour surface that cuts at least 0.5 m into *Bedform b*  
15  
16 347 and is amalgamated with an overlying pinch-and-swell sandstone bed (Fig. 9B). Medium- to thin-  
17  
18 348 bedded structured sandstones are present above and below *Bedform b* and *c*, which do not show  
19  
20 349 any facies or thickness changes over the exposed section.

21 350 The basal succession of subunit B2 in the DK01 core, at the same stratigraphic level as *Bedform b*  
22  
23 351 and *c*, comprises thick-bedded structureless (F1) to banded (F2) (>3 m) sandstones. Bed bases are  
24  
25 352 sharp and structureless and contain a variable amount of mudstone clasts (<1 cm). The middle to  
26  
27 353 upper parts of these beds show banded facies (F2) with clear mudstone clast-rich and -poor bands,  
28  
29 354 which pass through wavy lamination to climbing ripple (F3) and planar lamination at bed tops.  
30  
31 355 Above Section II, in both outcrop and core, a 15 m thick sandstone package shows a substantial  
32  
33 356 increase in bed thicknesses (max. 4.5 m), mainly due to bed amalgamation (Fig. 9A). Some of these  
34  
35 357 beds show a wave-like (asymmetric) morphology, similar to that observed in *Bedforms b* and *c*.  
36  
37 358 Abrupt bed thinning or pinch-out is common. These pinch-outs are primarily associated with  
38  
39 359 depositional geometry, with rare examples of bed truncation by erosion surfaces. Bounding surfaces  
40  
41 360 can be identified within the sandstone package, which are defined by successive upstream  
42  
43 361 depositional bed ~~pinch-out~~ pinch-out points (Fig. 10), with local (<2 m long) shallow (<0.3 m) erosion  
44  
45 362 surfaces. These bounding surfaces separate multiple packages of downstream shingling (three to  
46  
47 363 four) sandstone beds. The packages of pinch-and-swell beds are stacked in an aggradational to  
48  
49 364 slightly upstream orientated manner (Fig. 10) and are topped by a >60 m thick package of tabular  
50  
51 365 and laterally continuous medium- to thin-bedded structured sandstones. At the same interval in the  
52  
53 366 ~~DK01~~ DK01 core a transition can be observed from thick- to medium-bedded, dominantly banded  
54  
55  
56  
57  
58  
59  
60 367 (F2), sandstones towards more medium- to thin-bedded structured (F3) sandstones.

1  
2  
3  
4  
5  
6 **368 Bed architecture: Old Railway – Subunit B2**  
7

8 **369** At this locality on the southern limb of the Baviaans Syncline, the lower 10 m of subunit B2 is  
9  
10 **370** exposed for 100 m EW (Fig. 2C). Here, B2 is a medium- to thin-bedded sandstone-prone unit that  
11  
12 **371** shows substantial lateral thickness changes without evidence of a basal erosion surface (Fig. 11).  
13  
14 **372** Mean palaeoflow is ESE (121°) (Fig. 2C), indicating the exposure is sub-parallel to depositional dip.  
15  
16 **373** The sandstone beds are dominantly climbing ripple laminated (F3), with some banded/planar  
17  
18 **374** laminated (F2) and structureless divisions (F1).  
19  
20 **375** Multiple climbing ripple laminated beds contain dispersed small mudstone and siltstone clasts (Fig.  
21  
22 **376** 11C). The section is characterised by an alternation of beds showing typical pinch-and-swell  
23  
24 **377** geometries (0.5-2 m) and more tabular thin-bedded (<0.5 m) sandstones. Locally, individual beds  
25  
26 **378** pinch-and-swell multiple times over a distance of ~40 m, with wavelengths varying from 15 m to >40  
27  
28 **379** m. Where there are swells, bed bases truncate underlying beds (Fig. 11D). Siltstones comprise only  
29  
30 **380** ~10% of the succession and are thin-bedded and planar-laminated, with intercalated thin very fine-  
31  
32 **381** grained sandstones (<1 cm).  
33  
34 **382** Towards the top of the section, a 40 cm thick very fine-grained sandstone bed abruptly fines and  
35  
36 **383** thins downstream to a centimetre-thick siltstone bed (Fig. 12). This bed thickens and thins along a  
37  
38 **384** ~20 m distance (Fig. 12) forming sandstone lenses, before regaining original thickness (40 cm).  
39  
40 **385** Locally, within this zone, the bed longitudinally grades to siltstone and is perturbed from the top by  
41  
42 **386** decimetre-scale scour surfaces (0.2-3 m long, couple of cm's deep). At log 04 (Fig. 11A), a bed that  
43  
44 **387** pinches downstream has a downstream-orientated scour on its top surface, which is overlain by  
45  
46 **388** thin-bedded sandstones and siltstones that pass upstream beyond the confines of the scour surface.  
47  
48 **389** A downstream thickening bed with an erosive base truncates these beds. The majority of the  
49  
50 **390** observed pinch-and-swell bedforms stack in a downstream direction (Fig. 11A). However, in the  
51  
52 **391** middle of the package at log 1, one bed stacks in an upstream manner, giving the overall package an  
53  
54  
55  
56  
57  
58  
59  
60

392 aggradational character. This is similar to the stacking patterns observed within subunit B2 at the  
393 Doornkloof section (Fig. 10).

#### 394 **Sediment waves within channel-lobe transition zones**

395 The Doornkloof and Old Railway sections show bedforms with clear pinch-and-swell morphology  
396 that are subparallel to flow direction. These bedforms developed in a base-of-slope setting without  
397 any evidence of a large-scale basal confining surface. Bed-scale amalgamation and scouring are  
398 common in the two study areas, however the more significant component of downstream bed  
399 thickness changes is depositional. Their geometry and dimensions (>1 m height; 10-100 m  
400 wavelength), support their classification as sediment waves (Wynn & Stow, 2002). The bedforms  
401 described from the Doornkloof area (*Beds a-c*) show clear asymmetric pinch-and-swell  
402 morphologies, related to internal upstream-facing truncation surfaces (Figs 5 and 9). The well-  
403 constrained base-of-slope setting (Brunt *et al.*, 2013), the lack of confining erosion surfaces, and the  
404 lobe-dominated nature of Unit B downdip (Figs 3B and 3C) are consistent with an  
405 interpretation that the sediment waves formed within a CLTZ setting.

### 406 **DISCUSSION**

#### 407 **Topographic control on sediment wave inception**

408 The interpreted CLTZ setting for the sediment waves means that initial deposition is most likely  
409 related to flow expansion at the channel-mouth (e.g. Hiscott, 1994a; Kneller, 1995; Mulder &  
410 Alexander, 2001). The occurrence of abrupt downstream bedform thickening (e.g. *Bedform a*, Fig. 5),  
411 indicates a marked decrease in flow capacity resulting in a temporary increase of deposition rates  
412 (e.g. Hiscott, 1994a). Although deposition is expected in areas of flow expansion, this does not  
413 explain why sediment wave deposition appears to be localised (e.g. log 02-07; Fig. 5). Both the  
414 inception and localised deposition/development of the sediment waves are interpreted to be related  
415 to subtle and evolving the presence of seabed relief at the time of deposition. (dm's to m's  
416 amplitude). Seabed irregularities are common in base-of-slope settings, and minor defects (such as

Formatted: Font: Calibri

417 scours lined with mudstone clast conglomerates; Fig. 7) could have triggered deposition from flows  
418 close to the depositional threshold (Wynn *et al.*, 2002a). The presence of bedforms overlying swells  
419 of older bedforms, such as at the upstream location of *Bedform a* (Figs 5 (logs 2-7) and 8) or the  
420 sediment waves overlying *Bedform b* in subunit B2 (Fig. 10), suggest that relief of older bedforms,  
421 and consequent flow deceleration, may also act as a nucleus for later sediment wave development.  
422 The locally observed decimetre-scale deep scours probably had a more variable effect on sediment  
423 wave development. In some cases it resulted in topographic relief that could help sediment wave  
424 nucleation (e.g. log 4, Fig. 11) and in other cases the scours remove positive depositional relief (e.g.  
425 Fig. 12) and therefore they will have a slight negative effect on sediment wave nucleation. The  
426 aggradational character of the sediment wave packages (Figs 10 and 11A) supports a depositional  
427 feedback mechanism. Depositional bedforms form positive topography, which may help to nucleate  
428 sites of deposition and the development of composite sediment waves forming the complicated  
429 larger-scale sediment wave architecture (Figs 10 and 11A).

430

#### 431 **Bed-scale process record**

432 The sediment wave deposits from CLTZ settings in Unit B are diverse and show significant facies  
433 variations on the sub-metre scale. The characteristics of the sediment wave deposits from the two  
434 Unit B datasets are discussed and compared.

#### 435 *Bed-scale process record - Doornkloof section*

436 Facies of the sediment waves identified at the Doornkloof section are characterised by an  
437 assemblage of structureless (F1), banded and planar laminated (F2), and climbing ripple laminated  
438 (F3) sandstones. Local patches of structureless sandstone facies (F1) (Figs 5 and 9B) at bed bases,  
439 suggest periods of more enhanced deposition rates (e.g. Stow & Johansson, 2000). However, the  
440 sediment waves are dominated by banded facies, likely related either to traction-carpet deposition  
441 (Sumner *et al.*, 2008; Cartigny *et al.*, 2013) or low-amplitude bedwave migration under transitional

Formatted: Font: Calibri

1  
2  
3  
4  
5  
6 442 flows (Baas *et al.*, 2016). This suggests deposition from high concentration flows during bedform  
7  
8 443 development. The high degree of F2 variation (band thickness, presence of shallow truncations,  
9  
10 444 wavy nature) is explained by ~~either~~; 1) turbulent bursts interacting with ~~the~~ traction carpet (Hiscott,  
11  
12 445 1994b), ~~or~~; 2) waves forming at the density interface between ~~the~~ traction carpet and the  
13  
14 446 overlying lower-concentration flow, possibly as a result of Kelvin-Helmholtz instabilities, ~~or a~~  
15  
16 447 combination of both processes (Figs 4 and 6) (Sumner *et al.*, 2008; Cartigny *et al.*, 2013); ~~3) the~~  
17  
18 448 presence of bedwaves and associated development beneath mixed-load, mud-rich, transitional flows  
19  
20 449 (Baas *et al.*, 2016), or some combination of these processes. There is a strong spatial and  
21  
22 450 stratigraphic relationship between mudstone clast conglomerates (F4) (Figs 7 and 8) and banded  
23  
24 451 sandstone facies (F2) with a high proportion of mudstone clasts. As the deposits underlying the  
25  
26 452 shallow erosion surfaces are predominantly siltstones, the mudstone clast materials must have been  
27  
28 453 entrained farther upstream, and are therefore interpreted as lag deposits from bypass-dominated  
29  
30 454 high-concentration flows (e.g. Stevenson *et al.*, 2015). As scours are typically documented upstream  
31  
32 455 of sediment waves in modern CLTZs (Wynn *et al.*, 2002a), the source of these mudstone clasts is  
33  
34 456 likely linked to local upstream scouring, supported by the angularity of the clasts (Johansson & Stow,  
35  
36 457 1995). The transition from banded facies (F2) to climbing ripple-laminated facies (F3), common at  
37  
38 458 the top of individual beds, likely represents a ~~transition~~change from net depositional high  
39  
40 459 concentration flows, to steady deposition from moderate to low concentration flows, ~~and / or a~~  
41  
42 460 corresponding change from mud-rich transitional flows to mud-poor flows. The dominance of this  
43  
44 461 facies group (F3) at bed tops (Figs 5 and 9B) is interpreted as the product of less-energetic and more  
45  
46 462 depositional tails of bypassing flows.

47 463 To understand the process record and evolution of the Unit B sediment waves, it is important to be  
48  
49 464 able to distinguish the record of a single flow event, ~~from~~ a composite body comprised of deposits  
50  
51 465 from multiple flow events. The majority of the observed bed thickness changes within the sediment  
52  
53 466 waves at the Doornkloof section are attributed to depositional relief although internally they show  
54  
55 467 steep internal truncation surfaces (Figs 5, 6 and 9). The erosion surfaces may suggest that this

1  
2  
3  
4  
5  
6 468 depositional architecture is the result of multiple depositional and erosional flow events. However,  
7  
8 469 several lines of evidence suggest these are deposits produced from a single flow event. The  
9  
10 470 preservation of upstream-facing truncation surfaces (Figs 5 and 9B), implies a significant component  
11  
12 471 of bedform accretion at the upstream end (Figs 13 and 14A). To be able to preserve upstream  
13  
14 472 younging truncation surfaces with angles up to 25° (close to the angle-of-repose), the erosion and  
15  
16 473 deposition within each bedform, is likely to be the result of a single flow event. Within subunit B2,  
17  
18 474 no bed splitting is observed and all truncation surfaces of *Bedform b* and *c* merge towards the bed  
19  
20 475 base as a single surface (Fig. 9B), leaving underlying strata untouched. This suggests an origin from a  
21  
22 476 single flow event for the entire bedform.  
23  
24 477 In subunit B1, all upstream facing truncation surfaces in the main sandstone body of *Bedform a*  
25  
26 478 merge onto a single surface within the composite deposit, in a similar manner to *Bedform b* and *c*,  
27  
28 479 further suggesting a single flow origin for the main sediment wave morphology. Additionally,  
29  
30 480 *Bedform a* can be followed out for ~ 1 km in the upstream direction, and shows many small-scale (<5  
31  
32 481 m longitudinal distance) purely depositional undulations at the western end (Figs 5 and 8). These  
33  
34 482 flow parallel undulations are stratigraphically equivalent to the deposits above the most upstream  
35  
36 483 truncation surface and therefore, represent the youngest depositional phase of *Bedform a*  
37  
38 484 development. The absence of erosion surfaces or bedding planes between these undulations further  
39  
40 485 suggests that the main body of *Bedform a* was formed as a single event bed. The evidence therefore  
41  
42 486 supports the initiation and development of each wave-like bedform in the Doornkloof section  
43  
44 487 (*Bedform a, b* and *c*) to be during the passage of a single flow event. Therefore, the internal scour  
45  
46 488 surfaces and bedform undulations are interpreted to be the result of spatio-temporal flow  
47  
48 489 fluctuations from a single flow event. In contrast, the mudstone clast patches that underlie *Bedform*  
49  
50 490 *a* show upstream pinch-out of sandstone beds and downstream amalgamation (Fig. 7) indicating  
51  
52 491 multiple flow events formed these patches and the lower sandstone body prior to the initiation of  
53  
54 492 the main bedform. The presence of these mudstone clast patches results in a marked difference in  
55  
56 493 bedform architecture and bed thickness for *Bedform a* compared to *Bedform b* and *c*.  
57  
58  
59  
60



494 Bed-scale process record - Old Railway section

495 In the Old Railway section (Fig. 11), erosional bed bases and bed amalgamation are common,  
496 particularly where there is depositional thinning of underlying beds, indicating that the 'pinch-and-  
497 swell' bedforms present at this section are the result of multiple flow events in contrast to the  
498 Doornkloof area. However, bed amalgamation has limited impact on bedform thickness, as thickness  
499 increase dominantly occurs downdip of the point of amalgamation and is therefore of a depositional  
500 nature. The Old Railway bedforms classify as sediment waves (Wynn & Stow, 2002) with dimensions  
501 of 15 to >40 m wavelength (extending outside outcrop limits) and 1-2 m amplitude. However, the  
502 maximum bed thicknesses (1-1.5 m) are more limited than at the Doornkloof area (>2.5 m), climbing  
503 ripple-laminated facies (F3) is more dominant, and banded facies (F2) are almost absent. The  
504 sediment waves have a more uniform facies distribution and there is an absence of internal  
505 truncation surfaces (Fig. 11). The dominance of F3 indicates rapid deposition from dilute turbulent  
506 flows, which contrasts with the Doornkloof area.

508 Subcritical sediment waves: comparison with supercritical bedforms

509 The Doornkloof and Old Railway outcrops are both characterised by composite sediment waves.  
510 However, there are distinct differences between both areas. The Old Railway examples exhibit  
511 comparatively simple sediment waves, composed of multiple event beds, and dominated by lower  
512 flow-regime facies (F3) such as climbing ripple-lamination, accrete downstream, and lack significant  
513 internal erosive surfaces. Morphologically, stoss sides can be comparable to or longer than lee sides  
514 (Fig. 11). In contrast, the Doornkloof sediment waves were formed as single event beds and are  
515 characterized by short stoss sides, long lee sides, and exhibit erosion and more energetic facies (F1,  
516 F2, F4), with climbing ripple deposition (F3) becoming more dominant at the top of the beds (Fig.  
517 13A). The Doornkloof waves migrate upstream through erosional truncation and draping at bed  
518 swelling locations (up to >10 m; Fig. 9) followed by the development of another bed swell upstream

1  
2  
3  
4  
5  
6 519 (Fig. 13A). This means that each swell initiates individually, rather than simultaneously as a  
7 sinusoidal wave.  
8  
9  
10 521 The architecture of the Doornkloof sediment waves most closely resembles the smaller-scale type II  
11 and type III antidunal bedforms described by Schminke *et al.* (1973). However, these bedform  
12 architectures, which are an order of magnitude smaller, are interpreted to migrate through stoss-  
13 side deposition by supercritical flows based on the field observations, and have never been  
14 produced experimentally. In contrast, Kubo & Nakajima (2002) and Kubo (2004) observed sediment  
15 wave architectures with short stoss sides, long lee sides and variable wavelengths, similar to the  
16 Doornkloof sediment waves, under subcritical flow conditions in physical and numerical  
17 experiments. The depositional patterns of these sediment waves were defined by upstream  
18 migration of waveforms by individual growing mounds (Kubo & Nakajima, 2002; Kubo, 2004), and  
19 are therefore highly analogous to the observations from the Doornkloof waves.  
20  
21 526 The nature and variability of small-scale bedform structures (F3) (e.g., Fig. 13A for the Doornkloof  
22 waves) provide key indicators of flow type. This facies group consists of climbing ripples, sinusoidal  
23 lamination, biconvex ripples, and hummock-like structures, with biconvex ripples sometimes  
24 transitioning upwards into the hummocks. Climbing ripples and sinusoidal lamination are indicators  
25 of subcritical flow (Allen, 1973; Southard & Boguchwal, 1990), and the biconvex ripples and  
26 hummock-like structures have greater affinities with combined-flow ripples and hummocky cross  
27 stratification than with antidunes, again suggesting deposition under subcritical flow conditions.  
28  
29 533 *Spatio-temporal flow fluctuations – Doornkloof section*  
30  
31 539 In particular, the vertical change from biconvex ripples to hummock-like bedforms observed in the  
32 Doornkloof sediment waves is strongly analogous to structures associated with reflected flows in  
33 other turbidites (Tinterri, 2011; Tinterri & Muzzi Magalhaes, 2011), rather than deposits associated  
34 with supercritical flow conditions. The presence of topography in the form of the large-scale  
35 sediment wave may have led to flow reflection (Tinterri, 2011) and deflection as and when the flow  
36  
37  
38  
39  
40  
41  
42  
43  
44  
45  
46  
47  
48  
49  
50  
51  
52  
53  
54  
55  
56  
57  
58  
59  
60

Formatted: Font: Calibri

1  
2  
3  
4  
5  
6 544 waned. Importantly, these subcritical small-scale bedforms are observed over the full length of the  
7  
8 545 sediment waves, both on the stoss- and lee-side, at Doornkloof and the Old Railway (Figs 5, 9 and  
9  
10 546 11). This indicates subcritical deposition occurred across the entire sediment wave, and that the flow  
11  
12 547 remained subcritical throughout the depositional period over which the decimetre bedforms were  
13  
14 548 formed.

15  
16 549 The morphology and architecture of the sediment waves in this study contrast with large  
17  
18 550 supercritical bedforms, such as cyclic steps, since these exhibit short erosional lee-sides and long  
19  
20 551 depositional stoss-sides (Cartigny *et al.*, 2014; Hughes-Clark, 2016), and display upstream sediment  
21  
22 552 wave migration as a sinusoidal wave (Cartigny *et al.* 2014). Additionally, the sediment waves  
23  
24 553 described here are not single bedform structures such as described from supercritical bedforms  
25  
26 554 (e.g., Cartigny *et al.*, 2014; Covault *et al.*, 2017), but are composed of stacked smaller-scale  
27  
28 555 bedforms. The spatial and temporal extent of subcritical deposits also contrasts strongly with  
29  
30 556 'supercritical' bedforms where subcritical deposition can be expected only in some or all of the  
31  
32 557 stoss-side, downdip of a hydraulic jump (Vellinga *et al.*, 2018). Furthermore, tractional subcritical  
33  
34 558 bedforms are predicted to be limited to the downstream parts of the stoss side in aggradational  
35  
36 559 cyclic steps, or to be mixed-in with supercritical and non-tractional subcritical facies in  
37  
38 560 transportational cyclic steps (Vellinga *et al.*, 2018; their Fig. 9). Note that decimeter-scale bedforms  
39  
40 561 themselves could not be modelled in the CFD simulations of Vellinga *et al.* (2018). Lastly, the overall  
41  
42 562 signature of subcritical deposits within dominantly supercritical bedforms was one dominated by  
43  
44 563 amalgamation of concave-up erosional surfaces and low-angle foresets and backsets creating  
45  
46 564 lenticular bodies (Vellinga *et al.*, 2018). These bodies scale with the size of the overall bedform, and  
47  
48 565 the backsets show clear downstream fining (Vellinga *et al.*, 2018). Again, the sediment waves studied  
49  
50 566 herein show radically different architecture to that formed in cyclic steps, characterised by stacked  
51  
52 567 decimeter-scale bedforms and an absence of large-scale (scaling with the sediment wave) foresets,  
53  
54 568 backsets and lenticular bodies.  
55  
56  
57  
58  
59  
60

1  
2  
3  
4  
5  
6 569 In summary, the morphology, architecture, composite nature, and small-scale bedform types, all  
7  
8 570 indicate that the sediment waves were clearly deposited under subcritical conditions. The subcritical  
9  
10 571 nature of these sediment waves, the observation of upstream accretion via deposition on the stoss  
11  
12 572 side, and the associated upstream migration of the crestline, observed at Doornkloof, challenge the  
13  
14 573 assumption that all upstream-orientated expansion of sediment waves is the product of supercritical  
15  
16 574 conditions (Wynn & Stow, 2002; Symons *et al.*, 2016). That said, the Doornkloof bedforms appear to  
17  
18 575 have migrated sporadically over short distances (m's to tens of m's) through upstream accretion (Fig.  
19  
20 576 9B), before undergoing growth of new sediment wave lenses upstream, thus the entire bedform  
21  
22 577 does not continuously migrate as observed in some modern sediment wave examples (e.g., Hughes-  
23  
24 578 Clark, 2016). The presence of these subcritical sediment waves in the downstream parts of CLTZs  
25  
26 579 also challenges the idea that mid-sized fans, like those in the Karoo, likely exhibit flows close to  
27  
28 580 critical Froude numbers, at and beyond the CLTZ (Hamilton *et al.*, 2017), although such conditions  
29  
30 581 are likely in upstream parts of CLTZ where scouring occurs.

30 582

### 33 583 **Spatio-temporal flow fluctuations**

Formatted: Font: Bold

34  
35 584 The large-scale erosive truncations, and the wide variability of decimetre-scale bedforms in space  
36  
37 585 and time, observed in the Doornkloof waves indicate marked spatio-temporal flow fluctuations from  
38  
39 586 a single flow event. In contrast, the continuity of facies and absence of significant erosive surfaces  
40  
41 587 suggests that the Old Railway sediment waves were formed by flows with very limited spatio-  
42  
43 588 temporal variation. Here, we focus on these spatio-temporal fluctuations indicated by the  
44  
45 589 Doornkloof waves, and later address the issue of how the different types of sediment waves shown  
46  
47 590 in the Doornkloof and Old Railway outcrops could coexist.

48 591 Fluctuations in velocity and concentration can be expected in environments where turbidity currents  
49  
50 592 exit confinement (e.g. Kneller & McCaffrey, 1999, 2003; Ito, 2008; Kane *et al.*, 2009; Ponce &  
51  
52 593 Carmona, 2011), and where flows pass over depositional and erosional relief on the seabed (e.g.

594 Groenenberg *et al.*, 2010; Eggenhuisen *et al.*, 2011). Similar steep internal scour surfaces to those  
595 observed in the Doornkloof bedforms were interpreted to be generated by energetic sweeps from a  
596 stratified flow (Hiscott, 1994b). Furthermore, a similar depositional history of waxing and waning  
597 behaviour within a single flow was inferred from the sediment waves of the Miocene Austral  
598 foreland Basin, Argentina (Ponce & Carmona, 2011). However, the depositional model proposed by  
599 Ponce & Carmona (2011) assumes each independent lens-shaped geometry is created and reworked  
600 simultaneously, and subsequently draped as a result of flow deceleration. The Doornkloof sediment  
601 wave architecture cannot be explained by this process as the 'lenses' are clearly not disconnected  
602 (Figs 5 and 13). The distribution of truncation surfaces within the sediment waves of subunit B2 does  
603 however suggest there can be both phases of upstream swell formation as well as upstream  
604 migration of the crest line (e.g. *Bedform c* at log 34-35).

605 To explain the large fluctuations in flow concentration and depositional behaviour in CLTZ settings  
606 (Fig. 13), a number of factors can be considered. Here, we consider each of these factors in turn, and  
607 assess their potential for explaining the development of the sediment waves observed in this study.

#### 608 *Flow splitting in updip channel-levée systems*

609 Waxing and waning flow behaviour can be induced by splitting of the flow in the channel-levée  
610 system updip, where the primary 'channelised' flow may reach the sediment wave field earlier than  
611 the secondary 'overbank' flow (Peakall *et al.*, 2000). However, this would imply significant velocity  
612 and concentration differences and therefore significant depositional facies differences between the  
613 two stages, which does not fit the observations (Figs 13 and 14A). Furthermore, it would not explain  
614 the number of flow fluctuations interpreted within a single flow event bed (Figs 13 and 14A).

615 ~~Therefore, other mechanisms need to be proposed.~~

#### 616 *Mixed load (sand-clay) bedforms*

617 An alternative explanation for the sediment wave architecture could be that these bedforms formed  
 618 by flows with sand-clay mixtures. Complicated bedform architectures with both erosional and  
 619 depositional components have been created experimentally (Baas *et al.*, 2016). However, there are a  
 620 number of issues with this hypothesis: 1) the bedforms described from the two case studies are **one**  
 621 to two orders of magnitude larger than the 'muddy' bedforms described within flume tanks (Baas *et*  
 622 *al.*, 2016), and 2) the presence of clean climbing ripple-lamination suggests that at least part of the  
 623 flow was not clay-rich during deposition (Baas *et al.*, 2013; Schindler *et al.*, 2015).

Formatted: Space After: 10 pt, Don't hyphenate

624 *Froude number fluctuations*

Formatted: Font: Calibri

625 The net-depositional record of waxing and waning flow conditions (Fig. ~~*Froude number fluctuations*~~  
 626 ~~The net-depositional record of waxing and waning flow conditions (Fig. 14A)~~ **observed** at a single  
 627 **given** location within the Doornkloof sediment waves (Fig. 13) could be **hypothesised to be** a record  
 628 of temporal fluctuations around the critical Froude number separating sub- and **super-supercritical**  
 629 **flow conditions. However, the evidence for subcritical deposition across the full length of the**  
 630 **sediment waves, and over the timescale of bedform development, demonstrates that fluctuations**  
 631 **around the critical ~~flow~~ Froude number cannot be directly responsible for the formation of these**  
 632 **sediment waves. That said, fluctuations in velocity and capacity within a subcritical flow downstream**  
 633 **of a zone of hydraulic jumps may still play a role in controlling the observed sedimentation patterns.**

634 Fluctuations of the turbidity current Froude number are expected in areas of abrupt flow expansion  
 635 such as at the base-of-slope (Garcia, 1993; Wynn *et al.*, 2002b). Turbidity currents that undergo  
 636 rapid transitions from supercritical to subcritical conditions forming a single hydraulic jump, or  
 637 repeated hydraulic jumps across a CLTZ (Sumner *et al.*, 2013; Dorrell *et al.*, 2016), have been linked  
 638 to bedform formation (Vicente Bravo & Robles, 1995; Wynn & Stow, 2002; Wynn *et al.*, 2002b;  
 639 Symons *et al.*, 2016), and have been linked to the formation of erosive scours in upstream parts of  
 640 CLTZs in the Karoo Basin (Hofstra *et al.*, 2015). Due to the presence of multiple interacting hydraulic  
 641 jumps across a CLTZ, Froude number fluctuations around unity may be expected (Sumner *et al.*,

2013; Dorrell *et al.*, 2016). Such velocity fluctuations would change the capacity of the flow (Fig. 14A), however, whether this would translate to periodic changes in sediment concentration is less clear due in part to the lack of concentration measurements from natural and experimental subaqueous hydraulic jumps. That said, in turbidity currents generally, there is a close coupling between velocity and concentration changes (Felix *et al.*, 2005). Fluctuating velocities, and potentially concentration, related to variations in Froude numbers around critical may enable complicated and variable bedform architectures to be formed. ~~Here we examine the field evidence for such fluctuations.~~

~~The Doornkloof sediment waves (Fig. 13A) are composite features that show long depositional lee sides and short erosional stoss sides, and migrate upstream through truncation and draping at bed swelling locations (up to >10 m; Fig. 9) followed by the development of another bed swell upstream (Fig. 13A). This means that each swell initiates individually rather than simultaneously as a sinusoidal wave. The architecture most closely resembles the smaller scale type II and type III antidunal bedforms described by Schminke *et al.* (1973). However, these bedform architectures, which are an order of magnitude smaller, are interpreted to migrate through stoss side deposition by supercritical flows based on the field observations, and have never been produced experimentally. In contrast,~~

~~Kubo & Nakajima (2002) observed somewhat similar depositional patterns for sediment wave development, with individual growing mounds due to preferential deposition in combination with upstream migration of the waveform due to differential deposition, under subcritical flow conditions in physical and numerical experiments.~~

~~The morphology and architecture of the Doornkloof sediment waves contrast with large supercritical bedforms such as cyclic steps since these exhibit short erosional lee sides and long depositional stoss sides (Cartigny *et al.*, 2014; Hughes Clark, 2016), and form a single bedform structure rather than being composed of stacked smaller scale bedforms (e.g., Cartigny *et al.*, 2014; Covault *et al.*, 2017).~~

Formatted: Font: Calibri

667 In addition to the larger scale morphology and architecture, the nature and variability of small scale  
668 bedform structures (F3) (Fig. 13A) provide key indicators of flow type. This facies group (see Facies  
669 Characteristics) consists of climbing ripples, sinusoidal lamination, biconvex ripples, and hummock-  
670 like structures, with biconvex ripples sometimes transitioning upwards into the hummocks. Climbing  
671 ripples and sinusoidal lamination are indicators of subcritical flow (Allen, 1973; Southard &  
672 Boguchwal, 1990), and the biconvex ripples and hummock-like structures have greater affinities with  
673 combined flow ripples and hummocky cross stratification than with antidunes, again suggesting  
674 deposition under subcritical flow conditions. In particular, the vertical change from biconvex ripples  
675 to hummock-like bedforms is strongly analogous to structures associated with reflected flows in  
676 other turbidites (Tinterri, 2011; Tinterri & Muzzi Magalhaes, 2011), rather than with supercritical  
677 flow. The presence of topography in the form of the large-scale sediment wave may have led to flow  
678 reflection and deflection as and when the flow waned, in a similar manner to that envisaged by  
679 Tinterri (2011) for larger-scale topography.

680 The morphology, architecture, composite nature, and small-scale bedform types, all suggest that the  
681 sediment waves were clearly deposited under subcritical conditions. Consequently, fluctuations  
682 around the critical Froude number cannot be directly responsible for the formation of the sediment  
683 waves, albeit fluctuations in velocity and capacity within a subcritical flow downstream of a zone of  
684 hydraulic jumps may still play a role in controlling the observed sedimentation patterns.

685 The subcritical nature of these sediment waves, the observation of upstream accretion via  
686 deposition on the stoss side, and the associated upstream migration of the crestline, challenges the  
687 assumption that all upstream-orientated expansion of sediment waves is the product of supercritical  
688 conditions (Wynn & Stow, 2002; Symons *et al.*, 2016). That said, these bedforms appear to have  
689 sporadically migrated short distances (m's to tens of m's) through upstream accretion (Fig. 9B),  
690 before undergoing growth of new sediment wave lenses upstream (Fig. 14A), thus the entire  
691 bedform does not continuously migrate as observed in some modern sediment wave examples (e.g.,  
692 Hughes-Clark, 2016).



693 ~~Mixed load (sand-clay) bedforms~~

694 ~~An alternative explanation for the sediment wave architecture could be that these bedforms have~~

695 ~~been formed by flows with sand-clay mixtures. Complicated bedform architectures with both~~

696 ~~erosional and depositional components have been created experimentally (Baas et al., 2016).~~

697 ~~However, there are a number of issues with this hypothesis: 1) the bedforms described from the two~~

698 ~~case studies are of order of magnitude larger than the 'muddy' bedforms described within flume~~

699 ~~tanks (Baas et al., 2016), and 2) the presence of clean climbing ripple lamination suggests that at~~

700 ~~least part of the flow was not clay rich during deposition (Baas et al., 2013; Schindler et al., 2015).~~

701 ~~The 'hose effect' — Doornkloof section~~

702 A spatial control in flow character could also be invoked to explain the development of sediment

703 waves, based on flow-deposit interactions and the momentum of the flow core (Fig. 14B). As a

704 turbidity current exits channel confinement it does not directly lose its momentum (e.g. Choi &

705 Garcia, 2001). The flow core may shift around during bedform aggradation due to interactions with

706 depositional and erosional relief around the channel-mouth. Most studies on flow-deposit

707 interactions focus on temporal changes in flow conditions (e.g. Kneller & McCaffrey, 2003;

708 Groenenberg *et al.*, 2010), but rarely consider lateral changes within a single turbidity current

709 (Hiscott, 1994a). A single location within a sediment wave field may receive periods of high and low

710 energy linked to the lateral shifting of the flow core, where the energetic flow core can be linked to

711 periods of erosion and/or high concentration flow deposition, and the flow margin to deposition

712 from the less energetic and dilute parts of the flow. In this scenario, the upstream-orientated

713 truncation surfaces are the result of the interaction of the flow core with its self-produced obstacle

714 (Fig. 14B), linked to the inability to sustain the compensation process over time. Upstream

715 fluctuations in Froude number, related to an area of scour formation and hydraulic jumps, would

716 result in longitudinal waxing and waning flow behaviour downstream and could explain the

717 combination of both erosion and high concentration flow deposition of the flow core.

Formatted: Space After: 10 pt, Don't hyphenate

Formatted: Font: Calibri

1  
2  
3  
4  
5  
6 718 The compensational effects will form a stratigraphic record of fluctuating energy levels (Figs 13A and  
7  
8 719 14A). The lateral flow movement may explain deviation in palaeoflow direction between intra-bed  
9  
10 720 ripple-laminated intervals compared to sediment wave bed tops, observed within the Doornkloof  
11  
12 721 subunit B2 sediment waves (Figs 4A, 6F, 13 and ~~14A~~14B14), as it could represent (partial) flow  
13  
14 722 deflection affected by the evolving sediment wave morphology. Similar behaviour within a single  
15  
16 723 unconfined flow has been invoked in basin-floor settings of the Cloridorme Formation (Parkash,  
17  
18 724 1970; Parkash & Middleton, 1970) and at levée settings of the Amazon Channel (Hiscott *et al.*, 1997).  
19  
20 725 The 'hose effect' would result in a composite depositional record as the core of the flow sporadically  
21  
22 726 moves laterally, repeatedly superimposing high energy conditions onto lower energy conditions,  
23  
24 727 therefore explaining the inconsistency in ~~wavelength-sediment wave wavelengths~~. With this spatial  
25  
26 728 process, the locus of deposition will move laterally whilst the waning flow can lead to deposition  
27  
28 729 progressively migrating upstream. ~~This mechanism~~The hose effect may explain how sediment waves  
29  
30 730 are able to build upstream accreting geobodies without being deposited under supercritical  
31  
32 731 conditions. The mechanism also provides an explanation for the range and spatial variability of the  
33  
34 732 observed small-scale bedform structures (F3), and for the similarities with small-scale bedforms  
35  
36 733 interpreted to have been formed by turbidity currents interacting with topography (Tinterri, 2011;  
37  
38 734 Tinterri & Muzzi Magalhaes, 2011). As the flow migrates laterally, flows will interact at an angle with  
39  
40 735 the growing sediment wave, thus encouraging interaction of incident and reflected flow. ▲

Formatted: Font: +Body (Calibri)

41 736 As noted earlier, there is strong field-evidence (Parkash, 1970; Parkash & Middleton, 1970; Hiscott *et*  
42  
43 737 *al.*, 1997) for the 'hose effect' mechanism. However, the hose effect has not been experimentally or  
44  
45 738 numerically modelled, which reflects the ubiquity of bedform experiments in two-dimensional  
46  
47 739 flumes, and a paucity of three-dimensional flow effects on bedform development.  
48  
49 740 Spatio-temporal flow fluctuations - summary

50 741 In summary, the combination of waxing and waning flow behaviour in the subcritical flow core,  
51  
52 742 downstream of a zone of hydraulic jumps (Dorrell *et al.*, 2016), as well as spatial compensational  
53  
54  
55  
56  
57  
58  
59  
60

743 processes (hose effect) are invoked as the most probable mechanisms to explain the complicated  
744 architecture and facies patterns of the Doornkloof sediment waves.

745

746 ~~Bed-scale process record – Old Railway section~~

747 ~~In the Old Railway section (Fig. 11), erosional bed bases and bed amalgamation are common,~~

748 ~~particularly where there is depositional thinning of underlying beds, indicating that the ‘pinch and~~

749 ~~swell’ bedforms present at this section are the result of multiple flow events. However, bed~~

750 ~~amalgamation has limited impact on bedform thickness as thickness increase dominantly occurs~~

751 ~~down-dip of the point of amalgamation and is therefore of a depositional nature. The Old Railway~~

752 ~~bedforms classify as sediment waves (Wynn & Stow, 2002) with dimensions of 15 to >40 m~~

753 ~~wavelength (extending outside outcrop limits) and 1–2 m amplitude, however their maximum bed~~

754 ~~thicknesses (1–1.5 m) is more limited than at the Doornkloof area (>2.5 m), climbing ripple-laminated~~

755 ~~facies (F3) is more dominant, and banded facies (F2) are almost absent. The sediment waves have a~~

756 ~~more uniform facies distribution and there is an absence of internal truncation surfaces (Fig. 11).~~

757 ~~This suggests less spatial-temporal fluctuations of flows compared to the Doornkloof area. The~~

758 ~~dominance of F3 indicates rapid deposition from dilute turbulent flows, which contrasts with the~~

759 ~~Doornkloof area.~~

760 **Spatial variations within a sediment wave field**

Formatted: Font: 11 pt

761 ~~The character of the feeder channel could explain differences observed in CLTZ sediment wave~~

762 ~~character between the Doornkloof and Old Railway sections. As noted earlier, there are major~~

763 ~~differences between the sediment waves at the Old Railway outcrop with a low degree of spatial and~~

764 ~~temporal variability, and the high spatio-temporal variability observed in the Doornkloof sediment~~

765 ~~waves. Here, we will attempt to explain such variation between sediment waves in the same system.~~

766 ~~One potential mechanism is the character of the feeder channel, including factors such as channel~~

767 ~~dimensions and magnitude of the incoming flows. However, previous studies (Brunt *et al.*, 2013)~~

1  
2  
3  
4  
5  
6 768 suggest that the dimensions of feeder channels within the Unit B base-of-slope system were similar,  
7  
8 769 ~~suggesting~~implying that the character of sediment waves is unrelated to variations in feeder channel  
9  
10 770 character.

11  
12 771 Alternatively, the differences between the Doornkloof and Old Railway areas may be related to their  
13  
14 772 position relative to the mouth of the feeder channel. A dominance of lower flow-regime facies (F3)  
15  
16 773 such as climbing ripple-lamination is commonly associated with overbank or off-axis environments  
17  
18 774 (e.g. Kane & Hodgson, 2011; Brunt *et al.*, 2013; Rotzien *et al.*, 2014). As the Old Railway is  
19  
20 775 ~~characterized~~characterised by such facies, it could represent a fringe position through a sediment  
21  
22 776 wave field (Fig. 15). In contrast, the Doornkloof section is characterized by erosion and more  
23  
24 777 energetic facies (F1, F2, F4), suggesting it was situated in a more axial position in the sediment wave  
25  
26 778 field (Fig. ~~15~~15A). Furthermore, within the Doornkloof area, climbing ripple deposition (F3) becomes  
27  
28 779 more dominant at the top of the beds, likely reflecting progressive decrease in flow velocity and  
29  
30 780 concentration (Figs 5, 8 and 9B).

31 781 ~~Lateral~~These spatial and temporal variations can be integrated with the hypothesised lateral shifting  
32  
33 782 of the flow core (the ~~'hose effect')~~effect). The hose effect is likely to have more influence on  
34  
35 783 deposits within axial parts of the channel-mouth, such as within the Doornkloof area, where the flow  
36  
37 784 is most powerful. In contrast, the lateral fringes of the channel-mouth are most likely subject to  
38  
39 785 deposition from flow margins (Fig. ~~15~~15B), such as at the Old Railway section. This results in more  
40  
41 786 steady flow conditions and relatively uniform deposition of facies and explains the difference in  
42  
43 787 characteristics between the Old Railway sediment waves, which are dominated by F3 facies and  
44  
45 788 shows little evidence of erosion, and the Doornkloof sediment waves, which are dominated by F1  
46  
47 789 and F2 facies with substantial evidence of erosion.

48 790 The differences in the expression of the Unit B sediment waves suggest that the stratigraphic record  
49  
50 791 of CLTZ environments exhibit substantial spatial variability. The process model shows that initial  
51  
52 792 sediment wave architecture can involve both upstream orientated accretion (Doornkloof area), and  
53  
54  
55  
56  
57  
58  
59  
60

1  
2  
3  
4  
5  
6 793 | downstream orientated accretion (Old ~~railway~~Railway section) ~~within a single flow,~~ depending on  
7  
8 794 | the position with respect to the channel mouth. Despite the lack of 3D control on morphology, we  
9  
10 795 | predict that this variance in depositional behaviour between axial and fringe areas will have  
11  
12 796 | influence on planform crest morphology and will lead to the crest curvatures, which are commonly  
13  
14 797 | observed within the modern seafloor (e.g. Wynn *et al.*, 2002b). ~~Furthermore, due to the propagation~~  
15 798 | ~~of channel levée systems (e.g. Hodgson *et al.*, 2016), the preservation potential of sediment waves~~  
16  
17 799 | ~~in axial positions, such as those from the Doornkloof section, is lower than sediment wave deposits~~  
18  
19 800 | ~~in fringe positions, such as the Old Railway section (Fig. 15).~~ Similar observations on the importance  
20  
21 801 | of spatial variation have been made for the erosional bedform area (Fig. 15) of channel lobe  
22  
23 802 | transition zones (Hofstra *et al.*, 2015).

Formatted: Font: Not Italic

#### 804 Preservation of sediment waves in channel lobe transition zones

24  
25 803  
26  
27 804 | Preservation of sediment waves in channel lobe transition zones  
28  
29 805 | Two questions that remain unanswered are: 1) what conditions promoted stratigraphic preservation  
30  
31 806 | of the sediment waves in the examples herein, and 2) how likely is preservation of sediment waves  
32  
33 807 | in the stratigraphic record of channel lobe transition zones? Here, we interpret that the preservation  
34  
35 808 | of the sediment waves in the two field areas is related to the strongly aggradational character of  
36  
37 809 | subunits B1 and B2. This is also evident from the lobe deposits downdip that show strong  
38  
39 810 | aggradation and limited progradation (Fig. 3; Brunt *et al.*, 2013), in comparison to lobe deposits  
40  
41 811 | elsewhere in the Karoo Basin (e.g., Hodgson *et al.*). The preservation of the sediment waves in the  
42  
43 812 | Doornkloof area is interpreted to be related to the strong aggradational character of Unit B, also  
44  
45 813 | evident from the lobe deposits downdip (Brunt *et al.*, 2013). 2006; van der Merwe *et al.*, 2014).  
46  
47 814 | Furthermore, subunit B1 is abruptly overlain by a regional mudstone aiding preservation, whereas  
48  
49 815 | subunit B2 is overlain by thick levée successions (subunit B3), marking the progradation of the slope  
50  
51 816 | system across the CLTZ (Brunt *et al.*, 2013). This scenario has similarities to that proposed by

Formatted: Font: Not Italic

1  
2  
3  
4  
5  
6 817 Pemberton *et al.* (2016) who suggested that preservation of scours in a CLTZ was linked to a rapidly  
7  
8 818 prograding slope system.  
9  
10 819 For sediment waves in CLTZ settings in general, there are several scenarios that can be proposed to  
11  
12 820 facilitate their preservation. During system initiation at the start of a waxing-to-waning sediment  
13  
14 821 supply cycle, possibly driven by a relative sea-level fall and initial slope incision, the position of the  
15  
16 822 CLTZ on the base-of-slope might be relatively stable as slope conduits evolve prior to slope  
17  
18 823 progradation. The stratigraphic record of the resulting deposits is likely limited in thickness, and  
19  
20 824 probably preferentially associated with scour-fills (e.g., Pemberton *et al.*, 2016). The position of the  
21  
22 825 CLTZ could be fixed through physiographic features, such as a tectonic or diapiric break-in-slope,  
23  
24 826 which would aid the stratigraphic preservation of the CLTZ. Several studies have shown that when  
25  
26 827 submarine channel-levée systems avulse they do not return to their original route (e.g. Armitage *et*  
27  
28 828 *al.*, 2012; Ortiz-Karpf *et al.*, 2015; Morris *et al.*, 2016), which would help to preserve sediment waves  
29  
30 829 in an abandoned CLTZ. The stratigraphic evidence for this control would be in the sediment waves  
31  
32 830 abruptly overlain by mudstone or thin-bedded successions indicative of overbank deposition. Finally,  
33  
34 831 the preservation potential of sediment waves in CLTZs will be higher at the point of maximum  
35  
36 832 regression/progradation of the system (Hodgson *et al.*, 2016). Similar arguments were applied to the  
37  
38 833 preservation of scour-fills in CLTZ by Hofstra *et al.* (2015).  
39  
40 834 In summary, we hypothesise that preservation of sediment waves may require i) updip avulsion, ii)  
41  
42 835 represent the point of maximum system progradation, or iii) form during a period of relative spatial  
43  
44 836 stability, followed by system progradation. Subsequent rapid progradation of a slope system is then  
45  
46 837 important for long-term preservation, though an off-axis location relative to large-scale slope  
47  
48 838 channels is critical in order to avoid cannibalisation of the CLTZ deposits (e.g., Hofstra *et al.*, 2015).  
49  
50 839 Such propagation of channel-levée systems (e.g. Hodgson *et al.*, 2016), suggests that the  
51  
52 840 preservation potential of sediment waves in axial positions, for example the interpreted position of  
53  
54 841 the Doornkloof section, is lower than sediment wave deposits in fringe positions, such as the  
55  
56 842 interpreted position of the Old Railway section (Fig. 15A).  
57  
58  
59  
60

843

844 **CONCLUSIONS**

845 Detailed morphologies, architectures and facies of fine-sand grained sediment waves are reported  
846 from an ancient channel-lobe transition zone. -The sediment waves are constructed from banded  
847 and planar-laminated sandstones, as well as from progressive aggradation of a range of small-scale  
848 bedforms, including climbing ripples, sinusoidal lamination, biconvex ripples, and hummocky-like  
849 structures, interpreted as the products of subcritical deposition, with periods of flow reflection and  
850 deflection forming the biconvex ripples and hummocks. Morphologically, the sediment waves  
851 exhibit long-lee sides, and short erosively-cut stoss sides, and show upstream accretion over short  
852 distances (m's to tens of m's), punctuated by the upstream development of new sediment wave  
853 lenses. Consequently, the observations from these exhumed deposits challenge some current  
854 models of sediment wave development, which suggest that entire sediment waves continuously  
855 migrate upstream under supercritical conditions. In particular, the outcrops demonstrate that the  
856 formation of sediment waves in an upstream direction, as well as upstream migration of crestlines, is  
857 not solely the product of supercritical flows, but can also occur in subcritical conditions. The  
858 progressive development of the sediment waves is argued to be the product of lateral migration of  
859 the expanding flow across the channel-lobe transition zone, potentially coupled to fluctuations in  
860 velocity and flow capacity related to upstream hydraulic jumps. Variations in sediment waves, from  
861 more complex forms with multiple erosive surfaces and complex internal facies, to simple  
862 accretionary forms with abundant climbing ripples, is linked to position across the channel-lobe  
863 transition zone, from axial to lateral fringes respectively. -The preservation potential of sediment  
864 waves in CLTZs into the stratigraphic record is low due to subsequent system progradation and  
865 erosion. However, preservation is higher where there is updip avulsion and abandonment of a CLTZ,  
866 in off axis areas where sediment waves might be overlain by overbank sediments, and / or at the  
867 point of maximum system progradation.

1  
2  
3  
4  
5  
6 868 **ACKNOWLEDGEMENTS**  
7

8 869 This work forms part of the results of the LOBE 2 joint industry consortium research project. We are  
9  
10 870 grateful for the financial support from: Anadarko, Bayerngas Norge, BG Group, BHP Billiton, BP,  
11  
12 871 Chevron, Dong Energy, E.ON, GDF Suez, Maersk Oil, Marathon Oil, Petrobras, Shell, Statoil, Total,  
13  
14 872 VNG Norge, and Woodside. We are grateful to Matthieu Cartigny, [Brian Romans](#) and an anonymous  
15  
16 873 reviewer for the constructive reviews, ~~which greatly improved this manuscript~~, and for the input of  
17  
18 874 Associate Editor Jaco Baas, ~~which greatly improved this manuscript~~. We also acknowledge the  
19  
20 875 landowners from the Laingsburg area for access to their land. Finally, Renée de Bruijn, Nienke Lips  
21  
22 876 and Yvonne Spychala are thanked for their assistance in the field.  
23  
24  
25  
26  
27  
28  
29  
30  
31  
32  
33  
34  
35  
36  
37  
38  
39  
40  
41  
42  
43  
44  
45  
46  
47  
48  
49  
50  
51  
52  
53  
54  
55  
56  
57  
58  
59  
60



877 **REFERENCES**

- 878 **Alexander, J., Bridge, J.S., Cheel, R.J. and Leclair, S.F.** (2001) Bedforms and associated sedimentary  
879 structures formed under supercritical water flows over aggrading sand beds. *Sedimentology*, **48**,  
880 133-152.
- 881 **Allen, J.R.L.** (1973) A classification of climbing-ripple cross-lamination. *Journal of the Geological*  
882 *Society of London*, **129**, 537-541.
- 883 **Allen, J.R.L.** (1984) Parallel lamination developed from upper-stage plane beds: a model based on  
884 the larger coherent structures of the turbulent boundary layer. *Sedimentary Geology*, **39**, 227-242.
- 885 [Armitage, D.A., McHargue, T., Fildani, A. and Graham, S.A. \(2012\) Postavulsion channel evolution:](#)  
886 [Niger Delta continental slope. \*AAPG Bulletin\*, \*\*96\*\*, 823-843.](#)
- 887 **Baas, J.H. and de Koning, H.** (1995) Washed-out ripples: Their equilibrium dimensions, migration  
888 rate, and relation to suspended-sediment concentration in very fine sand. *Journal of Sedimentary*  
889 *Research*, **65**, 431-435.
- 890 **Baas, J.H., Davies, A.G. and Malarkey, J.** (2013) Bedform development in mixed sand-mud: The  
891 contrasting role of cohesive forces in flow and bed. *Geomorphology*, **182**, 19-32.
- 892 **Baas, J.H., Best, J.L. and Peakall, J.** (2016) Predicting bedforms and primary current stratification in  
893 cohesive mixtures of mud and sand. *Journal of the Geological Society*, **173**, 12-45.
- 894 **Best, J. and Bridge, J.** (1992) The morphology and dynamics of low amplitude bedwaves upon upper  
895 stage plane beds and the preservation of planar laminae. *Sedimentology*, **39**, 737-752.
- 896 **Bouma, A.H. and Boerma, J.A.K.** (1968) Vertical disturbances in piston cores. *Marine Geology*, **6**,  
897 231-241.

- 1  
2  
3  
4  
5  
6 898 **Brunt, R.L., Hodgson, D.M., Flint, S.S., Pringle, J.K., Di Celma, C., Prélat, A. and Grecula, M.** (2013)  
7  
8 899 Confined to unconfined: Anatomy of a base of slope succession, Karoo Basin, South Africa. *Marine*  
9  
10 900 *and Petroleum Geology*, **41**, 206-221.  
11  
12 901 **Campion, K.T., Dixon, B.T. and Scott, E.D.** (2011) Sediment waves and depositional implications for  
13  
14 902 fine-grained rocks in the Cerro Toro Formation (Upper Cretaceous), Silla Syncline, Chile. *Marine and*  
15  
16 903 *Petroleum Geology*, **28**, 761-784.  
17  
18 904 **Cartigny, M.J., Eggenhuisen, J.T., Hansen, E.W. and Postma, G.** (2013) Concentration-dependent  
19  
20 905 flow stratification in experimental high-density turbidity currents and their relevance to turbidite  
21  
22 906 facies models. *Journal of Sedimentary Research*, **83**, 1047-1065.  
23  
24 907 **Cartigny, M.J.B., Ventra, D., Postma, G. and Van Den Berg, J.H.** (2014) Morphodynamics and  
25  
26 908 sedimentary structures of bedforms under supercritical-flow conditions: New insights from flume  
27  
28 909 experiments. *Sedimentology*, **61**, 712-748.  
29  
30 910 **Choi, S.U. and Garcia, M.H.** (2001) Spreading of gravity plumes on an incline. *Coastal Engineering*  
31  
32 911 *Journal*, **43**, 221-237.  
33  
34 912 **Covault, J.A., Kostic, S., Paull, C.K., Sylvester, Z. and Fildani, A.** (2017) Cyclic steps and related  
35  
36 913 supercritical bedforms: Building blocks of deep-water depositional systems, western North America.  
37  
38 914 *Marine Geology*, **393**, 4-20, doi:10.1016/j.margeo.2016.12.009  
39  
40 915 **Damuth, J.E.** (1979) Migrating sediment waves created by turbidite currents in northern South China  
41  
42 916 Basin. *Geology*, **7**, 520-523.  
43  
44 917 **Dorrell, R.M., Peakall, J., Sumner, E.J., Parsons, D.R., Darby, S.E., Wynn, R.B., Özsoy, E. and Tezcan,**  
45  
46 918 **D.** (2016) Flow dynamics and mixing processes in hydraulic jump arrays: Implications for channel-  
47  
48 919 lobe transition zones. *Marine Geology*, **381**, 181-193.  
49  
50  
51  
52  
53  
54  
55  
56  
57  
58  
59  
60

- 1  
2  
3  
4  
5  
6 920 **Dumas, S. and Arnott, R.W.C.** (2006) Origin of hummocky and swaley cross-stratification— The  
7  
8 921 controlling influence of unidirectional current strength and aggradation rate. *Geology*, **34**, 1073-  
9  
10 922 1076.  
11  
12 923 **Dumas, S., Arnott, R.W.C. and Southard, J.B.** (2005) Experiments on oscillatory-flow and combined-  
13  
14 924 flow bed forms: Implications for interpreting parts of the shallow-marine sedimentary record.  
15  
16 925 *Journal of Sedimentary Research*, **75**, 501-513.  
17  
18 926 **Eggenhuisen, J.T., McCaffrey, W.D., Houghton, P.D. and Butler, R.W.** (2011) Shallow erosion  
19  
20 927 beneath turbidity currents and its impact on the architectural development of turbidite sheet  
21  
22 928 systems. *Sedimentology*, **58**, 936-959.  
23  
24 929 **Fedele, J.J., Hoyal, D., Barnaal, Z., Tulenko, J. and Awatt, S.** (2017) Bedforms created by gravity  
25  
26 930 flows. In: Budd, D.A., Hajek, E.A. and Purkis, S.J. (Eds) *Autogenic Dynamics and Self-organization in*  
27  
28 931 *Sedimentary Systems*. SEPM Special Publication 106, 95-121.  
29  
30 932 **Felix, M., Sturton, S. and Peakall, J.** (2005) Combined measurements of velocity and concentration  
31  
32 933 in experimental turbidity currents. *Sedimentary Geology*, **179**, 31-47.  
33  
34  
35 934 **Flint, S.S., Hodgson, D.M., Sprague, A., Brunt, R.L., Van Der Merwe, W.C., Figueiredo, J., Prélat, A.,**  
36  
37 935 **Box, D., Di Celma, C. and Kavanagh, J.P.** (2011) Depositional architecture and sequence stratigraphy  
38  
39 936 of the Karoo basin floor to shelf edge succession, Laingsburg depocentre, South Africa. *Marine and*  
40  
41 937 *Petroleum Geology*, **28**, 658-674.  
42  
43 938 **Garcia, M.H.** (1993) Hydraulic jumps in sediment-driven bottom currents. *Journal of Hydraulic*  
44  
45 939 *Engineering*, **119**, 1094-1117.  
46  
47 940 **Garcia, M.H.** (2008) *Sedimentation Engineering: Process, Measurements, Modeling and Practice.*  
48  
49 941 American Society of Civil Engineers, Reston, Virginia.  
50  
51  
52  
53  
54  
55  
56  
57  
58  
59  
60

- 1  
2  
3  
4  
5  
6 942 **Grechula, M., Flint, S.S., Wickens, H.DeV. and Johnson, S.D.** (2003) Upward-thickening patterns and  
7  
8 943 lateral continuity of Permian sand-rich turbidite channel fills, Laingsburg Karoo, South Africa.  
9  
10 944 *Sedimentology*, **50**, 831-853.  
11  
12 945 **Groenenberg, R.M., Hodgson, D.M., Pr lat, A., Luthi, S.M. and Flint, S.S.** (2010) Flow-deposit  
13  
14 946 interaction in submarine lobes: insights from outcrop observations and realizations of a process-  
15  
16 947 based numerical model. *Journal of Sedimentary Research*, **80**, 252-267.  
17  
18 948 [Hamilton, P., Gaillot, G., Strom, K., Fedele, J. and Hoyal, D. \(2017\) Linking hydraulic properties in](#)  
19  
20 949 [supercritical submarine distributary channels to depositional lobe geometry. \*Journal of Sedimentary\*](#)  
21  
22 950 [Research](#), **87**, 935-950.  
23  
24 951 **Harms, J.C.** (1969) Hydraulic significance of some sand ripples. *Geological Society of America*  
25  
26 952 *Bulletin*, **80**, 363-396.  
27  
28 953 **Harms, J.C., Southard, J.B., Spearing, D.R. and Walker, R.G.** (1975) *Depositional environments as*  
29  
30 954 *interpreted from primary sedimentary structures and stratification sequences*. Society for  
31  
32 955 Sedimentary Geology (SEPM) Short Course 2, pp. 161.  
33  
34 956 **Haughton, P., Davis, C., McCaffrey, W. and Barker, S.** (2009) Hybrid sediment gravity flow deposits-  
35  
36 957 classification, origin and significance. *Marine and Petroleum Geology*, **26**, 1900-1918.  
37  
38 958 **Heini , P. and Davies R.J.** (2009) Trails of depressions and sediment waves along submarine  
39  
40 959 channels on the continental margin of Espirito Santo Basin, Brazil. *Geological Society of America*  
41  
42 960 *Bulletin*, **121**, 698-711.  
43  
44 961 **Hiscott, R.N.** (1994a) Loss of capacity, not competence, as the fundamental process governing  
45  
46 962 deposition from turbidity currents. *Journal of Sedimentary Research*, **64**, 209-214.  
47  
48 963 **Hiscott, R.N.** (1994b) Traction-carpet stratification in turbidites-fact or fiction? *Journal of*  
49  
50 964 *Sedimentary Research*, **64**, 204-208.  
51  
52  
53  
54  
55  
56  
57  
58  
59  
60

965 **Hiscott, R.N., Hall, F.R., and Pirmez, C.** (1997) Turbidity-current overspill from the Amazon Channel:  
966 texture of the silt/sand load, paleoflow from anisotropy of magnetic susceptibility, and implications  
967 for flow processes. In: *Proceedings of the Ocean Drilling Program, Scientific Results* (Eds. Flood, R.D.,  
968 Piper, D.J.W., Klaus, A. and Peterson, I.C.), **155**, 53-78.

969 **Hodgson, D.M., [Flint, S.S., Hodgetts, D., Drinkwater, N.J., Johannessen, E.P. and Luthi, S.M. \(2006\)](#)**  
970 **[Stratigraphic evolution of fine-grained submarine fan systems, Tanqua depocenter, Karoo Basin,](#)**  
971 **[South Africa. \*Journal of Sedimentary Research\*, \*\*76\*\*, 20-40.](#)**

972 **[Hodgson, D.M., Di Celma, C.N., Brunt, R.L. and Flint, S.S. \(2011\)](#)** Submarine slope degradation and  
973 aggradation and the stratigraphic evolution of channel-levee systems. *Journal of the Geological*  
974 *Society*, **168**, 625-628.

975 **Hodgson, D.M., Kane, I.A., Flint, S.S., Brunt, R.L. and Ortiz-Karpf, A.** (2016). Time-transgressive  
976 confinement on the slope and the progradation of basin-floor fans: Implications for the sequence  
977 stratigraphy of deep-water deposits. *Journal of Sedimentary Research*, **86**, 73-86.

978 **Hofstra, M.** **[\(2016\) The Stratigraphic Record of Submarine Channel-lobe Transition Zones.](#)**  
979 **[Unpublished PhD thesis, University of Leeds, Leeds, 331p.](#)**

980 **[Hofstra, M., Hodgson, D.M., Peakall, J. and Flint, S.S. \(2015\)](#)** Giant scour-fills in ancient channel-lobe  
981 transition zones: Formative processes and depositional architecture. *Sedimentary Geology*, **329**, 98-  
982 114.

983 **Howe, J.A.** (1996) Turbidite and contourite sediment waves in the northern Rockall Trough, North  
984 Atlantic Ocean. *Sedimentology*, **43**, 219-234.

985 **Hughes Clarke, J.E.** (2016) First wide-angle view of channelized turbidity currents links migrating  
986 cyclic steps to flow characteristics. *Nature Communications*, 7:11896, doi: 10.1038/ncomms11896.

- 1  
2  
3  
4  
5  
6 987 **Ito, M.** (2008) Downfan transformation from turbidity currents to debris flows at a channel-to-lobe  
7  
8 988 transitional zone: the lower Pleistocene Otadai Formation, Boso Peninsula, Japan. *Journal of*  
9  
10 989 *Sedimentary Research*, **78**, 668-682.
- 11  
12 990 **Ito, M.** (2010) Are coarse-grained sediment waves formed as downstream-migrating antidunes?  
13  
14 991 Insight from an early Pleistocene submarine canyon on the Boso Peninsula, Japan. *Sedimentary*  
15  
16 992 *Geology*, **226**, 1-8.
- 17  
18 993 **Ito, M.** and **Saito, T.** (2006) Gravel waves in an ancient canyon: Analogous features and formative  
19  
20 994 processes of coarse-grained bedforms in a submarine-fan system, the lower Pleistocene of the Boso  
21  
22 995 Peninsula, Japan. *Journal of Sedimentary Research*, **76**, 1274-1283.
- 23  
24 996 **Ito, M.**, **Ishikawa, K.** and **Nishida, N.** (2014) Distinctive erosional and depositional structures formed  
25  
26 997 at a canyon mouth: A lower Pleistocene deep-water succession in the Kasuza forearc basin on the  
27  
28 998 Boso Peninsula, Japan. *Sedimentology*, **61**, 2042-2062.
- 29  
30 999 **Jobe, Z.R.**, **Lowe, D.R.** and **Morris, W.R.** (2012) Climbing-ripple successions in turbidite systems:  
31  
32 1000 depositional environments, sedimentation rates and accumulation times. *Sedimentology*, **59**, 867-  
33  
34 1001 898.
- 35  
36 1002 **Johansson, M.** and **Stow, D.A.V.** (1995) A classification scheme for shale clasts in deep water  
37  
38 1003 sandstones. In: Hartley, A.J. and Prosser, D.J. (eds.) *Characterization of Deep Marine Clastic Systems*,  
39  
40 1004 Geological Society Special Publication 94, 221-241.
- 41  
42 1005 **Jopling, A.V.** and **Walker, R.G.** (1968) Morphology and origin of ripple-drift cross-lamination, with  
43  
44 1006 examples from the Pleistocene of Massachusetts. *Journal of Sedimentary Research*, **38**, 971-984.
- 45  
46 1007 **Kane, I.A.** and **Hodgson, D.M.** (2011) Sedimentological criteria to differentiate submarine channel  
47  
48 1008 levee subenvironments: exhumed examples from the Rosario Fm. (Upper Cretaceous) of Baja  
49  
50 1009 California, Mexico, and the Fort Brown Fm. (Permian), Karoo basin, S. Africa. *Marine and Petroleum*  
51  
52 1010 *Geology*, **28**, 807-823.
- 53  
54  
55  
56  
57  
58  
59  
60

- 1  
2  
3  
4  
5  
6 1011 **Kane, I.A., McCaffrey, W.D. and Martinsen, O.J.** (2009) Allogenic vs. autogenic controls on  
7  
8 1012 megaflute formation. *Journal of Sedimentary Research*, **79**, 643-651.  
9  
10 1013 **Kennedy, J.F.** (1969) The formation of sediment ripples, dunes and antidunes. *Annual Review of*  
11  
12 1014 *Fluid Mechanics*, **1**, 147-168.  
13  
14  
15 1015 **Kidd, R.B., Lucchi, R.G., Gee, M. and Woodside, J.M.** (1998) Sedimentary processes in the Stromboli  
16  
17 1016 Canyon and Marsili Basin, SE Tyrrhenian Sea: results from side-scan sonar surveys. *Geo-Marine*  
18  
19 1017 *Letters*, **18**, 146-154.  
20  
21 1018 **Kneller, B.** (1995) Beyond the turbidite paradigm: physical models for deposition of turbidites and  
22  
23 1019 their implications for reservoir prediction. In: *Characterization of Deep Marine Clastic Systems* (Eds.  
24  
25 1020 Hartley, A.J. and Prosser, D.J.) *Geol. Soc. London, Spec. Publ.*, **94**, 31-49.  
26  
27 1021 **Kneller, B.C. and Branney, M.J.** (1995) Sustained high-density turbidity currents and the deposition  
28  
29 1022 of thick massive sands. *Sedimentology*, **42**, 607-616.  
30  
31 1023 **Kneller, B.C. and McCaffrey, W.D.** (1999) Depositional effects of flow nonuniformity and  
32  
33 1024 stratification within turbidity currents approaching a bounding slope: deflection, reflection, and  
34  
35 1025 facies variation. *Journal of Sedimentary Research*, **69**, 980-991.  
36  
37 1026 **Kneller, B.C. and McCaffrey, W.D.** (2003) The interpretation of vertical sequences in turbidite beds:  
38  
39 1027 the influence of longitudinal flow structure. *Journal of Sedimentary Research*, **73**, 706-713.  
40  
41 1028 **Kubo, Y.** (2004) [Experimental and numerical study of topographic effects on deposition from two-](#)  
42  
43 1029 [dimensional, particulate-driven density currents. \*Sedimentary Geology\*, \*\*164\*\*, 311-326.](#)  
44  
45 1030 **Kubo, Y.** and **Nakajima, T.** (2002) Laboratory experiments and numerical simulation of sediment-  
46  
47 1031 wave formation by turbidity currents. *Marine Geology*, **192**, 105-121.  
48  
49 1032 **Lonsdale, P. and Hollister, C.D.** (1979) Near-bottom traverse of Rockall Trough-Hydrographic and  
50  
51 1033 geological inferences. *Oceanologica Acta*, **2**, 91-105.  
52  
53  
54  
55  
56  
57  
58  
59  
60

- 1  
2  
3  
4  
5  
6 1034 **Lowe, D.R.** (1982) Sediment gravity flows: II Depositional models with special reference to the  
7  
8 1035 deposits of high-density turbidity currents. *Journal of Sedimentary Research*, **52**, 279-297.  
9  
10 1036 **Macdonald, H.A., Wynn, R.B., Huvenne, V.A., Peakall, J., Masson, D.G., Weaver, P.P. and McPhail,**  
11  
12 1037 **S.D.** (2011) New insights into the morphology, fill, and remarkable longevity (>0.2 m.y.) of modern  
13  
14 1038 deep-water erosional scours along the northeast Atlantic margin. *Geosphere*, **7**, 845-867.  
15  
16 1039 **Malinverno, A., Ryan, W.B., Auffret, G. and Pautot, G.** (1988) Sonar images of the path of recent  
17  
18 1040 failure events on the continental margin off Nice, France. In: *Sedimentological Consequences of*  
19  
20 1041 *Convulsive Geologic Events*, (Ed. Clifton, H.E.), *Geological Society of America Special Paper*, **229**, 59-  
21  
22 1042 76.  
23  
24 1043 **McHugh, C.M. and Ryan, W.B.** (2000) Sedimentary features associated with channel overbank flow:  
25  
26 1044 examples from the Monterey Fan. *Marine Geology*, **163**, 199-215.  
27  
28 1045 **Migeon, S., Savoye, B., Zanella, E., Mulder, T., Faugères, J.C. and Weber, O.** (2001) Detailed seismic-  
29  
30 1046 reflection and sedimentary study of turbidite waves on the Var Sedimentary Ridge (SE France):  
31  
32 1047 significance for sediment transport and deposition and for the mechanisms of sediment-wave  
33  
34 1048 construction. *Marine and Petroleum Geology*, **18**, 179-208.  
35  
36 1049 **Morris, S.A., Kenyon, N.H., Limonov, A.F. and Alexander, J.** (1998) Downstream changes of large-  
37  
38 1050 scale bedforms in turbidites around the Valencia channel mouth, north-west Mediterranean:  
39  
40 1051 implications for palaeoflow reconstruction. *Sedimentology*, **45**, 365-377.  
41  
42 1052 **Morris, E.A., Hodgson, D.M., Brunt, R.L. and Flint, S.S.** (2014) Origin, evolution and anatomy of silt-  
43  
44 1053 prone submarine external levées. *Sedimentology*, **61**, 1734-1763.  
45  
46 1054 [Morris, E.A., Hodgson, D.M., Flint, S., Brunt, R.L., Luthi, S.M. and Kolenberg, Y. \(2016\) Integrating](#)  
47  
48 1055 [outcrop and subsurface data to assess the temporal evolution of a submarine channel–levee system.](#)  
49  
50 1056 [AAPG Bulletin](#), **100**, 1663-1691.  
51  
52  
53  
54  
55  
56  
57  
58  
59  
60



- 1  
2  
3  
4  
5  
6 1057 **Mulder, T. and Alexander, J.** (2001) The physical character of subaqueous sedimentary density flows  
7  
8 1058 and their deposits. *Sedimentology*, **48**, 269-299.  
9  
10 1059 **Mukti, M.M.R. and Ito, M.** (2010) Discovery of outcrop-scale fine-grained sediment waves in the  
11  
12 1060 lower Halang Formation, an upper Miocene submarine-fan succession in West Java. *Sedimentary*  
13  
14 1061 *Geology*, **231**, 55-62.  
15  
16 1062 **Mutti, E. and Normark, W.R.** (1987) Comparing examples of modern and ancient turbidite systems:  
17  
18 1063 problems and concepts. In: *Marine Clastic Sedimentology: Concepts and Case Studies* (Eds. Leggett,  
19  
20 1064 J.K. and Zuffa, G.G.) *Graham and Trotman, Oxford*, pp. 1-38.  
21  
22 1065 **Mutti, E. and Normark, W.R.** (1991) An integrated approach to the study of turbidite systems. In:  
23  
24 1066 *Seismic Facies and Sedimentary Processes of Submarine Fans and Turbidite Systems* (Eds. Weimer, P.  
25  
26 1067 and Link, M.H.) *Springer, New York*, pp. 75-106.  
27  
28 1068 **Nakajima, T., Satoh, M. and Okamura, Y.** (1998) Channel-levee complexes, terminal deep-sea fan  
29  
30 1069 and sediment wave fields associated with the Toyama Deep-Sea Channel system in the Japan Sea.  
31  
32 1070 *Marine Geology*, **147**, 25-41.  
33  
34 1071 **Normark, W.R. and Dickson, F.H.** (1976) Sublacustrine fan morphology in Lake Superior. *AAPG*  
35  
36 1072 *Bulletin*, **60**, 1021-1036.  
37  
38 1073 **Normark, W.R. and Piper, D.J.W.** (1991) Initiation processes and flow evolution of turbidity currents:  
39  
40 1074 Implications for the depositional record. In: *From Shoreline to Abyss: Contributions in Marine*  
41  
42 1075 *Geology in Honor of Francis Parker Shepard* (Ed. Osborne, R.H.), *SEPM Special Publication*, **46**, 207-  
43  
44 1076 230.  
45  
46 1077 **Normark W.R., Hess, G.R., Stow, D.A.V. and Bowen, A.J.** (1980) Sediment waves on the Monterey  
47  
48 1078 Fan levee: a preliminary physical interpretation. *Marine Geology*, **37**, 1-18.  
49  
50 1079 **Normark, W.R., Piper, D.J., Posamentier, H. Pirmez, C. and Migeon, S.** (2002) Variability in form and  
51  
52 1080 growth of sediment waves on turbidite channel levees. *Marine Geology*, **192**, 23-58.  
53  
54  
55  
56  
57  
58  
59  
60

- 1  
2  
3  
4  
5  
6 1081 [Ortiz-Karpf, A., Hodgson, D.M. and McCaffrey, W.D. \(2015\) The role of mass-transport complexes in](#)  
7  
8 1082 [controlling channel avulsion and the subsequent sediment dispersal patterns on an active margin:](#)  
9  
10 1083 [the Magdalena Fan, offshore Colombia. \*Marine and Petroleum Geology\*, \*\*64\*\*, 58-75.](#)  
11  
12 1084 **Palanques, A., Kenyon, N.H., Alonso, B. and Limonov, A.** (1995) Erosional and depositional patterns  
13  
14 1085 in the Valencia mouth: An example of a modern channel-lobe transition zone channel. *Marine*  
15  
16 1086 *Geophysical Researches*, **17**, 503-517.  
17  
18 1087 **Parkash, B.** (1970) Downcurrent changes in sedimentary structures in Ordovician turbidite  
19  
20 1088 greywackes. *Journal of Sedimentary Research*, **40**, 572-590.  
21  
22 1089 **Parkash, B. and Middleton, G.V.** (1970) Downcurrent textural changes in Ordovician turbidite  
23  
24 1090 greywackes. *Sedimentology*, **14**, 259-293.  
25  
26 1091 **Peakall, J., McCaffrey, W.D. and Kneller, B.C.** (2000) A process model for the evolution, morphology,  
27  
28 1092 and architecture of sinuous submarine channels. *Journal of Sedimentary Research*, **70**, 434-448.  
29  
30 1093 [Pemberton, E.A.L., Hubbard, S.M., Fildani, A., Romans, B. and Stright, L. \(2016\) The stratigraphic](#)  
31  
32 1094 [expression of decreasing confinement along a deep-water sediment routing system: Outcrop](#)  
33  
34 1095 [example from southern Chile. \*Geosphere\*, \*\*12\*\*, 114-134.](#)  
35  
36 1096 **Piper, D.J.W. and Kontopoulos, N.** (1994) Bed forms in submarine channels: comparison of ancient  
37  
38 1097 examples from Greece with studies of Recent turbidite systems. *Journal of Sedimentary Research*,  
39  
40 1098 **64**, 247-252.  
41  
42 1099 **Piper, D.J.W., Shor, A.N., Farre, J.A., O'Connell, S. and Jacobi, R.** (1985) Sediment slides and  
43  
44 1100 turbidity currents on the Laurentian Fan: Sidescan sonar investigations near the epicenter of the  
45  
46 1101 1929 Grand Banks earthquake. *Geology*, **13**, 538-541.  
47  
48 1102 **Ponce, J.J. and Carmona, N.** (2011) Coarse-grained sediment waves in hyperpycnal clinoform  
49  
50 1103 systems, Miocene of the Austral foreland basin, Argentina. *Geology*, **39**, 763-766.  
51  
52  
53  
54  
55  
56  
57  
58  
59  
60

- 1  
2  
3  
4  
5  
6 1104 **Postma, G., Kleverlaan, K. and Cartigny, M.J.B.** (2014) Recognition of cyclic steps in sandy and  
7  
8 1105 gravelly turbidite sequences and consequences for the Bouma facies. *Sedimentology*, **61**, 2268-2290.  
9  
10 1106 **Praeg, D.B. and Schafer, C.T.** (1989) Seabed features of the Labrador slope and rise near 55° N  
11  
12 1107 revealed by SEAMARC I sidescan sonar imagery. *Atlantic Geoscience Centre, Bedford Institute of*  
13  
14 1108 *Oceanography*.  
15  
16 1109 **Prave, A.R. and Duke, W.L.** (1990) Small-scale hummocky cross-stratification in turbidites: a form of  
17  
18 1110 antidune stratification? *Sedimentology*, **37**, 531-539.  
19  
20 1111 **Prélat, A. and Hodgson, D.M.** (2013) The full range of turbidite bed thickness patterns in submarine  
21  
22 1112 lobes: controls and implications. *Journal of the Geological Society*, **170**, 209-214.  
23  
24 1113 [Prélat, A., Hodgson D.M. and Flint, S.S. \(2009\) Evolution, architecture and hierarchy of distributary](#)  
25  
26 1114 [deep-water deposits: a high-resolution outcrop investigation from the Permian Karoo Basin, South](#)  
27  
28 1115 [Africa. \*Sedimentology\*, \*\*56\*\*, 2132-2154.](#)  
29  
30 1116 [Prélat, A., Covault J.A., Hodgson D.M., Fildani, A. and Flint, S.S. \(2010\) Intrinsic controls on the](#)  
31  
32 1117 [range of volumes, morphologies, and dimensions of submarine lobes. \*Sedimentary Geology\*, \*\*232\*\*, 66-](#)  
33  
34 1118 [76.](#)  
35  
36 1119 **Pringle, J.K., Brunt, R.L., Hodgson, D.M. and Flint, S.S.** (2010) Capturing stratigraphic and  
37  
38 1120 sedimentological complexity from submarine channel complex outcrops to digital 3D models, Karoo  
39  
40 1121 Basin, South Africa. *Petroleum Geoscience*, **16**, 307-330.  
41  
42 1122 **Raudkivi, A.J.** (1998) *Loose Boundary Hydraulics*. A.A. Balkema, Rotterdam, The Netherlands, pp 260.  
43  
44 1123 **Rotzien, J.R., Lowe, D.R., King, P.R. and Browne, G.H.** (2014) Stratigraphic architecture and  
45  
46 1124 evolution of a deep-water slope channel-levee and overbank apron: The Upper Miocene Upper  
47  
48 1125 Mount Messenger Formation, Taranaki Basin. *Marine and Petroleum Geology*, **52**, 22-41.  
49  
50 1126 **Schindler, R.J., Parsons, D.R., Ye, L., Hope, J.A., Baas, J.H., Peakall, J., Manning, A.J., Aspden, R.J.,**  
51  
52 1127 **Malarkey, J., Simmons, S., Paterson, D.M., Lichtman, I.D., Davies, A.G., Thorne, P.D. and Bass, S.J.**  
53  
54  
55  
56  
57  
58  
59  
60

- 1  
2  
3  
4  
5  
6 1128 (2015) Sticky stuff: Redefining bedform prediction in modern and ancient environments. *Geology*,  
7  
8 1129 **43**, 399-402.  
9  
10 1130 **Schminke, H.U., Fisher, R.V. and Waters, A.C.** (1973) Antidune and chute and pool structures in the  
11  
12 1131 base surge deposits of the Laacher See area, Germany. *Sedimentology*, **20**, 553-574.  
13  
14 1132 **Sixsmith, P., Flint, S.S., Wickens, H.D. and Johnson, S.** (2004) Anatomy and stratigraphic  
15  
16 1133 development of a basin floor turbidite system in the Laingsburg Formation, main Karoo Basin, South  
17  
18 1134 Africa. *Journal of Sedimentary Research*, **74**, 239-254.  
19  
20 1135 **Skipper, K.**, (1971) Antidune cross-stratification in a turbidite sequence, Cloridorme Formation,  
21  
22 1136 Gaspé, Quebec. *Sedimentology*, **17**, 51-68.  
23  
24 1137 **Sohn, Y.K.** (1997) On traction-carpet sedimentation. *Journal of Sedimentary Research*, **67**, 502-509.  
25  
26  
27 1138 **Southard, J.B.** (1991) Experimental determination of bed-form stability. *Annual Review of Earth and*  
28  
29 1139 *Planetary Sciences*, **19**, 423-455.  
30  
31 1140 **Southard, J.B. and Boguchwal, L.A.** (1990) Bed configurations in steady unidirectional water flows.  
32  
33 1141 Part 2. Synthesis of flume data. *Journal of Sedimentary Research*, **60**, 658-679.  
34  
35 1142 **Stow, D.A. and Johansson, M.** (2000) Deep-water massive sands: nature, origin and hydrocarbon  
36  
37 1143 implications. *Marine and Petroleum Geology*, **17**, 145-174.  
38  
39 1144 **Stevenson, C.J., Jackson, C.A-L., Hodgson, D.M., Hubbard, S.M. and Eggenhuisen, J.T.** (2015) Deep-  
40  
41 1145 water sediment bypass. *Journal of Sedimentary Research*, **85**, 1058-1081.  
42  
43 1146 **Sumner, E.J., Amy, L.A. and Talling, P.J.** (2008) Deposit structure and processes of sand deposition  
44  
45 1147 from decelerating sediment suspensions. *Journal of Sedimentary Research*, **78**, 529-547.  
46  
47 1148 **Sumner, E.J., Peakall, J., Parsons, D.R., Wynn, R.B., Darby, S.E., Dorrell, R.M., McPhail, S.D.,**  
48  
49 1149 **Perrett, J., Webb, A. and White, D.** (2013) First direct measurements of hydraulic jumps in an active  
50  
51 1150 submarine density current. *Geophysical Research Letters*, **40**, 5904-5908.  
52  
53  
54  
55  
56  
57  
58  
59  
60

- 1  
2  
3  
4  
5  
6 1151 **Symons, W.O., Sumner, E.J., Talling, P.J., Cartigny, M.J. and Clare, M.A.** (2016) Large-scale sediment  
7  
8 1152 waves and scours on the modern seafloor and their implications for the prevalence of supercritical  
9  
10 1153 flows. *Marine Geology*, **371**, 130-148.  
11  
12 1154 **Talling, P.J., Masson, D.G., Sumner, E.J. and Malgesini, G.** (2012) Subaqueous sediment density  
13  
14 1155 flows: Depositional processes and deposit types. *Sedimentology*, **59**, 1937-2003.  
15  
16 1156 **Tinterri, R.** (2011). Combined flow sedimentary structures and the genetic link between sigmoidal  
17  
18 1157 and hummocky cross-stratification. *GeoActa (Bologna)*, **10**, 1-43.  
19  
20 1158 **Tinterri, R. and Muzzi Magalhaes, P.** (2011) Synsedimentary structural control on foredeep  
21  
22 1159 turbidites: An example from Miocene Marnoso-arenacea Formation, Northern Apennines, Italy.  
23  
24 1160 *Marine and Petroleum Geology*, **28**, 629-657.  
25  
26 1161 **Tinterri, R. and Tagliaferri, A.** (2015) The syntectonic evolution of foredeep turbidites related to  
27  
28 1162 basin segmentation: Facies response to the increase in tectonic confinement (Marnoso-arenacea  
29  
30 1163 Formation, Miocene, Northern Apennines, Italy). *Marine and Petroleum Geology*, **67**, 81-110.  
31  
32  
33 1164 **Van der Mark, C.F., Blom, A. and Hulscher, S.J.M.H.** (2008) Quantification of variability in bedform  
34  
35 1165 geometry. *Journal of Geophysical Research: Earth Surface*, **113**, F03020, doi:10.1029/2007JF000940.  
36  
37 1166 **Van Der Merwe, W.C., Hodgson, D.M., Brunt, R.L. and Flint, S.S.** (2014) Depositional architecture of  
38  
39 1167 sand-attached and sand-detached channel-lobe transition zones on an exhumed stepped slope  
40  
41 1168 mapped over a 2500 km<sup>2</sup> area. *Geosphere*, **10**, 1076-1093.  
42  
43 1169 [Vellinga, A.J., Cartigny, M.J.B., Eggenhuisen, J.T. and Hansen, E.W.M. \(2018\) Morphodynamics and](#)  
44  
45 1170 [depositional signature of low-aggradation cyclic steps: New insights from a depth resolved model.](#)  
46  
47 1171 [Sedimentology](#), **65**, 540-560.  
48  
49 1172 **Vicente Bravo, J.V. and Robles, S.** (1995) Large-scale mesotopographic bedforms from the Albian  
50  
51 1173 Black Flysch, northern Spain: characterization, setting and comparison with recent analogues. In:  
52 1174 *Atlas of Deep Water Environments; Architectural Style in Turbidite Systems* (Eds. Pickering, K.T.,  
53  
54  
55  
56  
57  
58  
59  
60

- 1  
2  
3  
4  
5  
6 1175 Hiscott, R.N., Kenyon, N.H., Ricci-Lucchi, F. and Smith, R.D.A.), *Chapman and Hall, London*, pp. 216-  
7  
8 1176 226.  
9  
10 1177 **Wickens H.DeV.** (1994) Basin floor fan building turbidites of the southwestern Karoo Basin, Permian  
11  
12 1178 Eccca Group, South Africa. *PhD-Thesis. University of Port Elizabeth*.  
13  
14 1179 **Winn, R.D. and Dott, R.H.** (1977) Large-scale traction-produced structures in deep-water fan-  
15  
16 1180 channel conglomerates in southern Chile. *Geology*, **5**, 41-44.  
17  
18 1181 **Wynn, R.B. and Stow, D.A.** (2002) Classification and characterisation of deep-water sediment waves.  
19  
20 1182 *Marine Geology*, **192**, 7-22.  
21  
22 1183 **Wynn, R.B., Kenyon, N.H., Masson, D.G., Stow D.A. and Weaver, P.P.** (2002a) Characterization and  
23  
24 1184 recognition of deep-water channel-lobe transition zones. *AAPG Bulletin*, **86**, 1441-1462.  
25  
26 1185 **Wynn, R.B., Piper, D.J.W. and Gee, M.J.R.** (2002b) Generation and migration of coarse-grained  
27  
28 1186 sediment waves in turbidity current channels and channel-lobe transition zones. *Marine Geology*,  
29  
30 1187 **192**, 59-78.  
31  
32 1188 **Yokokawa, M., Matsuda, F. and Endo, N.** (1995) Sand particle movement on migrating combined-  
33  
34 1189 flow ripples. *Journal of Sedimentary Research*, **A65**, 40-44.  
35  
36  
37 1190 **Zecchin, M., Caffau, M., Di Stefano, A., Maniscalco, R., Lenaz, D., Civile, D., Muto, F. and Crantelli,**  
38  
39 1191 **S.** (2013) The Messinian succession of the Crotona Basin (southern Italy) II: Facies architecture and  
40  
41 1192 stratal surfaces across the Miocene-Pliocene boundary. *Marine and Petroleum Geology*, **48**, 474-492.  
42  
43  
44  
45  
46  
47  
48  
49  
50  
51  
52  
53  
54  
55  
56  
57  
58  
59  
60

1193 **FIGURE CAPTIONS**

1194 **Figure 1.** Sediment wave dimensions (crest height *versus* wavelength) from modern and ancient  
1195 systems grouped on the basis of type of dataset (A), setting (B) and grain size (C). Data taken from  
1196 Normark & Dickson (1976); Winn & Dott (1977); Damuth (1979); Lonsdale & Hollister (1979); Piper *et*  
1197 *al.* (1985); Malinverno *et al.* (1988); Praeg & Schafer (1989); Piper & Kontopoulos (1994); Vicente  
1198 Bravo & Robles (1995); Howe (1996); Kidd *et al.* (1998); Morris *et al.* (1998); Nakajima *et al.* (1998);  
1199 McHugh & Ryan (2000); Migeon *et al.* (2001); Wynn *et al.* (2002a,b); Normark *et al.* (2002); Ito &  
1200 Saito (2006); Heinio & Davies (2009); Ito (2010); Mukti & Ito (2010); Campion *et al.* (2011); Ponce &  
1201 Carmona (2011); Ito *et al.* (2014); Morris *et al.* (2014); Postma *et al.* (2014). Note that a lack of sand-  
1202 prone sediment waves in modern examples can be ascribed to difficulties in retrieving piston cores  
1203 within such sediments (e.g. Bouma & Boerma, 1968). [The raw data are available as supplementary](#)  
1204 [material to this manuscript.](#)

1205 **Figure 2.** (A) Location map of the Laingsburg depocentre within the Western Cape. The transparent  
1206 overlay with black lining indicates the total exposed area of Unit B. Important outcrop areas are  
1207 highlighted, including the sections studied in this paper: Doornkloof and Old Railway; white  
1208 diamonds indicate locations discussed in Brunt *et al.* (2013). (B) Zoomed-in map of the Doornkloof  
1209 section including palaeocurrent distributions, sub-divided into subunit B1 and subunit B2. The  
1210 outcrop outlines are indicated by solid lines. Red line indicates Section I (Figure 5), blue line on DK-  
1211 unit B2 represents Section II (Figure 9). (C) Zoomed-in map of the Old Railway section including  
1212 palaeocurrent distributions.

1213 **Figure 3.** (A) [Simplified stratigraphic column of the deep-water stratigraphy within the Laingsburg](#)  
1214 [depocentre, based on Flint \*et al.\* \(2011\).](#) (B-C) Palaeogeographic reconstruction of subunit ~~B1~~ **B1** ~~(top~~  
1215 ~~B2~~ **(B)** and subunit ~~B2~~ **B2** ~~(bottom~~ **B1** ~~(C)~~ based on the regional study of Brunt *et al.* (2013). The two outcrop  
1216 locations discussed in this paper are indicated by the diamonds.

1  
2  
3  
4  
5  
6 1217 **Figure 4.** Examples of Internal bed structure and facies changes within subunit B2 (Doornkloof), with  
7  
8 1218 one example from *Bedform c* (A) and two from *Bedform b* (B and C) (see Fig. 9B for locations). All  
9  
10 1219 these examples show vertical internal facies changes, which include planar-lamination, wavy-  
11  
12 1220 lamination/banding and ripple-lamination.

13  
14 1221 **Figure 5.** Complete stratigraphic panel of the Doornkloof section showing the subdivision of Unit B,  
15  
16 1222 the location of the two detailed sedimentary sections (I, II), and the position of the DK01 core. The  
17  
18 1223 thin siltstone interval (TSI; Brunt *et al.*, 2013) between the AB interfan and subunit B1 has been used  
19  
20 1224 as a stratigraphic datum. The middle correlation panel shows section I of subunit B1; the position of  
21  
22 1225 *Bedform a* and the palaeoflow patterns have been indicated, as well as the location of the  
23  
24 1226 correlation panel in Figure 8. The bottom correlation panel shows the detailed facies distribution  
25  
26 1227 within *Bedform a* and its internal truncation surfaces. Outcrop photograph locations shown in Figure  
27  
28 1228 6 (A-D) and Figure 7 have been indicated.

29 1229 **Figure 6.** Representative outcrop photographs from Section I and II and descriptive DK01 core log of  
30  
31 1230 subunit B1, with (A) *Bedform a* with ripple-top morphology on top of a local mudstone clast  
32  
33 1231 conglomerate deposit; (B) Eastward-orientated internal truncation surface (dotted line) in banded  
34  
35 1232 division within *Bedform a*; (C) Mudstone clast conglomerate layer below *Bedform a*; (D) Mudstone  
36  
37 1233 clast-rich banded section of *Bedform a*; (E) Westward-orientated internal truncation surface (dotted  
38  
39 1234 line) with climbing ripple-laminated facies within *Bedform a*; (F) Climbing ripple-lamination in  
40  
41 1235 between banded sandstone and sigmoidal lamination, as part of *Bedform b*; (G) Lower section of  
42  
43 1236 westward orientated truncation surface in *Bedform b*; (H) Upper section of westward orientated  
44  
45 1237 truncation surface in *Bedform b*; (I) Banded sandstone division in *Bedform b*; (J) West-facing  
46  
47 1238 truncation surface in *Bedform c*. See Figure 5 and Figure 9B for locations. Interpreted position of  
48  
49 1239 *Bedform a* is indicated (by an asterisk) within the DK01 core log.

50 1240 **Figure 7.** Mudstone clast conglomerate patch at the bottom of *Bedform a*, with clean true-scale  
51  
52 1241 photopanel (top) and interpreted vertically exaggerated ( $V_e = 1.8$ ) photopanel (bottom). It shows a

53  
54  
55  
56  
57  
58  
59  
60



1  
2  
3  
4  
5  
6 1242 basal erosion surface overlying thin-bedded sandstones, multiple 'floating' sandstone patches,  
7  
8 1243 upstream orientated ~~pinchout~~ pinch-out and downstream orientated amalgamation. Location of  
9  
10 1244 photograph is shown in the lowest panel of Figure 5.

11  
12 1245 **Figure 8.** Facies correlation panel of local sandstone swell in subunit B1. *Bedform a* is located at the  
13  
14 1246 base of the package. Top panel shows its location within subunit B1. See middle panel of Figure 5 for  
15  
16 1247 more detailed facies correlation panel of the complete subunit B1, log locations, and lower panel of  
17  
18 1248 Figure 5 for symbol explanations.

19  
20 1249 **Figure 9.** (A) Panoramic view of the base of subunit B2 at the DK-section. The outlines of *Bedform b*  
21  
22 1250 and *c* are indicated with white lines. Numbers indicate the position of sedimentary logs. (B) Facies  
23  
24 1251 correlation of the II-section with *Bedform b* and *c*. The top panel shows the thickness variability of  
25  
26 1252 these beds and the surrounding stratigraphy, comprised of structured sandstones (ripple- or planar-  
27  
28 1253 laminated); the lower panel shows the internal facies distribution of *Bedform b* and *c*. Rose diagrams  
29  
30 1254 show palaeoflow measurements around Section II. Internal truncation surfaces and location of the  
31  
32 1255 facies photos shown in Figure 4 and Figure 6 (F-J) have been indicated. See Figure 2B and Figure 5 for  
33  
34 1256 location of section II and for meaning of log symbols.

35 1257 **Figure 10.** Bedset architecture within the main subunit B2 outcrop face in the Doornkloof area.  
36  
37 1258 Bounding surfaces have been defined based on successive bed pinch-out with multiple (3-4)  
38  
39 1259 downstream-orientated stacked and weakly amalgamated bedforms.

40  
41 1260 **Figure 11.** Subunit B2 within the Old Railway area. A- Facies correlation panels of the section with  
42  
43 1261 bedform distribution (top) and facies distribution (bottom). B- Zoomed-in facies correlation panel of  
44  
45 1262 most eastern section with C – mudstone clasts within a climbing-ripple laminated bed, indicating  
46  
47 1263 sediment overpassing, and D – bed splitting indicating erosion and amalgamation. See Figure 2 for  
48  
49 1264 location and lowest panel in Figure 5 for meaning of log symbols. Location of Figure 12 is indicated.

50 1265 **Figure 12.** Sketch of bed showing transient pinch-out to a thin siltstone bed (see Figure 11B for  
51  
52 1266 location), with (A1) pinch-out to siltstone, and (A2) local scouring of bed top.

1  
2  
3  
4  
5  
6  
7  
8  
9  
10  
11  
12  
13  
14  
15  
16  
17  
18  
19  
20  
21  
22  
23  
24  
25  
26  
27  
28  
29  
30  
31  
32  
33  
34  
35  
36  
37  
38  
39  
40  
41  
42  
43  
44  
45  
46  
47  
48  
49  
50  
51  
52  
53  
54  
55  
56  
57  
58  
59  
60

**Figure 13.** (A) Idealised model to illustrate the variation in sedimentary structure within sediment wave swells in the Doornkloof area. (B) Interpretation of changes in depositional behaviour through time, linked to the observed internal facies changes in (A). T1-T7 refer to successive time periods, and show the evolution of the sediment waves, and what this means in terms of flow conditions over time. F1 consists of structureless sands.

**Figure 14.** (A) Process explanation of the upstream-orientated accretion process, linked to flow capacity changes over time. Flow capacity may be linked to temporal variations in velocity from upstream hydraulic jumps, and/or to the lateral migration of the flow, shown in part B. (B) Illustration of the inferred spatial contribution (hose effect) during formation of the sediment waves. Lateral migration of the flow core during a single event is linked to capacity changes at a single location, as well as the formation of new swells upstream. The steps are interlinked between A and B; 'x' marks the same location throughout. Step 5 represents another phase of erosion, and thus a return to step 2.

**Figure 15.** (A) Spatial division within a channel-lobe transition zone between a depositional bedform area (DB) and an erosional bedform area (EB) following Wynn *et al.* (2002a). Differences in sediment wave deposit facies and architecture are explained by spatial differences between the axis and fringe areas of the deposition-dominated fields (DB) of a CLTZ. (B) Sketch model showing how the 'hose effect' within an active flow will dominantly influence sediment wave development in axial areas.

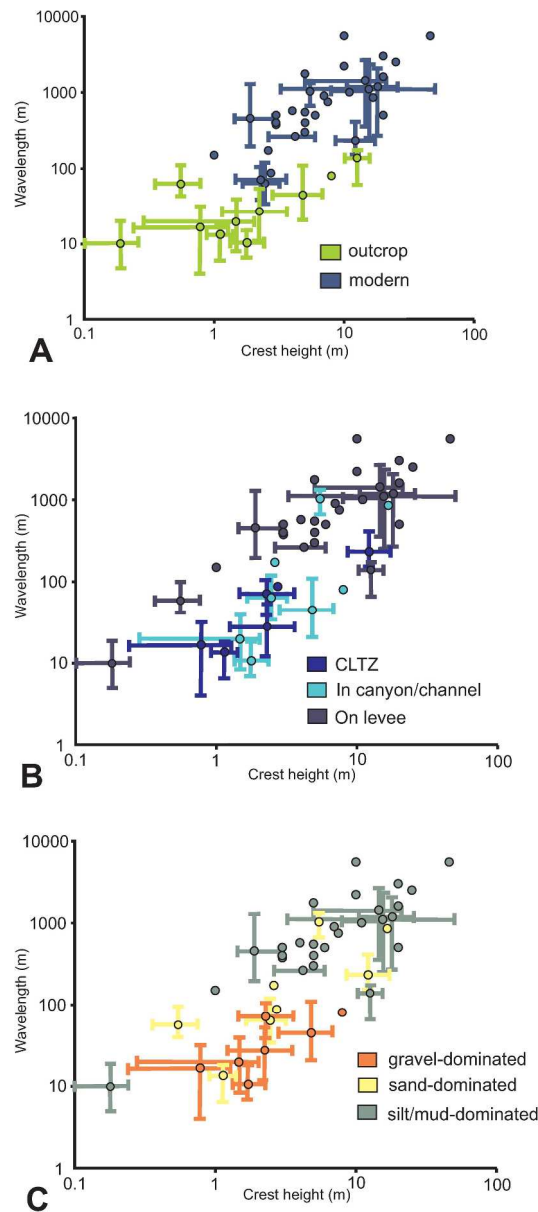


Figure 1: Sediment wave dimensions (crest height versus wavelength) from modern and ancient systems grouped on the basis of type of dataset (A), setting (B) and grain size (C). Data taken from Normark & Dickson (1976); Winn & Dott (1977); Damuth (1979); Lonsdale & Hollister (1979); Piper et al. (1985); Malinverno et al. (1988); Praeg & Schafer (1989); Piper & Kontopoulos (1994); Vicente Bravo & Robles (1995); Howe (1996); Kidd et al. (1998); Morris et al. (1998); Nakajima et al. (1998); McHugh & Ryan (2000); Migeon et al. (2001); Wynn et al. (2002a,b); Normark et al. (2002); Ito & Saito (2006); Heinö & Davies (2009); Ito (2010); Mukti & Ito (2010); Campion et al. (2011); Ponce & Carmona (2011); Ito et al. (2014); Morris et al. (2014); Postma et al. (2014). Note that a lack of sand-prone sediment waves in modern examples can be ascribed to difficulties in retrieving piston cores within such sediments (e.g. Bouma & Boerma, 1968). The raw data are available as supplementary material to this manuscript.

222x509mm (300 x 300 DPI)

1  
2  
3  
4  
5  
6  
7  
8  
9  
10  
11  
12  
13  
14  
15  
16  
17  
18  
19  
20  
21  
22  
23  
24  
25  
26  
27  
28  
29  
30  
31  
32  
33  
34  
35  
36  
37  
38  
39  
40  
41  
42  
43  
44  
45  
46  
47  
48  
49  
50  
51  
52  
53  
54  
55  
56  
57  
58  
59  
60

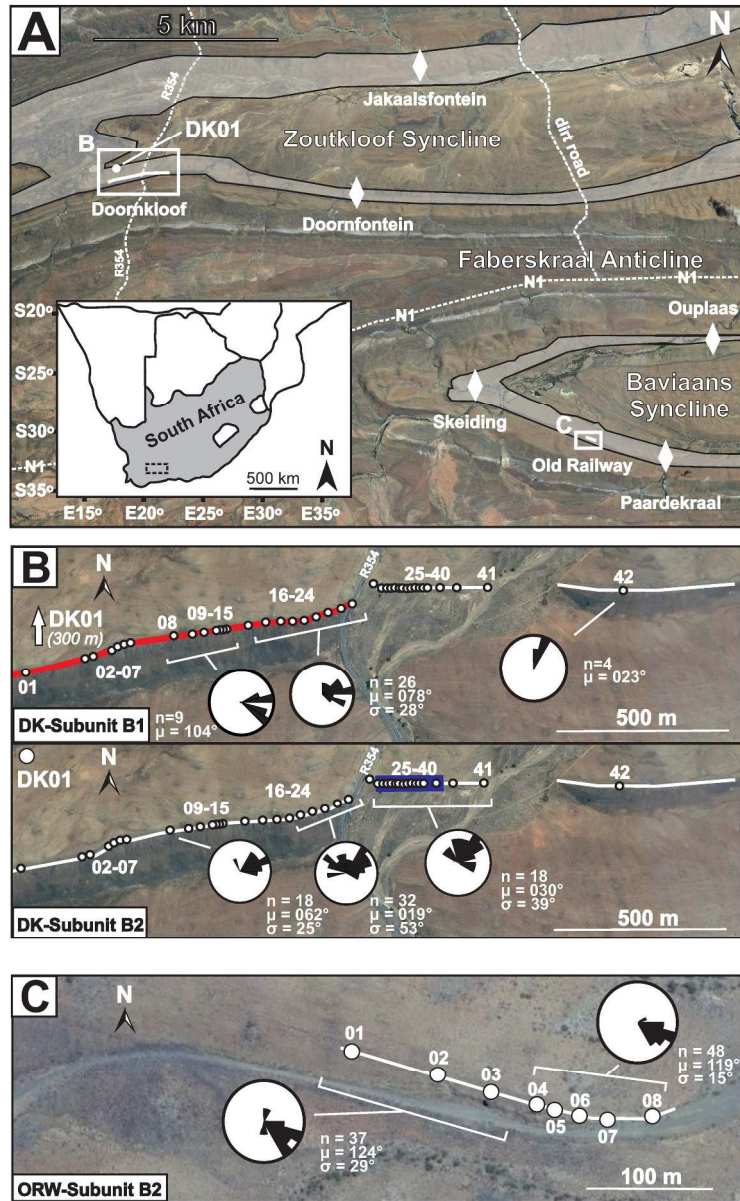


Figure 2: (A) Location map of the Laingsburg depocentre within the Western Cape. The transparent overlay with black lining indicates the total exposed area of Unit B. Important outcrop areas are highlighted, including the sections studied in this paper: Doornkloof and Old Railway; white diamonds indicate locations discussed in Brunt et al. (2013). (B) Zoomed-in map of the Doornkloof section including palaeocurrent distributions, sub-divided into subunit B1 and subunit B2. The outcrop outlines are indicated by solid lines. Red line indicates Section I (Figure 5), blue line on DK-unit B2 represents Section II (Figure 9). (C) Zoomed-in map of the Old Railway section including palaeocurrent distributions.

212x345mm (300 x 300 DPI)

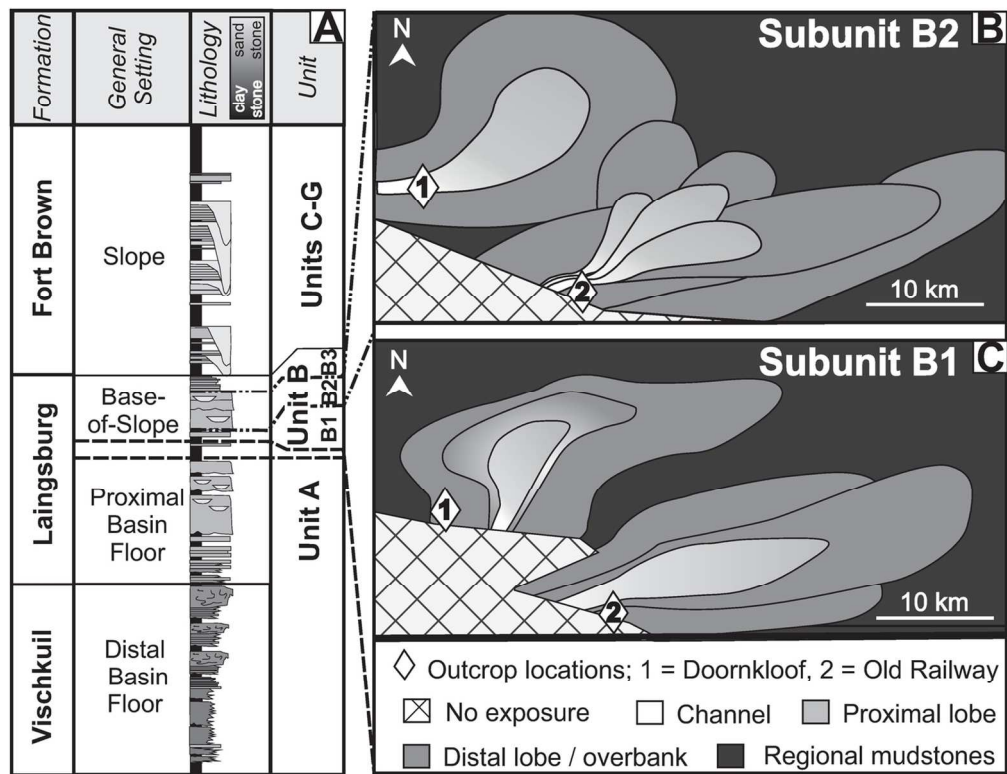


Figure 3: (A) Simplified stratigraphic column of the deep-water stratigraphy within the Laingsburg depocentre, based on Flint et al. (2011). (B-C) Palaeogeographic reconstruction of subunit B2 (B) and subunit B1 (C) based on the regional study of Brunt et al. (2013). The two outcrop locations discussed in this paper are indicated by the diamonds.

125x96mm (300 x 300 DPI)

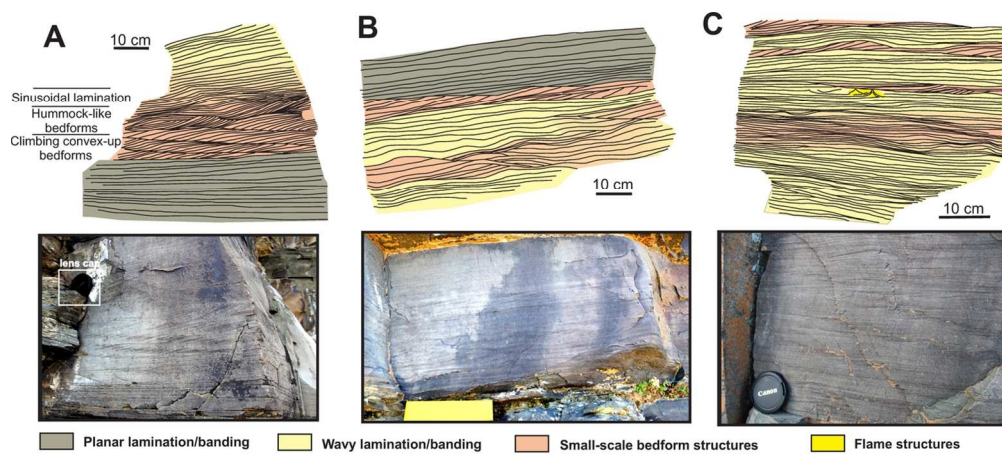


Figure 4: Examples of Internal bed structure and facies changes within subunit B2 (Doornkloof), with one example from Bedform c (A) and two from Bedform b (B and C) (see Fig. 9B for locations). All these examples show vertical internal facies changes, which include planar-lamination, wavy-lamination/banding and ripple-lamination.

122x54mm (300 x 300 DPI)

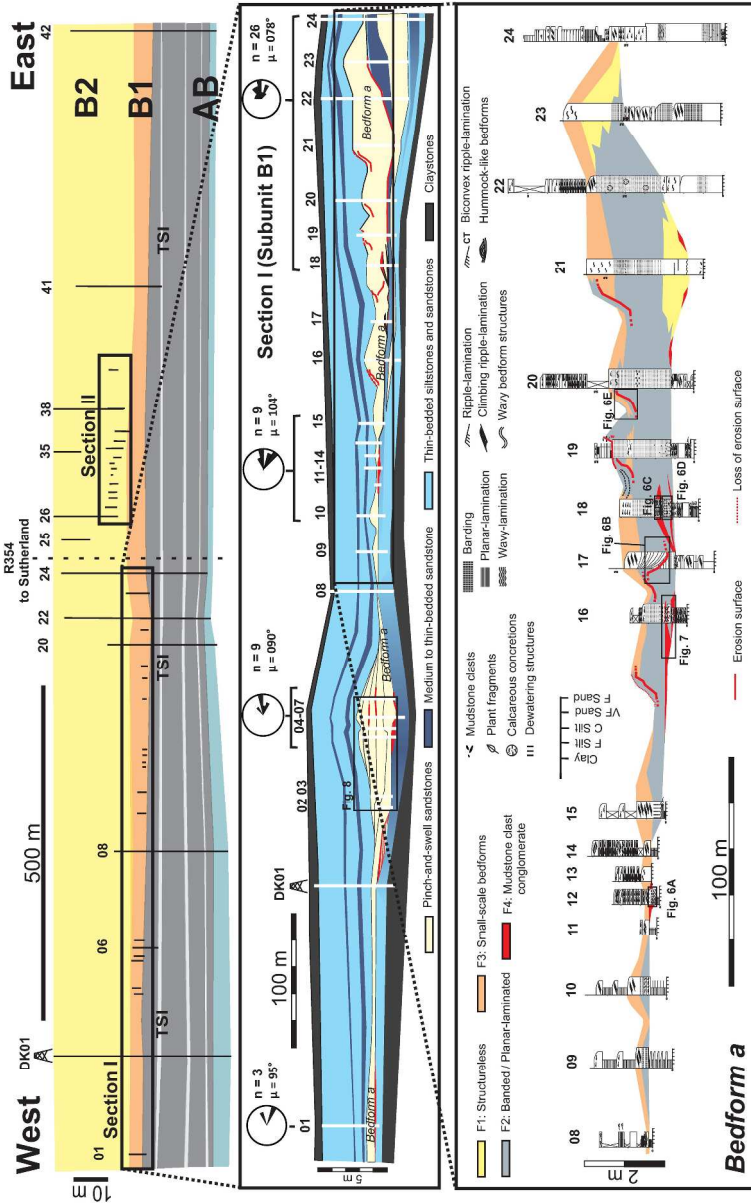
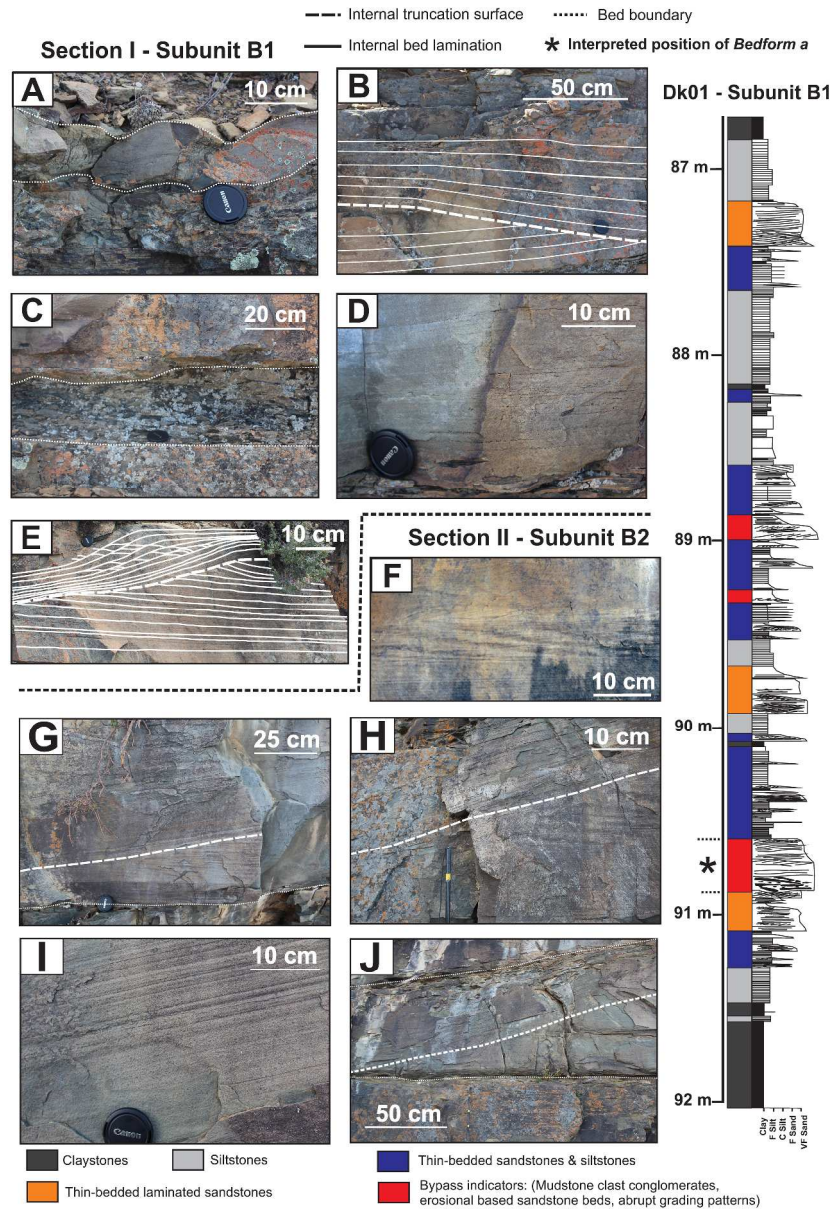


Figure 5: Complete stratigraphic panel of the Doornkloof section showing the subdivision of Unit B, the location of the two detailed sedimentary sections (I, II), and the position of the DK01 core. The thin siltstone interval (TSI; Brunt et al., 2013) between the AB interfan and subunit B1 has been used as a stratigraphic datum. The middle correlation panel shows section I of subunit B1; the position of Bedform a and the palaeoflow patterns have been indicated, as well as the location of the correlation panel in Figure 8. The bottom correlation panel shows the detailed facies distribution within Bedform a and its internal truncation surfaces. Outcrop photograph locations shown in Figure 6 (A-D) and Figure 7 have been indicated.

287x453mm (300 x 300 DPI)





46 Figure 6: Representative outcrop photographs from Section I and II and descriptive DK01 core log of subunit  
47 B1, with (A) Bedform a with ripple-top morphology on top of a local mudstone clast conglomerate deposit;  
48 (B) Eastward-orientated internal truncation surface (dotted line) in banded division within Bedform a; (C)  
49 Mudstone clast conglomerate layer below Bedform a; (D) Mudstone clast-rich banded section of Bedform a;  
50 (E) Westward-orientated internal truncation surface (dotted line) with climbing ripple-laminated facies within  
51 Bedform a; (F) Climbing ripple-lamination in between banded sandstone and sigmoidal lamination, as part of  
52 Bedform b; (G) Lower section of westward orientated truncation surface in Bedform b; (H) Upper section of  
53 westward orientated truncation surface in Bedform b; (I) Banded sandstone division in Bedform b; (J) West-  
54 facing truncation surface in Bedform c. See Figure 5 and Figure 9B for locations. Interpreted position of  
55 Bedform a is indicated (by an asterisk) within the DK01 core log.

446x653mm (300 x 300 DPI)

56  
57  
58  
59  
60

1  
2  
3  
4  
5  
6  
7  
8  
9  
10  
11  
12  
13  
14  
15  
16  
17  
18  
19  
20  
21  
22  
23  
24  
25  
26  
27  
28  
29  
30  
31  
32  
33  
34  
35  
36  
37  
38  
39  
40  
41  
42  
43  
44  
45  
46  
47  
48  
49  
50  
51  
52  
53  
54  
55  
56  
57  
58  
59  
60

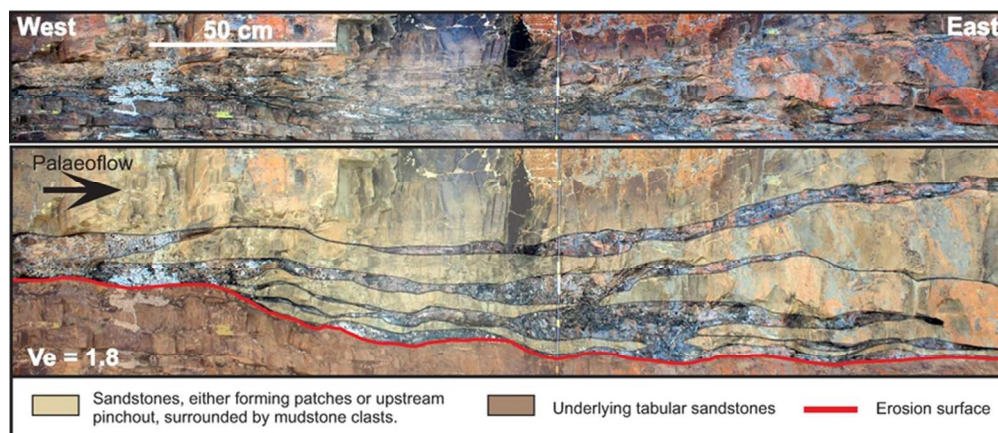


Figure 7: Mudstone clast conglomerate patch at the bottom of Bedform a, with clean true-scale photopanel (top) and interpreted vertically exaggerated ( $V_e = 1.8$ ) photopanel (bottom). It shows a basal erosion surface overlying thin-bedded sandstones, multiple 'floating' sandstone patches, upstream orientated pinch-out and downstream orientated amalgamation. Location of photograph is shown in the lowest panel of Figure 5.

73x31mm (300 x 300 DPI)

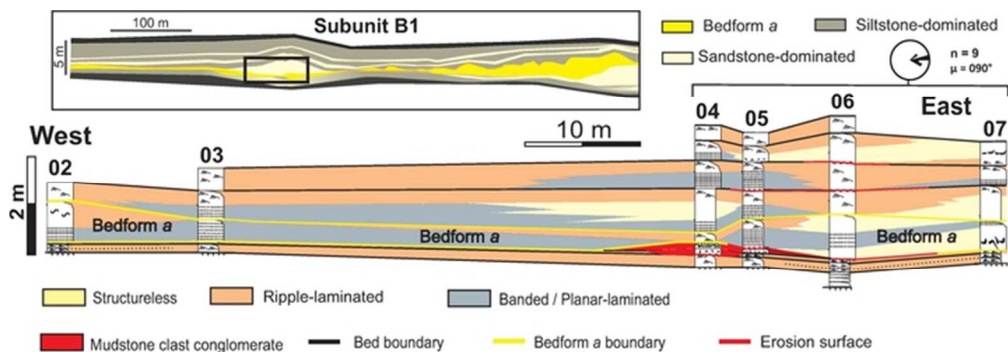


Figure 8: Facies correlation panel of local sandstone swell in subunit B1. Bedform a is located at the base of the package. Top panel shows its location within subunit B1. See middle panel of Figure 5 for more detailed facies correlation panel of the complete subunit B1, log locations, and lower panel of Figure 5 for symbol explanations.

60x20mm (300 x 300 DPI)

1  
2  
3  
4  
5  
6  
7  
8  
9  
10  
11  
12  
13  
14  
15  
16  
17  
18  
19  
20  
21  
22  
23  
24  
25  
26  
27  
28  
29  
30  
31  
32  
33  
34  
35  
36  
37  
38  
39  
40  
41  
42  
43  
44  
45  
46  
47  
48  
49  
50  
51  
52  
53  
54  
55  
56  
57  
58  
59  
60

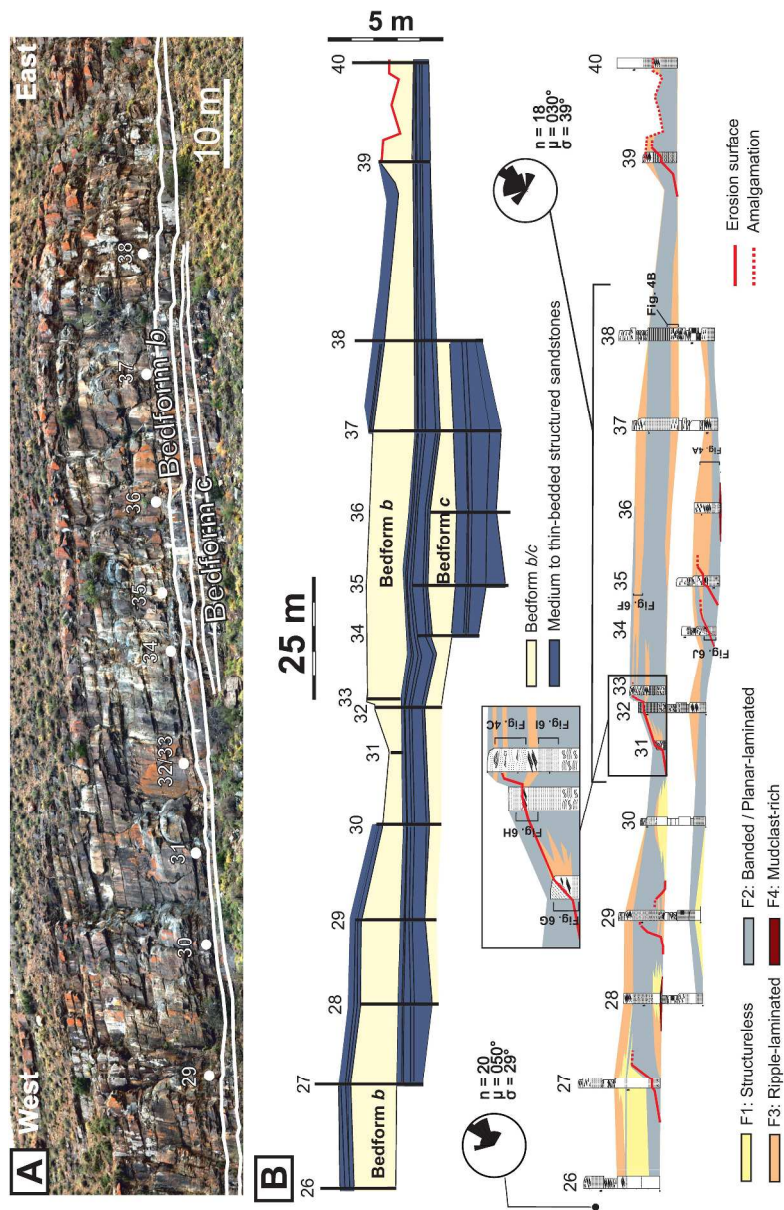


Figure 9: (A) Panoramic view of the base of subunit B2 at the DK-section. The outlines of Bedform b and c are indicated with white lines. Numbers indicate the position of sedimentary logs. (B) Facies correlation of the II-section with Bedform b and c. The top panel shows the thickness variability of these beds and the surrounding stratigraphy, comprised of structured sandstones (ripple- or planar-laminated); the lower panel shows the internal facies distribution of Bedform b and c. Rose diagrams show palaeoflow measurements around Section II. Internal truncation surfaces and location of the facies photos shown in Figure 4 and Figure 6 (F-J) have been indicated. See Figure 2B and Figure 5 for location of section II and for meaning of log symbols.

286x440mm (300 x 300 DPI)

1  
2  
3  
4  
5  
6  
7  
8  
9  
10  
11  
12  
13  
14  
15  
16  
17  
18  
19  
20  
21  
22  
23  
24  
25  
26  
27  
28  
29  
30  
31  
32  
33  
34  
35  
36  
37  
38  
39  
40  
41  
42  
43  
44  
45  
46  
47  
48  
49  
50  
51  
52  
53  
54  
55  
56  
57  
58  
59  
60

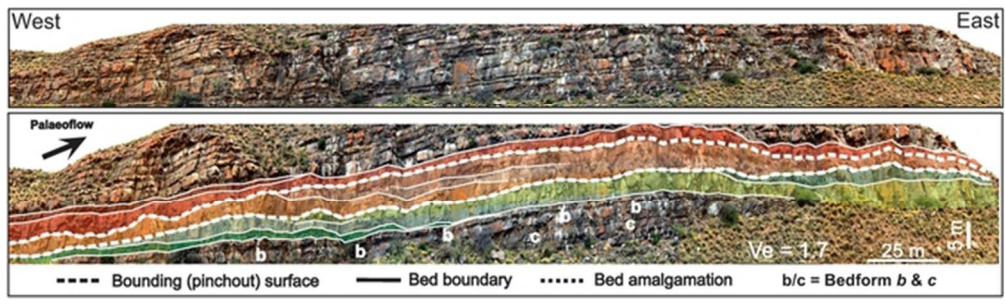


Figure 10: Bedset architecture within the main subunit B2 outcrop face in the Doornkloof area. Bouding surfaces have been defined based on successive bed pinch-out with multiple (3-4) downstream-orientated stacked and weakly amalgamated bedforms.

57x16mm (300 x 300 DPI)

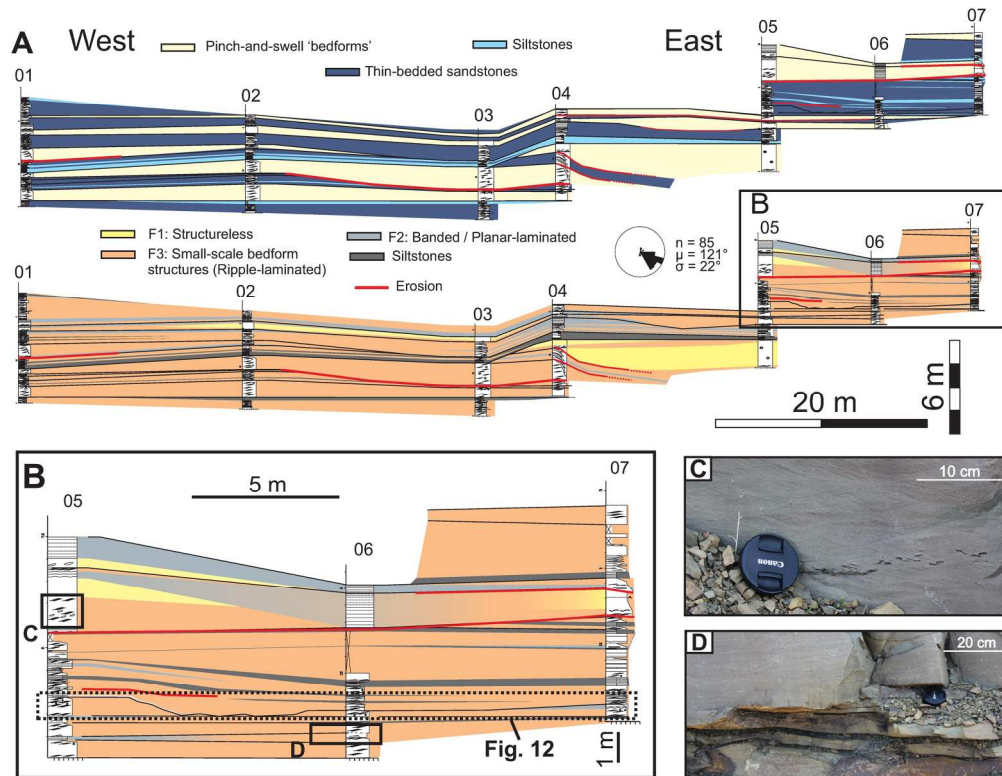


Figure 11: Subunit B2 within the Old Railway area. A- Facies correlation panels of the section with bedform distribution (top) and facies distribution (bottom). B- Zoomed-in facies correlation panel of most eastern section with C – mudstone clasts within a climbing-ripple laminated bed, indicating sediment overpassing, and D – bed splitting indicating erosion and amalgamation. See Figure 2 for location and lowest panel in Figure 5 for meaning of log symbols. Location of Figure 12 is indicated.

196x151mm (300 x 300 DPI)

1  
2  
3  
4  
5  
6  
7  
8  
9  
10  
11  
12  
13  
14  
15  
16  
17  
18  
19  
20  
21  
22  
23  
24  
25  
26  
27  
28  
29  
30  
31  
32  
33  
34  
35  
36  
37  
38  
39  
40  
41  
42  
43  
44  
45  
46  
47  
48  
49  
50  
51  
52  
53  
54  
55  
56  
57  
58  
59  
60

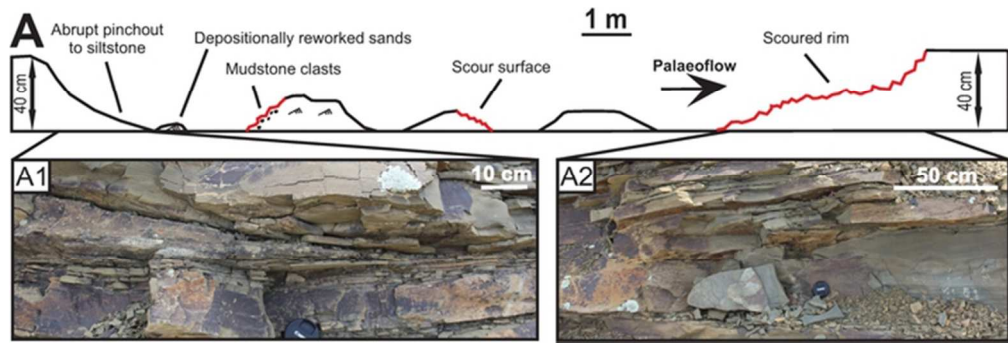


Figure 12: Sketch of bed showing transient pinch-out to a thin siltstone bed (see Figure 11B for location), with (A1) pinch-out to siltstone, and (A2) local scouring of bed top.

60x20mm (300 x 300 DPI)



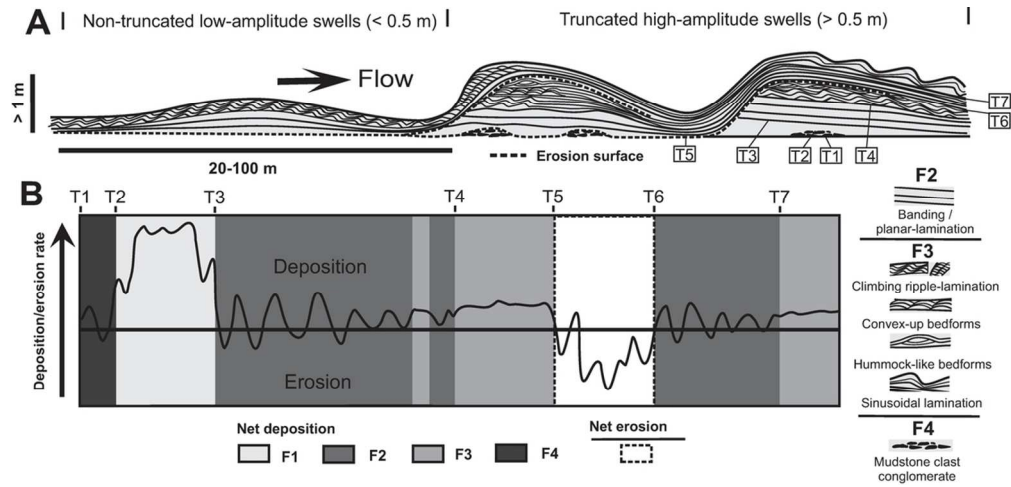


Figure 13: (A) Idealised model to illustrate the variation in sedimentary structure within sediment wave swells in the Doornkloof area. (B) Interpretation of changes in depositional behaviour through time, linked to the observed internal facies changes in (A). T1-T7 refer to successive time periods, and show the evolution of the sediment waves, and what this means in terms of flow conditions over time. F1 consists of structureless sands.

105x50mm (300 x 300 DPI)

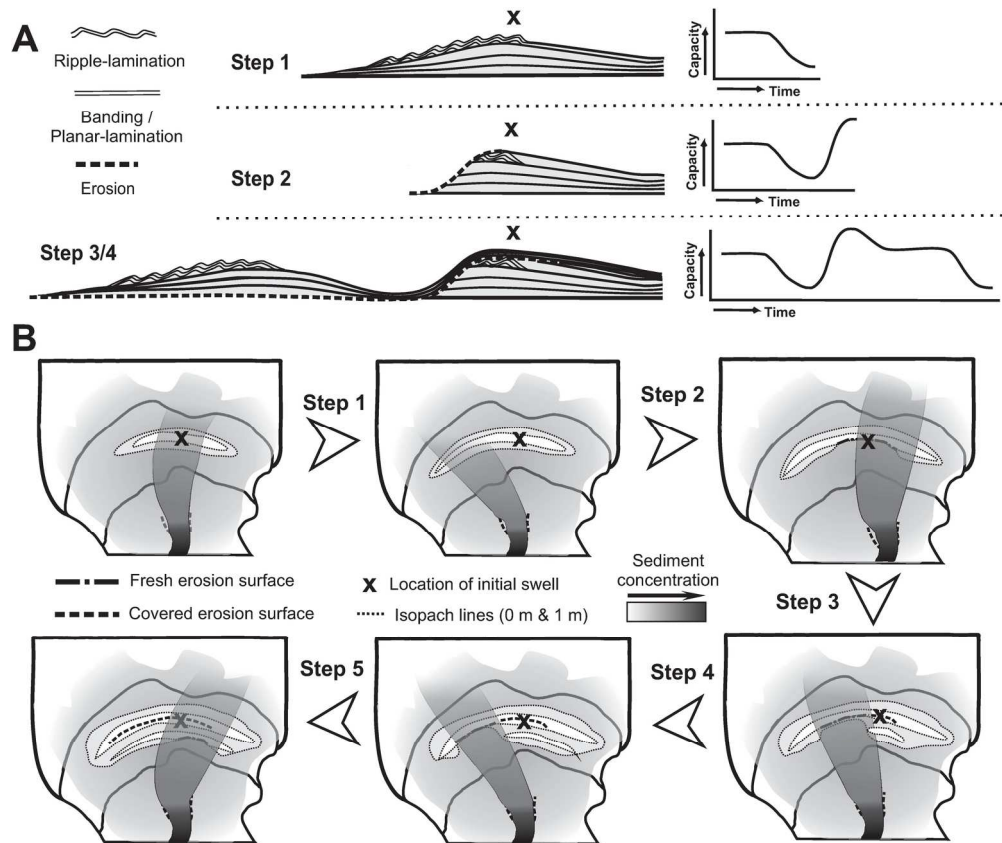


Figure 14: (A) Process explanation of the upstream-orientated accretion process, linked to flow capacity changes over time. Flow capacity may be linked to temporal variations in velocity from upstream hydraulic jumps, and/or to the lateral migration of the flow, shown in part B. (B) Illustration of the inferred spatial contribution (hose effect) during formation of the sediment waves. Lateral migration of the flow core during a single event is linked to capacity changes at a single location, as well as the formation of new swells upstream. The steps are interlinked between A and B; 'x' marks the same location throughout. Step 5 represents another phase of erosion, and thus a return to step 2.

173x145mm (300 x 300 DPI)

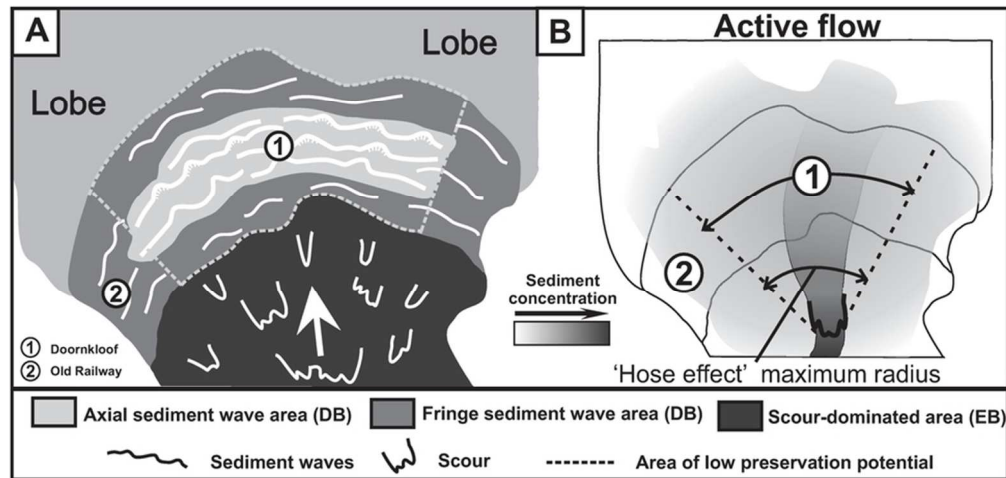


Figure 15: (A) Spatial division within a channel-lobe transition zone between a depositional bedform area (DB) and an erosional bedform area (EB) following Wynn et al. (2002a). Differences in sediment wave deposit facies and architecture are explained by spatial differences between the axis and fringe areas of the deposition-dominated fields (DB) of a CLTZ. (B) Sketch model showing how the 'hose effect' within an active flow will dominantly influence sediment wave development in axial areas.

81x38mm (300 x 300 DPI)

<u>Publication</u>	<u>Dataset type</u>	<u>Formation/System</u>	<u>Environment</u>	<u>Dimensions (WL = Wavelength; CH = Crest Height)</u>	<u>(Average) grain size</u>
Campion et al. (2011)	Outcrop	Cerro Toro Formation	Channel-levee	CH 1.5-15 m, WL 60-200 m	mud to very fine sand
Ito, Saito (2006); Ito (2010)	Outcrop	Boso Peninsula	Canyon	CH 0.4-2 m; WL 7-60 m	gravel
Ito et al. (2014)	Outcrop	Boso Peninsula	Canyon-mouth	CH <2 m; WL <20 m	medium to very coarse
Morris et al. (2014)	Outcrop	Laingsburg Formation	Channel-levee	CH 0.8 m; WL > 100 m	very fine sandstone
Mukti, Ito (2010)	Outcrop	Halang Formation	Channel-levee	CH 0.13 m; WL 10.7 m	mud-dominated
Piper, Kontopoulos (1994)	Outcrop	Pleistocene south side Gulf of Corinth	Confined channel	CH 8 m; WL 80 m	pebbly sands to gravel
Ponce, Carmona (2011)	Outcrop	Austral foreland Basin	CLTZ	CH < 5 m, WL 10-40 m	coarse-grained
Postma et al. (2014)	Outcrop	Tabernas Basin	Canyon/channel	CH 3-8 m; WL 20-100 m	coarse sands to gravel
Vicento-Bravo, Robles (1995)	Outcrop	Albian Black Flysch	Channel-fill; CLTZ	CH 0.3-1.5 m; WL 5-40 m	pebbly sands to gravel
Winn, Dott (1977)	Outcrop	Cerro Toro Formation	Confined channel	CH <4 m; WL 8-12 m	gravel
Damuth (1979)	Modern	Manila trench	Channel-levee	CH 5-20 m; WL 300-3000 m	silt-dominated
Heinö, Davies (2009)	Modern	Espirito Santo Basin	Channel/CLTZ	CH 10-30 m ; WL 100-300 m	coarse-grained
Howe (1996)	Modern	Barra Fan	Channel-levee	CH 5 m; WL 1750 m	silt-dominated
Kidd et al. (1998)	Modern	Stromboli Canyon	Canyon	CH 3-4m high; WL 200m long; CH 18 m, WL 800 m	sand-dominated
Lonsdale, Hollister (1979)	Modern	Reynidsjup Fan	Channel-levee	CH 20 m; WL 500 m	silt-dominated
Malinverno et al. (1988)	Modern	Var Cayon	Canyon	CH <5 m; WL 35-100 m	sand to boulders
McHugh, Ryan (2000)	Modern	Monterey Fan	Channel-levee	CH 10-25 m; WL 300-2500 m	silt-dominated
Migeon et al. (2001)	Modern	Var Fan	Channel-levee	CH 7-46 m high, WL 900-5500 m	silt-dominated
Morris et al. (1998)	Modern	Valencia Channel mouth	Channel-mouth	CH m-scale; WL 70-80 m	coarse-grained
Nakajima et al. (1998)	Modern	Toyama Fan	Channel-levee	CH <70 m; WL <3000 m	silt-dominated
Normark, Dickson (1976)	Modern	Reserve Fan	Channel-levee	WL 120-400 m	silt-dominated
Normark et al. (2002)	Modern	Hueneme Fan	Channel-levee	CH 1-8 m; WL 150 - 550 m	silt-dominated
Piper et al. (1985)	Modern	Laurentian Fan	Channel-mouth	CH 2-5 m; WL 50-100 m	gravel and gravelly sand
Praeg, Schafer (1989)	Modern	Labrador Sea	Channel-levee	CH 5-30 m; WL 500-3000 m	silt-dominated
Wynn et al. (2000a)	Modern	Selvage Fan	Channel-levee	CH <5 m, WL <1100 m	silt-dominated
Wynn et al. (2000b)	Modern	La Palma Fan	Slope/levee	CH 5-70 m; WL 400-2400 m	silt-dominated
Wynn et al. (2000b)	Modern	El Hierro Fan	Channel	CH 6m; WL <1200 m	coarse-grained